

USING CONDITIONAL GENE MANIPULATION TO STUDY REPRODUCTIVE
PHYSIOLOGY AND PATHOLOGY

A Dissertation

by

XIN FANG

Submitted to the Graduate and Professional School of
Texas A&M University
in partial fulfillment of the requirements for the degree of

DOCTOR OF PHILOSOPHY

Chair of Committee,	Qinglei Li
Committee Members,	Ivan Ivanov
	Kayla J. Bayless
	Monique Rijnkels
Head of Department,	Todd M. O'Hara

August 2022

Major Subject: Biomedical Sciences

Copyright 2022 Xin Fang

ABSTRACT

Reproductive development and tumorigenesis are the two main topics in reproductive research. Enhancer of zeste (EZH2), a core component of Polycomb Repressive Complexes 2, possesses histone methyltransferase activity that catalyzes the trimethylation of lysine 27 of histone H3. It has been shown that EZH2 is involved in epithelial to mesenchymal transition (EMT), a key event in development and carcinogenesis. However, the role of EZH2 in the uterus and endometrial cancer remains poorly defined. In Aim 1, we generated a mouse model harboring conditional deletion of *Ezh2* in the uterus. The uterine epithelium became stratified and further developed into endometrial hyperplasia in this mouse model. Fertility defects accompanied by altered uterine growth and function were also found in the *Ezh2* conditional knockout (*Ezh2* cKO) mice. Findings suggest EZH2 protects epithelial integrity partially by inhibiting the differentiation of basal-like cells and preventing epithelial stratification. To study the role of *Ezh2* in endometrial cancer development, we generate a mouse model with double deletion of both *Ezh2* and *Pten* in Aim 2. Compared to *Pten*^{d/d} mice, reduced tumor burdens were observed in the *Pten*^{d/d}; *Ezh2*^{d/d} mice. However, the deletion of *Ezh2* induced altered immune response, enhanced inflammation, and exacerbated epithelial stratification, leading to unfavorable disease outcomes. These results suggest EZH2 plays dual roles in endometrial cancer development. Aim 3 of the dissertation was to study mechanism underlying the development of testicular granulosa cell tumors (TGCTs), a type of rare tumor in the testis. A mouse model with constitutively activative transforming growth factor beta receptor 1 (TGFBR1) in the testis was generated. The development of sex cord-stromal tumor, resembling TGCT, led to overproliferation in Sertoli cells and defective spermatogenesis. The testicular tumors were identified as TGCTs for the positive staining of granulosa cell markers

including INHA, FOXO1, and FOXL2 essential for ovarian granulosa cell differentiation and functions. Thus, Aim 3 uncovered an oncogenic role of TGF β signaling in the testis. In summary, these studies have identified mechanisms of reproductive development and tumorigenesis and will potentially guide the development of targeted therapy for pregnancy failure and tumors in the reproductive system.

ACKNOWLEDGEMENTS

I would like to thank my committee chair, Dr. Qinglei Li and my committee members, Dr. Ivan Ivanov, Dr. Kayla J. Bayless and Dr. Monique Rijnkels for their guidance and support during my Ph.D. program at Texas A&M University. I sincerely appreciated my mentor Dr. Li, for his great effort in training me to become a qualified Ph.D. candidate. With great patience, Dr. Li taught me how to conduct the experiment and figure out an excellent resolution for experiment questions. I will benefit from the habit learned from him for my entire life. I also want to thank Dr. Ivanov for he taught me about data analysis which greatly support my research and helped me develop critical thinking skills during my study. I also want to thank Dr. Monique Rijnkels and Kayla J. Bayless for they not only gave good suggestions on my projects, but also helped me to build up my knowledge base of epigenetics and cell culture. Their enthusiasm for science and the hard work made them great role models for me. I cherish every moment I spend with my committee members.

I would like to extend my gratitude to all the past and current members of the Li laboratory including Nan Ni, Yang Gao for their generous help and encouragement.

Finally, I would like to thank my parents and parents-in-law for their invaluable support. Their encouragement motivated me to the present position. I sincerely express my love and appreciation to my husband, Yifei Liao, for his continuous support. His love brings me out from the stress and difficulty during the research progress. Also, thanks to my adorable cat, Archie, for relieving my pressure with his companion.

CONTRIBUTORS AND FUNDING SOURCES

Contributors section

Part 1, faculty committee recognition

This work was supervised by a dissertation committee consisting of Dr. Qinglei Li (Chair), Dr. Ivan Ivanov of the Department of Veterinary Physiology and Pharmacology, Dr. Kayla J. Bayless of the Department of Molecular and Cellular Medicine and Dr. Monique Rijnkels of the Department of Veterinary Integrative Biosciences.

Part 2, student/collaborator contributions

The work presented in Section 2 is reprinted with slight modification from Fang et al. “Enhancer of zeste 2 polycomb repressive complex 2 subunit is required for uterine epithelial integrity” published in June 2019 with permission from The American Journal of Pathology. All work was completed by the student, under the supervision of Dr. Qinglei Li. We thank Dr. John P. Lydon of Department of Molecular and Cellular Biology, Baylor College of Medicine for providing *Pgr*-Cre mice and Dr. Yang Gao of Baylor College of Medicine for setting up the initial mouse breeding colony.

The work presented in Section 3 is partially reprinted from Fang et al. “EZH2 and Endometrial Cancer Development: Insights from a Mouse Model” published in March 2022 with permission from Cells. All work was completed by the student, under the supervision of Dr. Qinglei Li. We thank Dr. Ivan Ivanov of the Department of Veterinary Physiology and Pharmacology, Dr. Kayla J. Bayless of the Department of Molecular and Cellular Medicine and Dr. Monique Rijnkels of

the Department of Veterinary Integrative Biosciences for critical reading of the manuscript and helpful discussions. I also want to thank for Dr. Xiaofang Wang of Department of Biomedical Sciences, Dr. Yanan Tian of Department of Veterinary Physiology and Pharmacology and Dr. John P. Lydon of Department of Molecular and Cellular Biology for their help in methodology and paper editing. The authors thank the staff in the Comparative Medicine Program for animal care and the histology core facility for sample processing and embedding.

The work presented in Section 4 is reprinted with slight modification from Fang *et al.*

“A Novel Mouse Model of Testicular Granulosa Cell Tumors” which is published in July 2019 with permission from Molecular Human Reproduction. All work was completed by the student, under the supervision of Dr. Qinglei Li. We thank Dr. John P. Lydon and Dr. Laurent Bartholin of Centre de Recherche en Cancérologie de Lyon for providing mice containing the latent constitutively active TGFBR1. We thank Dr. Yang Gao and Mrs. Nan Ni for technical assistance.

Funding sources

The work in Aim 1 was supported by National Institutes of Health grant R01HD087236 from the Eunice Kennedy Shriver National Institute of Child Health & Human Development and Texas A&M University T3 grant (Q.L.)

The work in Aim 2 was supported by the Texas A&M University T3 grant (to Q.L.), NICHD/NIH grant R01HD087236 (to Q.L.), and NIAID/NIH grant R21AI152050 (to Y.T.). The University of Virginia Center for Research in Reproduction Ligand Assay and Analysis Core is supported by the Eunice Kennedy Shriver NICHD/NIH Grant R24HD102061.

The work in Aim 3 was supported by National Institutes of Health grant R03HD082416 from the Eunice Kennedy Shriver National Institute of Child Health & Human Development and the New Faculty Start-up Funds from Texas A&M University (to Q.L.).

NOMENCLATURE

EZH2	Enhancer of Zeste
cKO	Conditional Knockout
TGCTs/ GrCTs	Testicular Granulosa Cell Tumors
TGF β /TGFB	Transforming Growth Factor β
TGFBR1	Transforming Growth Factor β Receptor 1
TGFBR1-CA	Constitutively Activated TGFBR1
PcG	Polycomb Group
H3K27me3	Trimethylation of Lysine 27 of Histone H3
TCGA	The Cancer Genome Atlas
POLE	DNA Polymerase Epsilon Catalytic Subunit
ProMisE	Proactive Molecular Risk Classifier for Endometrial Cancer
TNM Stage	Tumor, Nodes, and Metastases Stage
mT/mG	Membrane-localized tdTomato / Membrane-targeted EGFP
H.E.	Hematoxylin and Eosin
PAS staining	Periodic Acid Schiff Staining
ELISA	Enzyme-Linked Immunosorbent Assay
PCR	Polymerase Chain Reaction
qRT-PCR	Quantitative Reverse Transcription -PCR
HPRT	Phosphoribosyltransferase
IHC	Immunohistochemistry
IF	Immunofluorescence
ACTB	β -Actin

RPL19	Ribosomal Protein L19
AMH	Anti-Mullerian Hormone
AMHR2	Anti-Mullerian Hormone Receptor Type 2

TABLE OF CONTENTS

	Page
ABSTRACT.....	ii
ACKNOWLEDGEMENTS.....	iv
CONTRIBUTORS AND FUNDING SOURCES	v
NOMENCLATURE	viii
TABLE OF CONTENTS.....	x
LIST OF FIGURES	xi
LIST OF TABLES.....	xiii
INTRODUCTION	1
1 Polycomb repressive complex and uterine function and disease.....	1
2 Transforming growth factor β signaling and testicular granulosa cell tumors	8
3 Rationale and significance	20
AIM 1. EZH2 IS REQUIRED FOR UTERINE EPITHELIAL INTEGRITY	23
1 Material and methods.....	23
2 Results.....	28
3 Discussion	42
AIM 2. EZH2 AND ENDOMETRIAL CANCER DEVELOPMENT: INSIGHTS FROM A MOUSE MODEL	47
1 Material and methods.....	47
2 Results.....	52
3 Discussion	65
AIM 3. A NOVEL MOUSE MODEL OF TESTICULAR GRANULOSA CELL TUMORS	71
1 Material and methods.....	71
2 Results.....	75
3 Discussion	92
SUMMARY	97

REFERENCES	99
APPENDIX A.....	128

LIST OF FIGURES

FIGURE		Page
1	EZH2 and gene regulation	1
2	The canonical functions of PRC1 and PRC2 groups	3
3	Proposed genetic labeling to trace TGCT origin in TGFBR1-CA mice.....	19
4	Key regulators of TGCT development	20
5	Conditional deletion of <i>Ezh2</i> in the mouse uterus	29
6	Ablation of EZH2 results in focal formation of stratified uterine epithelium	31
7	Epithelial stratification and endometrial hyperplasia in aged <i>Ezh2</i> cKO mice	33
8	Dysregulation of forkhead box A2 (FOXA2) in the uteri of <i>Ezh2</i> cKO mice.....	35
9	Minimal forkhead box A2 (FOXA2) expression in cytokeratin 14 (KRT14)-positive cells	36
10	Ablation of EZH2 produces basal-like cell types with up-regulation of basal cell makers	38
11	Reproductive defects in <i>Ezh2</i> cKO mice	39
12	Generation of mice with conditional deletion of <i>Pten</i> and <i>Ezh2</i> in the uterus	54
13	Reduced Ki67 index in the uteri of <i>Pten</i> ^{d/d} ; <i>Ezh2</i> ^{d/d} mice compared with <i>Pten</i> ^{d/d} mice	56
14	Deletion of <i>Ezh2</i> promotes accumulation of intraluminal neutrophils in PTEN inactivated uteri.....	58
15	Deletion of <i>Ezh2</i> in PTEN-inactivated uteri causes heightened inflammation.....	59
16	Analysis of ELA2 and TNF α levels using ELISA.....	60

17	Deletion of <i>Ezh2</i> intensifies epithelial stratification in PTEN-depleted uteri.....	62
18	Reduced hypoxia in the uteri of <i>Pten^{d/d}; Ezh2^{d/d}</i> mice compared with <i>Pten^{d/d}</i> mice .	63
19	Expression of PGR in <i>Pten^{d/d}</i> and <i>Pten^{d/d}; Ezh2^{d/d}</i> uteri.....	64
20	Constitutive activation of TGFBR1 in mouse testes	77
21	Sustained activation of TGFBR1 in the testis leads to sex cord-stromal tumor formation	79
22	Depletion of germ cells and alteration of cell proliferation in the testes of TGFBR1- CA ^{Acre} males	82
23	Immunofluorescence analysis of testicular tumor development in TGFBR1-CA ^{Acre} males	84
24	Testicular tumors of TGFBR1-CA ^{Acre} males express granulosa cell tumor markers	86
25	Immunofluorescence analysis of DMRT1 and FOXL2 distribution during testicular tumor development	88
26	Analysis of Sertoli cell and Leydig cell markers in tumors from TGFBR1-CA ^{Acre} males	90
27	WNT/CTNNB1 signaling is active in GrCTs resulting from overactivation of TGFBR1	92

LIST OF TABLES

TABLE		Page
1	EZH2 and the endometrial carcinoma	6
2	Mouse models used in endometrial cancer studies	8
3	Differences between the TGCT subtypes	12
4	Information of primary antibodies (Aim 1)	25
5	Real-time RT-PCR primers.....	26
6	Information of primary antibodies (Aim2)	49
7	Primary antibodies for immunostaining and western blotting analyses (Aim 3).....	73

INTRODUCTION

1 Polycomb repressive complex and uterine function and disease

1.1 Polycomb repressive complexes

EZH2 is a well-established histone methyltransferase, catalyzing the trimethylation of lysine 27 of histone H3 (H3K27) [1] or functionally interacting with DNA methyltransferases (Fig. 1) [2].

EZH2 regulates a wide spectrum of physiological and pathological events including, but not limited to, cell differentiation, germline development, X-chromosome inactivation, stem cell pluripotency, cell-cycle progression, DNA repair, and cancer development [3-6].

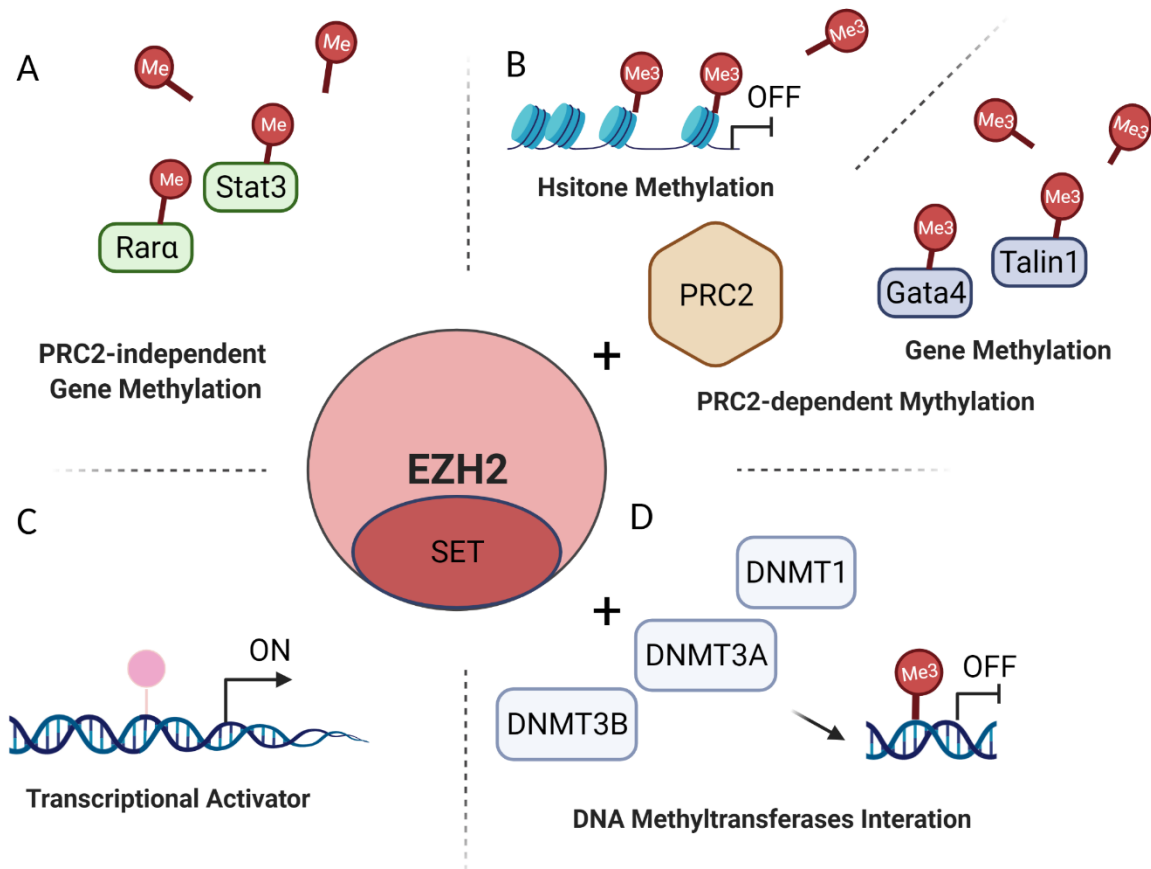


Figure 1. EZH2 and gene regulation. (A) EZH2 can methylate genes independent from PRC2 group. (B) EZH2, as the core component of PRC2 group, represses gene expression by catalyzing trimethylation on the histone or genes. (C) EZH2 can activate gene expression as a transcriptional factor. (D) EZH2 interacts with DNA methyltransferases to repress gene expression. The model was adapted from Refs [7, 8].

Polycomb Group (PcG) proteins are conserved epigenetic regulators of gene silencing and cell fate determination and maintenance [9]. Two major PcG complexes have been characterized in mammals, including Polycomb Repressive Complex (PRC) 1 and PRC2 [1].

The PRC1 consists of the catalytic core, ring finger protein (RING) 1A/B, one of Polycomb group RING finger (PCGF) proteins (PCGF1/2/3/4/5/6), and chromobox (CBX) and PHC subunits [10] (Fig. 2A). The PRC1 complexes can be categorized into six groups (PRC1.1-PRC1.6) based on the combination of RING1A/B with different PCGF proteins [11]. The different PRC1 complexes have different functions [11, 12]. The traditional function of PRC1 complexes is to repress gene expression mainly by inducing histone H2A at lysine 119 (H2AK119ub1) monoubiquitylation [13]. The PRC1 complexes also interact with PRC2 group to repress gene expression in different ways [14, 15]. It was reported that the CBX proteins of PRC1.2/4 groups lead the PRC1 complexes to PRC2 pre-occupied loci [14, 16]. Meanwhile, the Jarid2 and Aebp2 of PRC2 group can bind to H2Aub which is induced by PRC1 complexes and then mediate histone trimethylation [17]. New studies showed PRC1 complexes also activate gene expression [18-20]. Very little information is known about the PRC1 complexes in transcriptional activation [11]. It has been reported that Autism Susceptibility Candidate 2 (AUTS2) in PRC1.5 group induces gene activation by recruiting P300 [21].

PRC2 group consists of four core components in mammals [22] including EZH1/2, SUZ12 polycomb repressive complex 2 subunit (SUZ12), embryonic ectoderm development (EED), chromatin remodeling factor (RBBP4/7), and other protein including RB binding protein 4,

jumonji and AT-rich interaction domain containing 2 (JARID2) and AE binding protein 2 (AEBP2), PHD finger protein (PCL) 1-3, elongin BC and polycomb repressive complex 2 associated protein (EPOP/C17orf96), and ligand dependent nuclear receptor corepressor (LCOR/C10orf12) (Fig. 2B) [23, 24]. Similar to the PRC1 complexes, different combinations of PRC2 group catalyze mono-methylation, di-methylation, and tri-methylation of lysine 27 on Histone H3 (H3K27me_{1/2/3}) to regulate gene expression [25, 26]. The inhibition of EZH2 represses the levels of H3K27me_{1/2/3} differently [26]. SUZ12, independent from EZH2 and EED, controls H3K27 methylation patterns by binding to CpG islands [26].

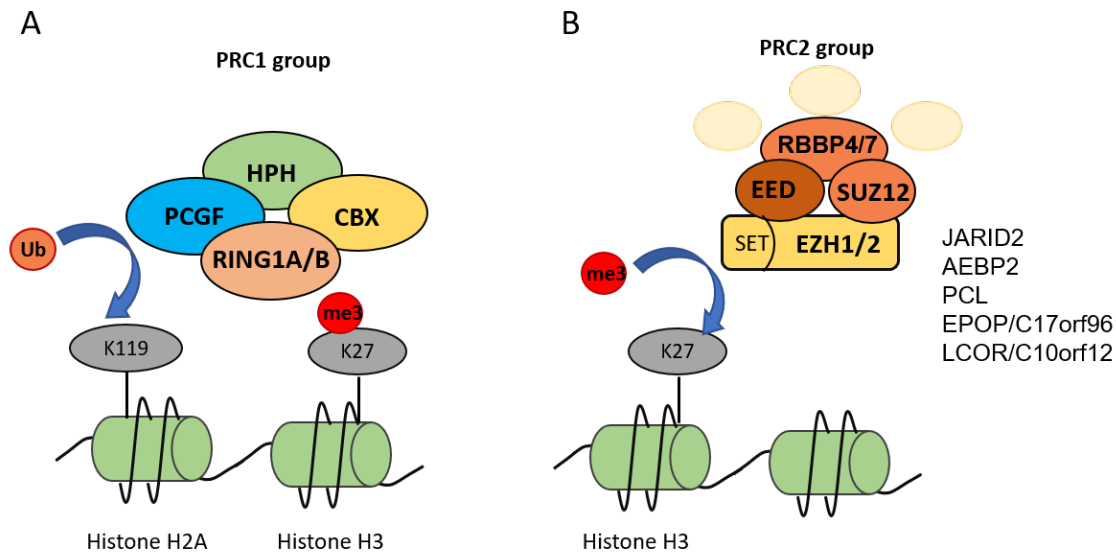


Figure 2. The canonical functions of PRC1 and PRC2 groups. (A) Canonical PRC1 complexes were composed of RING1A/B, PCGF proteins, one of CBX proteins and one of HPH proteins. CBX proteins recognize H3K27me₃ deposited by PRC2. Canonical PRC1 catalyzes monoubiquitylation on histone H2A at lysine 119 (H2AK119ub1). (B) The PRC2 complex consists of four core proteins including SUZ12, EZH1/2, EED and RBBP4/7 in mammals. EZH2 is the methyltransferase responsible for methylation of lysine 27 of histone H3, and this methylation activity resides in the SET domain. Interaction with other proteins in the complex is required for EZH2 activity.

Among the PRC2 core proteins, EZH1 and EZH2 are the functional enzymatic components that contain the SET domain [27]. PRC2-EZH1 and PRC2-EZH2 can both catalyze methylation on

H3K27. Although EZH1 has some functional redundancy with EZH2 by sharing part of target genes, the mechanism of gene repression by EZH1 may differ from EZH2 [27]. For example, the PRC2-EZH1 regulates chromatin compaction independent from SAM, the methyltransferase cofactor [27]. In addition, knockdown of *Ezh1* does not affect the global level of H3K27me_{2/3}, while deletion of *Ezh2* can induce a great reduction of H3K27me_{2/3} in NIH-3T3 cells [27].

1.2. EZH2 and uterine function

The endometrium of the uterus comprises both luminal and glandular epithelia, the integrity of which is critical for uterine function. In mice, the proliferation of luminal epithelium is reduced prior to blastocyst implantation; and high proliferative activity of luminal epithelium resulting from imbalanced hormonal signaling prevents blastocyst implantation [28]. Enhanced uterine epithelial proliferation has also been linked to endometrial hyperplasia, a pre-malignant condition of endometrial cancer [29]. It was shown that uterine epithelial stratification arising from ablation of fibroblast growth factor receptor 2 (FGFR2) causes pregnancy complications [30]. The murine endometrium contains slightly coiled glands which are formed postnatally [31]. Uterine glands play an indispensable role in mice during pregnancy via producing secretory substances that regulate uterine receptivity and decidualization [32, 33]. The requirement of uterine glands in pregnancy was also demonstrated by using the ovine uterine gland knockout model [34]. Furthermore, the importance of uterine gland secretions in mouse pregnancy was shown by studies using uterine-specific knockout mice of forkhead box A2 (*Foxa2*), in which the production of leukemia inhibitory factor essential for implantation is impaired [35].

Evidence supports a link between altered expression of EZH2 and in vitro decidualization of human endometrial cells [36], environmental estrogen exposure [37], uterine fibroids [4], endometriosis [38], and endometrial cancer development [39]. However, the role of EZH2 in normal uterine epithelial cells remains undefined.

1.3 EZH2 and endometrial cancer

Endometrial cancer is the most common cancer in the genital tract in women, with approximately 65,570 new cases and 12,940 deaths each year in the United States [40].

Endometrial cancer is classified into two distinct types [41]. The type I cancer represents the major type (~90%) and is often accompanied by endometrial hyperplasia [41, 42]. The type II cancer accounts for ~10% of the total cases and is more aggressive than the type I cancer [41-44]. Histologically, the type I cancer is endometrioid carcinoma while the type II cancer consists of several subtypes, including serous carcinoma and clear-cell carcinoma [45]. Notably, the type I, but not the type II, endometrial cancer is related to estrogen stimulation [46]. Using molecular sequencing technologies, endometrial cancer has been classified into the following types by The Cancer Genome Atlas (TCGA) Research Network: DNA polymerase epsilon catalytic subunit (POLE) (ultramutated), microsatellite-instability (MSI) (hypermuted), copy-number low, as well as copy-number high [47]. To facilitate the classification in clinical practice, the Proactive Molecular Risk Classifier for Endometrial Cancer (ProMisE) has been developed and validated, with the inclusion of immunohistochemical analysis of DNA mismatch repair (MMR) protein and tumor protein p53 (TP53) [48-50]. Interestingly, a recent report shows that a combination of tumor-infiltrating lymphocytes pattern and MMR may be used as a surrogate for the POLE

mutation group [51]. ProMisE has been used in molecular diagnosis of human endometrial cancer [52].

High expression levels of EZH2 in endometrial cancer tissue are correlated with the histological grade, invasion status, lymphatic metastasis and tumor, nodes, and metastases (TNM) stage (Table 1) [53]. Repression of *EZH2* in the endometrial carcinoma cells, such as RL-952 cells and Ishikawa cells, significantly reduces cell invasion [53-55]. Genome-wide analysis revealed reduced expression of tumor growth associated genes including peroxiredoxin 6 (PRDX6) induced by *EZH2* silencing in endometrial cancer and ovarian cell lines (i.e., Hec-1A and SKOV3-ip1) [55]. However, the role of *Ezh2* in endometrial cancer development remains incompletely understood.

Table 1. EZH2 and the endometrial carcinoma

Species	EC tissue or cell lines	EZH2 expression	Role in cancer development	Ref
Human	Low grade endometrioid and clear cell uterine carcinoma	Overexpression	<i>EZH2</i> inhibits the proliferation of ARID1A-mutated tumors	[56, 57]
	Hyperplasia, atypical hyperplasia, and EC	Overexpression	Upregulation of <i>EZH2</i> is correlated with myometrial invasion and lymph-vascular space invasion	[58]
	endometrial carcinoma (EC)	Overexpressed in 141 (69.8%) type I tumors and 63% of type II tumors	Upregulation of <i>EZH2</i> is correlated with histologic grade, angiolymphatic invasion, lymph node metastasis, myometrial invasion, and cervical involvement	[59]

Table 1. Continued

Species	EC tissue or cell lines	EZH2 expression	Role in cancer development	Ref
	EC	Overexpression	Correlation with disease-free and overall survival of patients	[55]
	EC	Overexpression	Correlation with the histological grade, depth of tumor invasion, lymph node metastasis and TNM stage (P<0.05).	[53]
	EC	Overexpression	Correlation with poor prognosis of EC	[60]
Cells	HEC-1-A and Ishikawa	Knockdown	Reduced cell proliferation	[58]
	RL95-2	Knockdown	Reduced proliferation and invasion	[53]
	SPAC-1-L and Ishikawa	Knockdown	Suppressed cell proliferation and invasion in vitro, and decreased tumor size and weight in EC cells in xenografted mice	[54]
	ECC-1, RL95-2, and HEC-1-A	Knockdown	Decreased cell proliferation, migration and invasion. Increased cells arrested in G2/M	[61]
	HEC-1-A and Ishikawa	Knockdown	Decreased angiogenesis and cell proliferation, and enhanced apoptosis	[55]
	ISK (well-differentiated), and KLE	Inhibition	Inhibited cell proliferation and upregulation of p21 and TCF3	[60]

Significant challenges remain for endometrial cancer treatment. Determining the histological subtype of endometrial cancer is an effective strategy that guides cancer treatment, with an emerging need to incorporate more molecular details into clinical interventions [62]. While surgery remains to be the most common option to treat this gynecological malignancy, new therapeutic strategies targeting actionable mutations and/or molecular pathways are potentially

valuable [63, 64]. Of particular importance, knowledge gaps need to be filled in areas of early cancer diagnostics, cancer risk stratification, and molecular identity-based treatment options [62]. Below lists several mouse models used to study endometrial cancer (Table 2).

Table 2. Mouse models used in endometrial cancer studies

Mouse model	Endometrial cancer studies	Ref
<i>Mig-6</i> ablation mouse	Endometrial hyperplasia and E2-dependent EC	[65]
<i>Pgr^{cre/+}Pten^{fl/fl}Kras^{G12D}</i>	Immune system and microenvironment in hematogenous metastatic EC	[66]
<i>BAC-Sprp2f-Cre⁺LSL-Pole^{P286R/+}</i> and <i>BAC-Sprp2f-Cre⁺LSL-Pole^{P286R/+}Msh2^{L/L}</i>	Immune response driven by <i>POLE</i> -activated EC	[67]
<i>Sprp2f-Cre; Lkb1^{L/L}</i>	<i>Lkb1</i> deletion induced invasive EC by regulating mTOR signaling	[68]
<i>Ksp1.3-Cre; Trp53fl/fl</i>	P53 suppresses type II endometrial cancer	[69]
<i>Pten^{d/d}</i>	Neutrophils combat endometrial cancer development	[70]
<i>Pten^{d/d}; Tgfbr1^{d/d}</i>	Metastatic EC and TGFβ signaling	[71]
<i>cyclin D1^{FL/WT CreER}</i>	<i>Cyclin D1</i> T286A mutation and EC development with inflammation	[72]

2. Transforming growth factor β signaling and testicular granulosa cell tumors*

2.1 Background

Granulosa cell tumors (GCTs) comprise granulosa cells and stromal components [73]. GCTs are generally low-grade malignancies, manifested by indolent growth and a low risk of metastasis [73]. However, the prognosis of GCTs is stage-dependent, and patients at advanced tumor stages tend to have higher recurrence [74], making long-term surveillance necessary. The recurrence

* Reprinted in a modified form with permission from “New insights into testicular granulosa cell tumors” by Fang X, Li Q. *Oncol Lett.* 2020;20(6):293.

also increases the mortality rate and the economic/emotional burden of the patients. Thus, it is critical to understand the molecular mechanism of GCT development and identify predictors for tumor recurrence and optimal regimen for tumor treatment.

Ovarian GCTs account for 3-5% of all ovarian tumors and are the major type of malignant sex cord-stromal tumors (~70%) [75]. There are two subtypes of ovarian GCTs, namely the adult type and the juvenile type [76]. It has been reported that >80% of girls <8 years of age with juvenile-type GCTs demonstrate precocious pseudopuberty [77]. By contrast, adult-type GCTs often occur in perimenopausal women, with an unpredictable outcome of relapse. The development of adult-type GCTs is often accompanied by symptoms of hormone dysregulation (e.g., amenorrhea, uterine bleeding and endometrial hyperplasia) [78, 79]. The clinical symptoms, diagnostic imaging, histology of surgery-obtained tumor samples and presence of tumor markers [(e.g., inhibins and anti-Mullerian hormone (AMH))] provide useful information for the diagnosis of GCTs [80, 81].

GCTs can also occur in the testis. Similar to ovarian GCTs, testicular GCTs (TGCTs) contain the adult and the juvenile subtypes. While ovarian GCTs account for ~90% of ovarian sex cord-stromal tumors (reported in 2012) [76], the adult or juvenile type of TGCTs accounts for <0.5% of testicular sex cord-stromal tumors (reported in 2017) [82]. Although similarities exist between GCTs in the testis and the ovary, mechanisms underlying the development of these tumors remain poorly characterized, partially owing to the rarity of this type of testicular malignancy. In the present review, the subtypes and pathology of TGCTs and important signaling pathways associated with tumorigenesis are discussed. The study delves into forkhead box L2 (FOXL2)-

related signaling, wntless-related MMTV integration site (WNT)/ β -Catenin (CTNNB1) signaling, the phosphoinositide 3-kinase (PI3K) pathway and the transforming growth factor β (TGF β) pathway in the development of TGCTs. With the development of new mouse models that focus on TGCTs, it is anticipated that the pace of investigation into the molecular and genetic basis of these tumors will be accelerated.

2.2 Tumors in the testes

Testicular tumors occur mostly in males of 14-44 years old [83]. Based on the 2016 classification by the World Health Organization, testicular tumors contain seven different subtypes, including but not limited to, germ cell tumors of two groups and sex cord-stromal tumors [84]. Germ cell tumors account for the majority of testicular tumors. Sex cord-stromal tumors make up 4% of tumors in the testis [85] and consist of Leydig cell tumors, Sertoli cell tumors, GCTs, fibroma and thecoma group tumors, mixed-type tumors and unclassified tumors [84]. Leydig cell tumors are the most common type of sex cord-stromal tumors. These tumors are often well circumscribed and appear brown, yellow or gray-white in color on the cut surface [86]. The cell types in a given Leydig cell tumor may be variable. Histologically, the cells are often medium to large in size and polygonal in shape, with eosinophilic granular cytoplasm [86, 87]. Due to the histological and immunohistochemical similarities between GCTs in females and males [88, 89], a comparative approach is likely to be valuable in gaining mechanistic insights into tumorigenesis and discovering common regulatory pathways. As the causes and pathogenesis of these rare testicular tumors are poorly defined, clinically relevant mouse models are particularly useful in this research field to determine the oncogenic insult and potential therapeutic targets [89-91].

2.3 TGCTs: subtypes and histopathology

TGCTs can be divided into the juvenile type and the adult type (Table 3). Juvenile-type TGCT is a more common form compared with adult-type TGCT. The juvenile type represents the most common tumors in the male gonad in patients <6 months of age and can even be diagnosed shortly after birth due to the increased size of the testis [92]. Histologically, follicular components are present in juvenile-type TGCTs [82, 92]. Tumor cells have round dense nuclei with infrequent nuclear grooves, and abundant mitosis can be found [93]. The juvenile-type tumors are generally benign, with rarely observed metastasis. In a report of 70 cases, only 2 cases showed lymphovascular invasion and 4 cases exhibited rete testis invasion [93]. The juvenile-type TGCTs were reported to be positively stained for FOXL2, steroidogenic factor-1 and vimentin [93]. Some tumors also express inhibin, calretinin, Wilms tumor 1 and SRY-box transcription factor 9 (SOX9) [93]. As inhibin is expressed by both granulosa cells and Sertoli cells, it is unclear whether the variable expression of the inhibin observed in juvenile TGCTs is stage-dependent or merely reflects the individual variation of these tumors.

Some studies have suggested that the formation of granulosa cell tumors is associated with sex chromosome abnormalities and aberrant gonadal development [94, 95]. It has been shown that infants with mixed gonadal dysgenesis or intersexual disorder develop juvenile-type GCTs [95]. Another example of this link was found in the case of a newborn baby with the X/XY karyotype who developed congenital juvenile-type TGCT [94]. The levels of inhibin B, β -hCG and testosterone appear normal in some juvenile-type GCT patients [92]. High levels of serum α -fetoprotein (AFP) are observed in some juvenile-type TGCTs [92, 93]; however, AFP levels are physiologically high in infants and newborns [96].

Table 3. Differences between the TGCT subtypes.

TGCT-related factors/features	Juvenile-type TGCTs	Adult-type TGCTs	(Ref.)
Age	Most common tumors in the testis at <6 months of age	Median age, 44 years (range, 12-87 years)	[82, 97]
Metastasis	Rare	Metastatic potential	[93, 98]
Macroscopic feature	Yellow to tan-white cut surface; cystic or solid structures	Yellow-tan cut surface; solid and/or cystic structures	[82, 93]
Microscopic feature	Round dense nuclei; infrequent nuclear grooves; abundant mitosis	Vague cell borders; pale nuclei with nuclear grooves; Call-Exner bodies	[82, 93, 99]
Genomics/genetics	Abnormal sex chromosome and gonadal development	Some tumors contain the <i>FOXL2</i> mutation	[94, 95, 100]

Adult-type TGCTs are extremely rare, with 91 cases described to date [97]. Microscopically, the tumor cells have vague cell borders and pale nuclei containing nuclear grooves [82, 99]. The tumor cells are less mitotic compared with those of juvenile-type GCTs [82]. It is notable that juvenile-type TGCTs lack Call-Exner bodies (i.e., small eosinophilic fluid-filled spaces within microfollicular structures) that are observed in the adult-type TGCTs [82]. Although most adult-type TGCTs are benign, the metastatic potential of these tumors remains of concern. For instance, in a previous study, one patient was found to develop metastases 10 years after the first diagnosis, while additional metastasis was found in the inguinal lymph node of another patient 1 year after the diagnosis and detection of retroperitoneal lymph node metastasis [98]. In another

case, metastasis was found in the bone of a patient 6 years after orchidectomy surgery [101]. Thus, long-term follow-up/monitoring is needed for patients with TGCTs. Histopathologically, the adult-type GCTs are identified as solid and/or cystic tumors [82]. Laterality has been reported in most documented adult-type GCT cases in males [97]. The histological/pathological criteria or clinical features that predict the malignant/benign disposition of TGCTs are not well defined. It appears that tumor size (> 5 cm), but not mitotic count, tumor necrosis or other parameters, is positively associated with the malignancy of adult-type TGCTs [102]. Orchidectomy and testis-sparing surgery have been used to treat TGCTs [97]. Currently, it remains unclear with regard to the genetic or molecular determinants that contribute to the phenotypic and prognostic outcomes of the juvenile-type versus the adult-type TGCTs. Answering this question may help develop tailored treatment options for the two subtypes of TGCTs.

2.4 *FOXL2* mutation in GCT development

FOXL2, a granulosa cell-expressed gene, regulates granulosa cell fate and ovarian function [103]. Supporting a critical role of *Foxl2* as a female gene, disruption of *FOXL2* in adult ovaries induces the expression of *SOX9* specific to the male gonad [104]. *FOXL2* is expressed in juvenile-type TGCTs [105]. Notably, the expression of *SOX9* is found in the cytoplasm of *FOXL2*-positive cells in some juvenile-type TGCTs [105]. As *FOXL2* is a granulosa cell lineage marker, this finding suggests potential Sertoli cell-granulosa cell transdifferentiation during the formation of TGCTs [105].

A missense mutation of *FOXL2* [nt. 402C>G (C134W)] is vital in the pathogenesis of adult-type ovarian GCTs [106]. With regard to its contribution to GCT development, studies have shown that this mutation impairs the capability of growth differentiation factor 9, an oocyte-produced protein, in promoting follistatin transcription in the presence of SMAD3 [107]. This may lead to increased cell proliferation due to unopposed activin signaling [107, 108]. In addition, *FOXL2* mutation also reduces apoptosis and increases the induction of aromatase (CYP19), which promotes estrogen synthesis [109-111]. Lima et al [100] identified a *FOXL2* mutation in adult-type TGCTs, with a lower mutation frequency compared with that in ovarian GCTs. However, this mutation was not found by the same researchers in other testicular tumors such as juvenile-type TGCTs and Sertoli-Leydig cell tumors, likely due to the limited number of cases examined and/or the low mutation frequency or lack of mutation in those tumors [100]. Thus, mutational analysis of *FOXL2* may prove beneficial in the differential diagnosis of the two subtypes of TGCTs if they demonstrate a different profile of *FOXL2* mutation. Moreover, in-depth understanding of the potential pathogenic function of the *FOXL2* mutation in TGCTs will be instrumental for developing tailored treatment modalities.

2.5 Genetically modified mouse models to study TGCTs

Elegant reviews on molecular pathogenesis, signaling pathways and mouse models of ovarian GCTs have been published [76, 112, 113]. The present review focuses on mouse models that have been reported to develop testicular tumors with a sex cord-stromal origin. Compared with mouse models for ovarian GCTs, there are only a limited number of genetically engineered mouse models that are known to develop testicular sex cord-stromal tumors. Inhibins and activins are key regulators of ovarian development and function. In the ovary, inhibins are

mainly synthesized by granulosa cells and negatively regulate the secretion of follicle-stimulating hormone (FSH) [114]. In the male gonad, Sertoli cells produce inhibins that regulate the testicular function [115]. Inhibin α (*Inha*)-knockout mice develop sex cord-stromal tumors in both sexes [116]. The neoplasms are mixed or incompletely differentiated tumors, accompanied by increased serum FSH levels [116]. Deletion of both *Inha* and gonadotropin-releasing hormone inhibits tumor development and reduces the levels of FSH and luteinizing hormone [117]. CDKN1B (also known as p27) is a cyclin-dependent kinase inhibitor that suppresses G1 phase progression. Compound deletion of *Cdkn1b* and *Inha* accelerates the development of testicular tumors in males compared with deletion of *Inha* alone [118]. Deletion of another regulator of the G1/S transition, *cyclin D2*, inhibits tumor progression in *Inha* null mice [119]. Loss of inhibins potentiates the activin signaling. It has been found that SMAD3 acts as an essential mediator of the unopposed activin signaling in testicular tumor development induced by *Inha* deletion [120]. A sexually dimorphic function has been observed for SMAD3 in gonadal tumor development induced by the loss of inhibins, where depletion of SMAD3 has a more pronounced protective effect on tumorigenesis in the male compared with that in the female [120].

WNT/CTNNB1 and PI3K/AKT signaling pathways play important roles in regulating the development of multiple types of cancer [121-124]. In the female, dysregulation of CTNNB1 signaling triggers the formation of ovarian GCTs [122]. Male mice bearing conditional expression of a stable CTNNB1 mutant and deletion of phosphatase and tensin homolog (*Pten*) using AMH type 2 receptor (*Amhr2*)-Cyclization recombinase/ causes recombination (Cre) develop TGCTs at an early age, with lung metastases in nearly half of the mice by 4 months [90]. These tumors express *Wnt4* and FOXL2 [90]. The mechanism underlying tumor development in

this mouse model remains unclear. A loss of PTEN enhances PI3K/AKT signaling activity and promotes the phosphorylation of FOXO1A [90]; however, the role of FOXO1A in tumorigenesis awaits further elucidation. Notably, it was recently found that the conditional overactivation of CTNNB1 in mouse Sertoli cells using *Amh*-Cre through elimination of a *Ctnnb1* exon required for CTNNB1 protein degradation induces transdifferentiation of Sertoli cells into granulosa-like cells and the formation of TGCTs [125]. Mechanistically, activation of WNT signaling increases the expression of FOXL2 via the binding of CTNNB1 to the *FOXL2* promoter at the T-cell factor/lymphoid enhancer factor binding sites [125]. This finding may also partially explain how overactivation of CTNNB1 promotes the formation of a TGCT in the aforementioned mouse model containing simultaneous activation of WNT and PI3K/AKT signaling [90].

Kirsten rat sarcoma viral oncogene homolog (*Kras*) is an oncogene that encodes a small GTPase [126]. Expression of KRAS^{G12D} inhibits granulosa cell proliferation and differentiation in early ovarian follicles, but slightly enhances cell proliferation in large antral follicles, revealing follicular stage-dependent roles of the KRAS mutant [127]. The mitotic index of antral follicle was increased from approximately 0.7 in the wildtype to 1.4 in KRAS mutant mouse. Mouse models with oncogenic KRAS^{G12D} expression or PTEN ablation in conjunction with CTNNB1 overactivation using *Amhr2*-Cre or *Cyp19*-Cre have been created to determine interactions between WNT and PI3K/RAS signaling [91]. It was found that constitutive activation of KRAS or loss of PTEN promotes the development of ovarian GCTs or TGCTs in stable CTNNB1-expressing mice [91]. Consistent with the benign feature of TGCTs, metastasis was not found and the viability of mice was not compromised up to 8 months. As expected, these mice are infertile due to tumor development and impaired spermatogenesis [91].

Members of the FOX family are implicated in multiple developmental processes and diseases [128, 129]. FOXL2 and FOXO3 play key roles in ovarian development and function [129]. FOXO1 acts as a tumor suppressor through inhibiting CYP19 expression via mutant FOXL2 (C134W) and SMAD3 in the human non-luteinized granulosa HGrC1 cell line [130]. In addition, ~20% of *Foxo1/3* double conditional knockout mice in the ovary using *Amhr2-Cre* or *Cyp19-Cre* develop ovarian GCTs by 6-8 months [131]. These tumors cause increased levels of inhibins and estradiol [131]. It is yet unclear whether FOXO1/3 is involved in TGCT development.

TGF β superfamily signaling is implicated in numerous physiological and pathological processes [132]. TGF β ligands signal through membrane-associated type II and type I receptors (TGFBR2/TGFBR1) and activate receptor-regulated SMADs (R-SMADs), including SMAD2/3 (TGF β /activin-responsive SMADs) and SMAD1/5/8 [bone morphogenetic protein (BMP)-responsive SMADs]. R-SMADs then complex with SMAD4 to elicit biological responses via the regulation of gene transcription [133]. TGF β signaling plays divergent roles in cancer development [134] and is important for GCT development [133]. A study by Pangas *et al* [135] revealed a role of BMP signaling in GCT development by demonstrating that conditional deletion of *Smad1* and *Smad5* promotes the development of GCTs in the ovary, but not in the testis. Instead, Sertoli-Leydig tumors form in *Smad1/5* conditionally deleted males [135]. In a continuum of research interrogating the role of TGF β signaling in reproductive development and function, a mouse model has been generated with constitutively activated TGFBR1 (TGFBR1-CA) in the gonad [89, 136]. Both male and female TGFBR1-CA mice develop GCTs [89, 136]. The cellular origin of TGCTs remains enigmatic. In male TGFBR1-CA mice, constitutive

activation of TGFBR1 is induced by *Amhr2*-Cre, which is expressed in both Sertoli cells and Leydig cells [137-139]. Notably, Sertoli cells and granulosa cells appear to arise from the same progenitor cells [140]. Moreover, Sertoli cells with dysregulated gene expression can transdifferentiate into granulosa-like cells [125]. Thus, it is conceivable that TGCTs in TGFBR1-CA males are derived from Sertoli cells. To unambiguously define the origin of TGCTs in the TGFBR1-CA mouse model [89], it is necessary to specifically activate TGFBR1 using a Cre driver specific to Sertoli cells (Fig. 3). It is anticipated that sustained activation of TGFBR1 in Sertoli cells (TGFBR1-CASC) will induce TGCT development (Fig. 3). Future studies may use genetic labeling with a dual fluorescence reporter mouse line, membrane-targeted tdTomato (mT)/membrane-targeted EGFP (mG) [141], to elucidate tumor cell origin. In the mT/mG mouse, Cre-negative cells express tdTomato, a red fluorescent protein [141] (Fig. 3A). By contrast, Cre-positive cells are expected to express GFP that can be tracked by green fluorescence [141, 142] (Fig. 3B). Should TGCTs not occur in these mice, efforts will be undertaken to investigate how interactions between Sertoli cells and Leydig cells contribute to the formation of TGCTs in the context of TGFBR1 activation (Fig. 3B). Aim 3 of this thesis will detail the findings of TGCTs in TGFBR1-CA males.

Overall, several key genes and signaling pathways have been associated with TGCT development (Fig. 4). Although robust genetic evidence supports the phenotypic relevance of these mouse models to TGCTs, their potential utility for investigating the etiology and pathogenesis of TGCTs, as well as testing therapeutic agents, requires further evaluation.

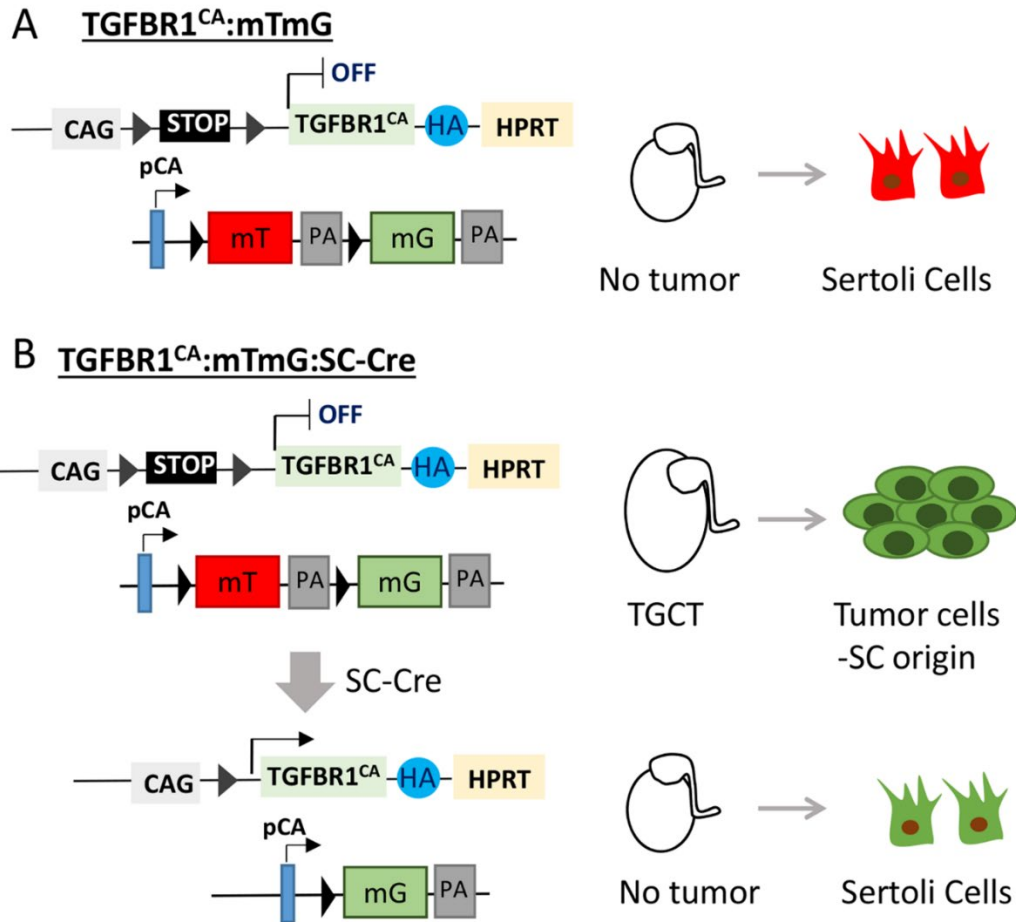


Figure 3. Proposed genetic labeling to trace TGCT origin in TGFBR1-CA mice. Mice harboring constitutively active TGFBR1 will be bred with mTmG mice and Sertoli cell-specific Cre mice. (A) Sertoli cells in the testes of control mice express tdTomato (red). (B) In the TGFBR1-CA:mTmG:SC-Cre testes, Sertoli cells express constitutively active TGFBR1 and EGFP (green). The experiment is expected to elucidate whether Sertoli cells contribute to the development of TGCTs and whether activation of TGFBR1 in Sertoli cells is sufficient to induce TGCTs. mT, membrane-targeted tdTomato; mG, membrane-targeted EGFP; PA, polyadenylation sequences; pCA, chicken β -actin promoter with CMV enhancer; CAG, human cytomegalovirus enhancer and chicken β -actin; HA, hemagglutinin; SC, Sertoli cell; TGCT, testicular granulosa cell tumor; TGFBR1, TGF- β receptor type-1; HPRT, hypoxanthine guanine phosphoribosyl transferase.

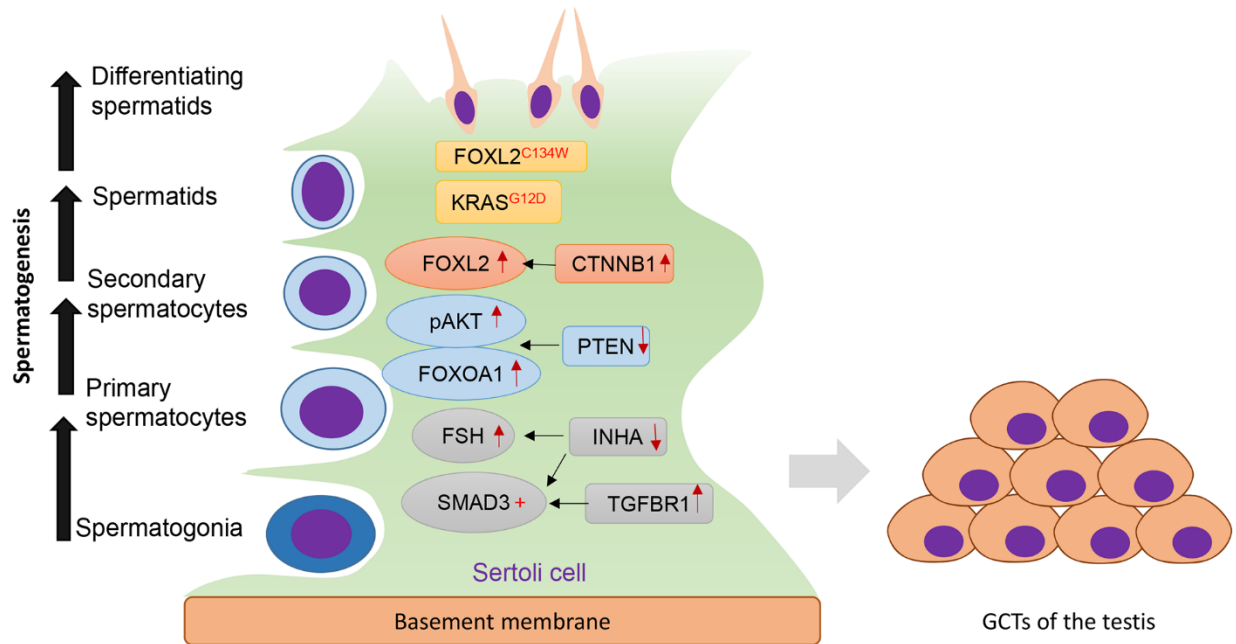


Figure 4. Key regulators of TGCT development. Sertoli cells serve an important role in maintaining normal spermatogenesis. Dysregulation of several genes/signaling pathways induces the formation of TGCTs. Increased TGF β signaling via TGFBR1 activates SMAD3, whereas ablation of INHA increases FSH levels and enhances SMAD3 signaling. Loss of PTEN promotes pAKT and FOXO1A signaling. Activation of CTNNB1 results in increased expression of FOXL2. In addition, KRAS^{G12D} and FOXL2 mutation (FOXL2^{C134W}) are also implicated in TGCT development. TGCT, testicular granulosa cell tumor; FOXL2, forkhead box L2; KRAS, Kirsten rat sarcoma viral oncogene homolog; CTNNB1, β -Catenin; PTEN, phosphatase and tensin homolog; FSH, follicle-stimulating hormone; INHA, inhibin α ; TGFBR1, TGF- β receptor type-1; p, phosphorylated.

3 Rationale and significance

The proposed studies will focus on two topics in reproduction and disease. The first topic is to determine the role of a key epigenetic regulator, EZH2, in uterine development (Aim 1) and endometrial cancer development (Aim 2). The hypothesis is that EZH2 regulates uterine epithelial integrity and endometrial cancer development. EZH2 is a core subunit of PRC2 group and plays critical roles in regulating epithelial cell properties. The structural and functional integrity of the uterine epithelium is indispensable for the normal function of the uterus, which is

a prerequisite for pregnancy success. As the role of EZH2 is poorly defined in the uterus, I will use a Cre-LoxP strategy to conditionally target *Ezh2* specifically in the epithelial and stromal compartments of the uterus. Using this mouse model, I will not only investigate the physiological role of EZH2 in uterine development and function (Aim 1), but also determine how loss of EZH2 impacts the development of endometrial cancer induced by PTEN depletion (Aim 2). In Aim 1, I will first perform histological and immunohistochemical analysis to determine the structural phenotype of the reproductive tract. Then, I will examine the pregnancy-related events including decidual development. Last, I will attempt to understand molecular changes that may affect pregnancy success. In Aim 2, I will perform histological, cellular and molecular analyze to determine the impact of *Ezh2* deletion on tumor development and progression induced by *Pten* conditional deletion. Then I will study the cell proliferation and hormone regulation during the endometrial cancer development. Last but not least, I will examine the immune cell recruitment and inflammation which may affect the progression of endometrial cancer. Knowledge gained from this study will help a better understanding of epigenetic regulation in the mouse uterus in both physiological and pathological conditions. These findings are expected to ultimately benefit the treatment of uterine dysfunction, pregnancy failure, and endometrial malignancies.

The second topic will focus on the signaling mechanisms underlying the development of granulosa cell tumors in the male gonad. TGF β superfamily signaling regulates fundamental events of reproduction and development. Unbalanced TGF β signaling can cause multiple defects in the reproductive tract [143, 144]. The research is built on our early findings of dysregulated TGF β signaling in the pathogenesis of ovarian granulosa cell tumors. Although our initial histological and immunological studies have provided evidence suggesting activated TGF β

signaling may alter the cell identity of Sertoli cells, unambiguous genetic evidence indicating the cellular origin of TGCTs is lacking. Thus, in the second part of this proposal, I will study molecular changes in the mouse testis with constitutively activative TGFBR1 and genetically trace TGCT origin using an mTmG reporter line (Aim 3). The hypothesis is that constitutive activation of TGF β signaling alters Sertoli cell identity, leading to TGCT formation. Due to the complexity of TGF β superfamily signaling, I will focus on manipulating TGFBR1, the type 1 receptor that mediates TGF β signaling. This proposal is expected to determine the mechanism underlying TGCT development and identify TGCT origin. These studies will demonstrate a key role of TGFBR1 activation in the development of gonadal tumors in both sexes. Findings will have a potential implication in the diagnosis and treatment of a rare type of tumor in the testis. Overall, completion of proposed work in this thesis will identify mechanisms underlying reproductive development and carcinogenesis, opening new doors for the treatment of pregnancy failure and cancers in the reproductive system.

Aim 1. EZH2 IS REQUIRED FOR UTERINE EPITHELIAL INTEGRITY*

1 Materials and methods

1.1 Animals and tissue collection

The animal use protocol was approved by the Texas A&M University Institutional Animal Care and Use Committee (IACUC). Animals were handled according to the animal care and use guidelines from the National Institutes of Health and Texas A&M IACUC. Mice were housed under a 12-hour light/12-hour dark cycle in the Laboratory Animal Resources and Research (LARR) facility. Animal care was provided by experienced technicians from the Comparative Medicine Program. Mice were on C57BL/6; 129SvEv background. Generation of progesterone receptor (*Pgr*)-Cre mice [145] and *Ezh2*^{flox/flox} mice [146] was described previously. The *Ezh2*^{flox/flox} mice (Stock no. 022616) were purchased from The Jackson Laboratory (Bar Harbor, ME). Vaginal smears were analyzed to confirm the cycling, and all mice utilized in this experiment had intact ovaries. Uterine epithelia were collected by a mild trypsin digestion [147], followed by mechanical separation using fine forceps under a stereo dissection microscope (Olympus, Waltham, MA). Uterine samples used for histological studies were fixed with 10% (v/v) neutral buffered formalin (Millipore Sigma, St. Louis, MO). Samples were embedded and processed using the on-campus Core Histology Laboratory of the Veterinary Integrative Biosciences Department. Hematoxylin and eosin (H.E.) staining was used to determine general histopathological features of the reproductive tract.

* Reprinted in slight modified form with permission from “Enhancer of Zeste 2 Polycomb Repressive Complex 2 Subunit Is Required for Uterine Epithelial Integrity” by Fang X, Ni N, Lydon JP, Ivanov I, Bayless KJ, Rijnkels M, and Li Q. *Am J Pathol.* 2019 ;189(6):1212-1225.

1.2 Generation of mice with uterine conditional knockout of *Ezh2*

Control (*Ezh2*^{flox/flox}; Ctrl) and *Ezh2* conditional knockout (*Ezh2*^{flox/flox}; *Pgr*^{Cre/+}; *Ezh2* cKO) mice were generated. The genotype of mice was analyzed by genomic PCR based on an established Jackson Laboratory protocol using mouse tail DNA and primers *Ezh2* flox-F (5'-CATGTGCAGCTTTCTGTTCA-3') and *Ezh2* flox-R (5'-CACAGCCTTTCTGCTCACTG-3') (WT band = 203 bp and flox band = ~300 bp). The primers used to amplify recombinant/mutant *Ezh2* band (200 bp) were 5'-CCCATGTTTAAGGGCATAGTGACATG-3' and 5'-TCGAGGGACCTAATAACTCGTATAGCA-3' [146]. Hypoxanthine guanine phosphoribosyltransferase (*Hprt*) was used as an internal control [71]. Genotyping of *Pgr*-Cre and analysis of PCR products were described elsewhere [89, 148].

1.3 Immunohistochemistry and Immunofluorescence

Immunostaining was detailed previously [89, 144]. Briefly, 5 µm paraffin sections were deparaffinized, rehydrated, and boiled in citrate buffer (pH = 6) to expose the antigen, followed by incubation with 3% H₂O₂ solution for 10 min. Inactivation of endogenous peroxidase activity was only performed for the immunohistochemical procedure. Sections were blocked before incubation with primary antibodies (Table 4) overnight at 4°C. After primary antibody incubation, the avidin-biotin complex kit (ABC; Catalog no. PK-6100; Vector Laboratories, Burlingame, CA) was used, with NovaRed (Catalog no. SK-4800; Vector Laboratories) being the developing substrate (for immunohistochemistry). Sections were mounted using mounting media (Catalog no. 17986-01; Thermo Fisher Scientific, Waltham, MA or Catalog no. 3801743; Leica Biosystems, Buffalo Grove, IL). For Immunofluorescence microscopy, sections were

mounted using medium that contains 4', 6-diamidino-2-phenylindole (DAPI), a nuclear counterstain (Catalog no. P36931; Thermo Fisher Scientific).

Table 4. Information of primary antibodies (Aim 1)

Name	Manufacture	Cat. No.	Host	IHC/IF	WB
EZH2	Cell Signaling, Danvers, MA	5246	Rabbit	1:400	1:1000
FOXA2	Abcam, Cambridge, MA	Ab108422	Rabbit	1:250	
Ki67	Abcam, Cambridge, MA	Ab16667	Rabbit	1:200	
VIM	Cell Signaling, Danvers, MA	5741	Rabbit	1:200	
ACTA2	Cell Signaling, Danvers, MA	19245	Rabbit	1:500	
KRT8	DSHB*, Iowa City, Iowa	TROMA-I	Rat	1:200	
KRT14	Thermo fisher Scientific, Waltham, MA	PA5-16722	Rabbit	1:400	
KRT14	Santa Cruz Biotechnology, Dallas, TX	SC-53253	Mouse	1:100	
KRT5	BioLegend, San Diego, CA	905501	Rabbit	1:3000	
KRT6A	BioLegend, San Diego, CA	905701	Rabbit	1:1000	
p63 (Δ N)	BioLegend, San Diego, CA	619001	Rabbit	1:500	

1.4 *Dolichos biflorus agglutinin* (DBA) lectin staining

DBA staining was performed as detailed elsewhere with slight modifications [149]. After deparaffinization and rehydration, sections were boiled in citrate buffer (pH = 6) for 20 min, blocked with 5% BSA in Tris-buffered saline (TBS) for 30 min, and incubated with fluorescein-labeled DBA (Catalog no. FL-1031; Vector Laboratories) diluted 1:100 in 1% BSA/TBS overnight at 4°C. Sections were mounted with DAPI-containing medium described above.

1.5 Western blotting

Uterine protein samples were prepared and western blotting was conducted based on our previously reported procedures [89]. Information for primary antibodies is listed in Table 4.

Chemiluminescent substrate (Catalog no. WBKLS0100; Millipore Sigma) was used for signal detection. Digital images were captured using ChemiDoc imaging system (Bio-Rad, Hercules, CA) and processed using Adobe Photoshop CS5.

1.6 Reverse transcription (RT)-quantitative PCR (qPCR)

RNA isolation and RT-qPCR were conducted as described [150]. RT was carried out using 500 ng (for uterine or decidual tissues) or 200 ng (for uterine epithelium) total RNA and superscript III reverse transcriptase (Catalog no. 18080044; Thermo Fisher Scientific). Quantitative PCR was performed in duplicates using either SYBR Green (Catalog no. 1725121; Bio-Rad) or TaqMan Mix (Catalog no. 4304437; Thermo Fisher Scientific). The sequences of gene-specific primers [30, 143, 144, 146, 148, 150-162] and information of Taqman probes are listed in Table 5. The average cycle threshold (CT) value for each gene was normalized to that of ribosomal protein L19 (*Rpl19*), and relative gene expression levels were calculated as described [163].

Table 5. Real-time RT-PCR primers

Primers used for SYBR assays			
Name		Sequence	Reference
<i>Ezh2^{del}</i>	Forward	5'-TTACTGCTGGCACCGTCTGATGTG-3'	[146]
	Reverse	5'-TGTCTGCTTCATCCTGAGAAATAATCTCC-3'	
<i>Foxa2</i>	Forward	5'-AGCAGAGCCCAACAAGA-3'	[30]
	Reverse	5'-AGAGAGAGTGGCGGATGGAG-3'	
<i>Krt8</i>	Forward	5'-TCCATCAGGGTGAAGTCAAGAA-3'	PrimerBank ID 52789a1
	Reverse	5'-CCAGCTTCAAGGGGCTCAA-3'	
<i>Krt14</i>	Forward	5'-GCTGGATGTGAAGACAAGGCTGGAG-3'	[30]
	Reverse	5'-ATTGGGAAGATGAAAGGTGG-3'	
<i>Krt17</i>	Forward	5'-TCCCAGCTCAGCATGAAAGC-3'	[151]
	Reverse	5'-CTTGTAAGTCAAGTCAAGTGGGC-3'	
<i>TAp63</i>	Forward	5'-GTGGATGAACCTTCCGAAAA-3'	[152]
	Reverse	5'-GAGGAGCCGTTCTGAATCTG-3'	
Δ <i>Np63</i>	Forward	5'-GAGCAGCCTTGACCAGTCTC-3'	[152]
	Reverse	5'-GAGGAGCCGTTCTGAATCTG-3'	

Table 5. Continued

Primers used for SYBR assays			
Name		Sequence	Reference
<i>Fgfr2</i>	Forward	5'-CCTCGATGTCGTTGAACGGTC-3'	PrimerBank ID 198594a1
	Reverse	5'CAGCATCCATCTCCGTCACA-3'	
<i>Wnt4</i>	Forward	5'-CATCGAGGAGTGCCAATACCA-3'	[153]
	Reverse	5'-GGAGGGAGTCCAGTGTGGAA-3'	
<i>Wnt7a</i>	Forward	5'-CGACTGTGGCTGCGACAAG-3'	[154]
	Reverse	5'-CTTCATGTTCTCCTCCAGGATCTTC-3'	
<i>Pten</i>	Forward	5'-ACACCGCCAAATTTAACTGC-3'	[155]
	Reverse	5'-TACACCAGTCCGTCCTTTTC-3'	
<i>Bmp2</i>	Forward	5'-GGGACCCGCTGTCTTCTAGT-3'	[143]
	Reverse	5'-TCAACTCAAATTCGCTGAGGAC-3'	
<i>Il15</i>	Forward	5'-ACATCCATCTCGTGCTACTTGT-3'	[148]
	Reverse	5'-GCCTCTGTTTTAGGGAGACCT-3'	
<i>Klrg1</i>	Forward	5'-TTTGGGGCTTTTGACTGTGAT-3'	[148]
	Reverse	5'-TGTAAGGAGATGTGAGCCTTTGT-3'	
<i>Prf1</i>	Forward	5'-TCTCCTCCTATGGCACGCAC-3'	[148]
	Reverse	5'-TGTAAGGACCGAGATGCGG-3'	
<i>Bmpr2</i>	Forward	5'-TTGGGATAGGTGAGAGTCGAAT-3'	[161]
	Reverse	5'-TGTTTCACAAGATTGATGTCCCC-3'	
<i>Tgfb1</i>	Forward	5'-TGCCATAACCGCACTGTCA-3'	[144]
	Reverse	5'-AATGAAAGGGCGATCTAGTGATG-3'	
<i>Vegfa</i>	Forward	5'-AGACAGAACAAAGCCAGAAAATCA-3'	[162]
	Reverse	5'-AATGCTTTCTCCGCTCTGAA-3'	
<i>Angpt2</i>	Forward	5'-GATCTTCCTCCAGCCCCTAC-3'	[148]
	Reverse	5'-TTTGTGCTGCTGTCTGGTTC-3'	
<i>Wnt6</i>	Forward	5'-GCGGAGACGATGTGGACTTC-3'	[156]
	Reverse	5'-ATGCACGGATATCTCCACGG-3'	
<i>Sfrp4</i>	Forward	5'-AGAAGGTCCATACAGTGGGAAG-3'	[157]
	Reverse	5'-GTTACTGCGACTGGTGCGA-3'	
<i>Dact1</i>	Forward	5'-TCAGGGTTTTATGAGCTGAGT-3'	[158]
	Reverse	5'-GAACACGGAGTTGGAGGAGTTA-3'	
<i>Mtor</i>	Forward	5'-ACCGGCACACATTTGAAGAAG-3'	PrimerBank ID 9910228a1
	Reverse	5'-CTCGTTGAGGATCAGCAAGG-3'	
<i>Ptgs2</i>	Forward	5'-TGAGCAACTATTCCAAACCAGC-3'	[159]
	Reverse	5'-GCACGTAGTCTTCGATCACTATC-3'	
<i>Hoxa10</i>	Forward	5'-CCTGCCGCGAACTCCTTTT-3'	PrimerBank ID 6680243a1
	Reverse	5'-GGCGCTTCATTACGCTTGC-3'	
<i>Fkbp3</i>	Forward	5'-TTGCCAAGACTGCTAATAAGGAC-3'	PrimerBank ID 7305061a1
	Reverse	5'-TTGGTGGACCCTCATCAAGAG-3'	
<i>Fkbp4</i>	Forward	5'-CCTCTCGAAGGAGTGGACATC-3'	PrimerBank ID 6753882a1
	Reverse	5'-TCCCCGATCATGGGTGTCT-3'	
<i>Fkbp5</i>	Forward	5'-TGAGGGCACCAGTAACAATGG-3'	PrimerBank ID 6753884a1
	Reverse	5'-CAACATCCCTTTGTAGTGGACAT-3'	
<i>Rpl19</i>	Forward	5'-ATGAGTATGCTCAGGCTACAGA-3'	[150]
	Reverse	5'-GCATTGGCGATTTTCATTGGTC-3'	
Taqman gene expression assay			
Name	ID		Manufacturer
<i>Ezh1</i>	Mm01292494_g1		Thermo Fisher Scientific

Table 5. Continued

Taqman gene expression assay		
Name	ID	Manufacturer
<i>Krt5</i>	Mm00503549_m1	Thermo Fisher Scientific
<i>Prl8a2</i>	Mm01135453_m1	Thermo Fisher Scientific
<i>Corin</i>	Mm00444120_m1	Thermo Fisher Scientific
<i>Rpl19</i>	Mm02601633_g1	Thermo Fisher Scientific

1.7 Statistical analysis

Statistical difference between two groups was examined using the unpaired two-tailed t-test.

Data are mean \pm SEM. A P value less than 0.05 denotes statistical significance ($*P < 0.05$, $**P < 0.01$, and $***P < 0.001$).

2 Results

2.1 Conditional ablation of EZH2 in the uterus

Expression of EZH2 has been reported in the glandular epithelium and stroma of the human uterus [36]. To verify the expression of EZH2 in the mouse uterus, we performed immunohistochemistry using an antibody directed to EZH2. The results showed strong immunoreactive signals of EZH2 in both luminal and glandular epithelia of the mouse uterus (Appendix A-1A-D). Lower levels of EZH2 were detected in the myometrium (Appendix A-1). Immunostaining for EZH2 in the stroma appeared to be variable during the estrous cycle (Appendix A-1).

EZH2 is involved in epithelial-mesenchymal transition (EMT) in cancer cells [164]. To determine if EZH2 is required for uterine epithelial integrity, we deleted uterine *Ezh2* using *Pgr-Cre* that is expressed in both epithelial and mesenchyme-derived cells of the uterus [145]. Figure 5A depicts the conditional allele of *Ezh2* in which exons 14 and 15 are flanked by two LoxP sites

[146]. Cre-mediated deletion of the target exons is expected to cause a frameshift mutation that eliminates the SET domain [146]. As anticipated, deletion of *Ezh2* was evidenced by the presence of a recombined *Ezh2* allele in the *Ezh2* cKO uterus (Fig. 5A and B). Consistently, real-time PCR detected a significant reduction of *Ezh2* mRNA levels in 1-month-old *Ezh2* cKO mice (Fig. 5C). Ablation of EZH2 was further examined using uteri from 2-month-old mice by Western blotting (Fig. 5D) and immunohistochemical analyses (Fig. 5E and F), which demonstrated reduced expression of EZH2 in the uteri of *Ezh2* cKO mice compared with age-matched controls. Thus, EZH2 was efficiently depleted in the uterus.

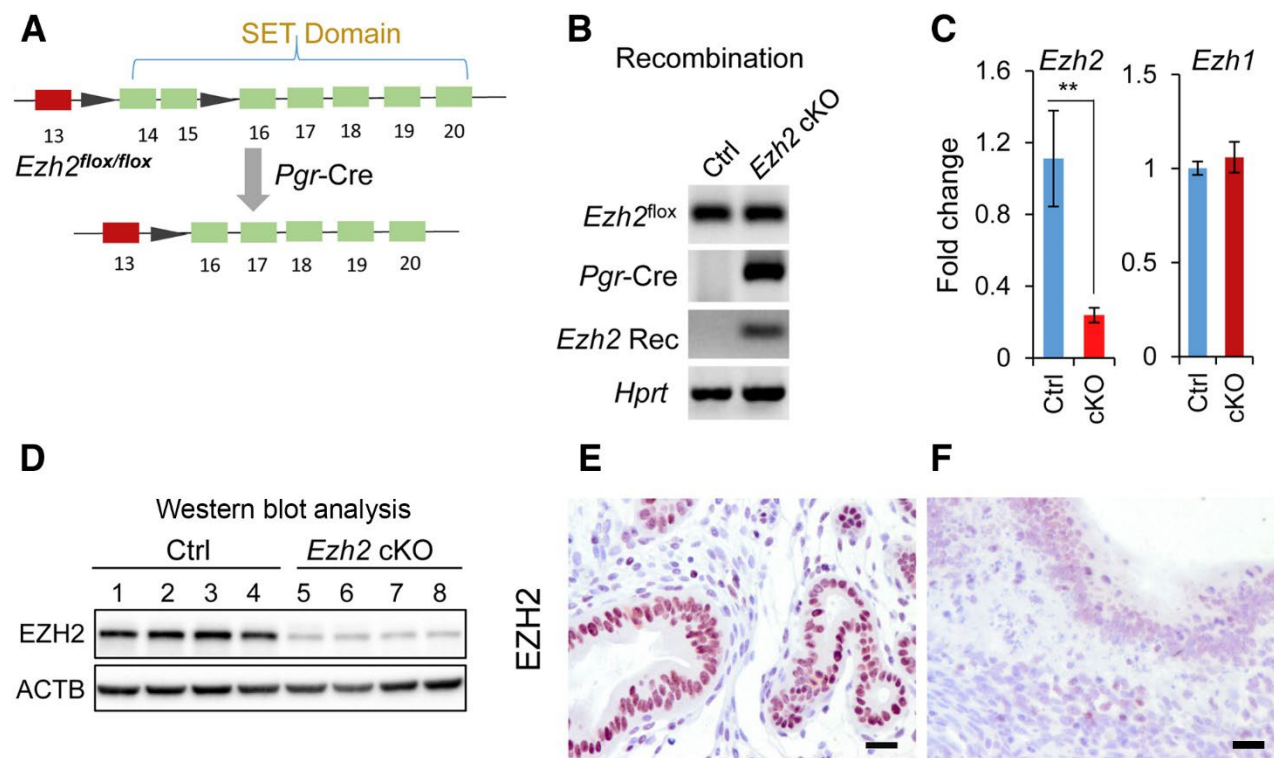


Figure 5. Conditional deletion of *Ezh2* in the mouse uterus. **A:** Schematic representation of *Pgr-Cre*-mediated inactivation of *Ezh2* floxed allele. **B:** Recombination of *Ezh2* floxed allele in *Ezh2* cKO uteri. The *Ezh2* recombined allele (*Ezh2 Rec*) was only detectable in the uterus of the *Ezh2* cKO mouse but not the control (Ctrl). **C:** Reduction of *Ezh2*, but not *Ezh1*, mRNA levels in the uteri of 1-month-old *Ezh2* cKO mice versus controls. **D:** Western blot analysis of EZH2 protein levels in control and *Ezh2* cKO mice. Each lane represents an independent uterine sample from a 2-month-old mouse. β -Actin (ACTB) was included as an internal control. **E** and **F:** Immunohistochemical staining of EZH2 in the uteri of 2-month-old

control and *Ezh2* cKO mice. Three independent samples per group were examined. Note the diminished immunoreactive signals in the epithelia of *Ezh2* cKO uteri (F) compared with controls (E). Data are expressed as means \pm SEM (C). $n = 4$ Ctrl mice (C and D); $n = 5$ cKO mice (C); $n = 4$ cKO mice (D). $**P < 0.01$. Scale bars = 20 μm (E and F).

2.2 Depletion of EZH2 leads to the formation of stratified uterine epithelium

To determine potential impact of EZH2 depletion on uterine development, we examined the morphology of the uterus at 1 month of age. The uterus was histologically normal, consisting of major structural components including the myometrium and endometrium revealed by H.E. staining (Fig. 6A-D). It is well established that cytokeratin 8 (KRT8) is expressed in simple epithelia, whereas KRT5, KRT6, and KRT14 are produced by stratified epithelia [165]. Immunostaining of KRT8 showed the presence of both luminal and glandular epithelium within the endometrium (Appendix A-2A and D). Stromal cells of both control and *Ezh2* cKO uteri expressed vimentin (VIM) (Appendix A-2B and E). The myometrium of *Ezh2* cKO mice appeared to be indistinguishable from that of controls by immunostaining of alpha smooth muscle actin (ACTA2; Appendix A-2C and F). However, further immunohistochemical analysis of the uterus using antibodies directed to basal cell markers KRT14 and transformation-related protein 63 (p63) demonstrated focal expression of these proteins beneath luminal and/or glandular epithelial cells in *Ezh2* cKO uteri (arrows; Fig. 6H-J), which is in sharp contrast to normal controls (Fig. 6E-G).

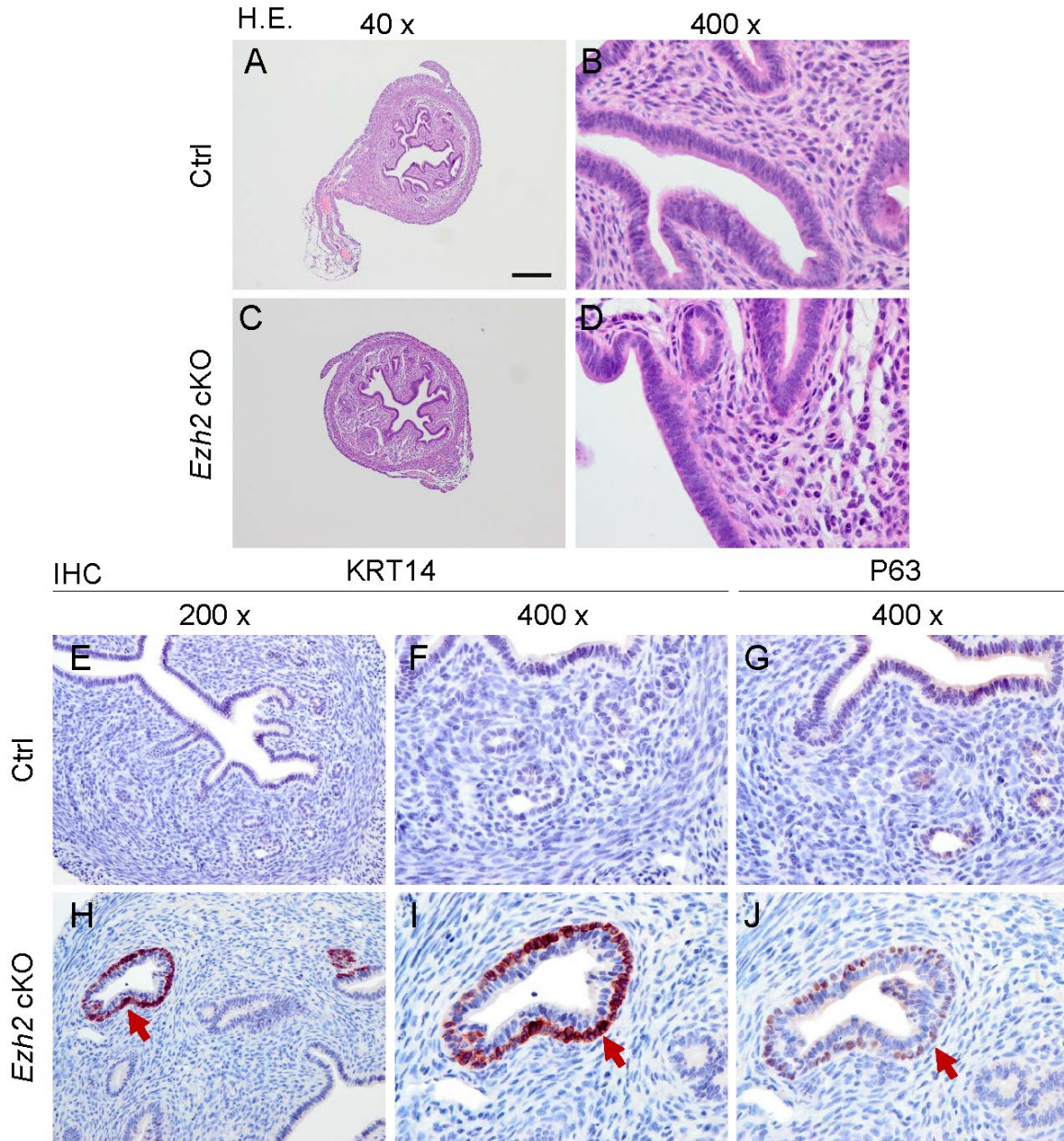


Figure 6. Ablation of EZH2 results in focal formation of stratified uterine epithelium. A–D: Hematoxylin and eosin staining of uterine samples from 1-month-old control (Ctrl) and *Ezh2* cKO mice. A–D: Higher-magnification images (B and D) for A and C, respectively. E–J: Immunostaining of cytokeratin 14 (KRT14) and tumor protein 63 (p63) using 1-month-old control and *Ezh2* cKO uteri. Note the immunoreactive signals of KRT14 beneath the epithelial layer of a uterine gland and the p63-specific signals in the same gland on an adjacent section (arrows). E, F, H, and I: Higher-magnification images (F and I) for E and H, respectively. Three independent samples per group were examined. Scale bars: 250 μ m (A and C); 25 μ m (B, D, F, G, I, and J); 50 μ m (E and H). Original magnification: \times 40 (A and C); \times 400 (B, D, F, G, I, and J); \times 200 (E and H). H&E, hematoxylin and eosin staining; IHC, immunohistochemistry.

Similar epithelial abnormalities in limited regions were found in the uteri of 2-month-old *Ezh2* cKO mice (arrows; Fig. 7A and B) compared with controls (Fig. 7C). At around 8 months of age, epithelial stratification was escalated in *Ezh2* cKO mice. The lesion was evidenced by the presence of cells positively stained for KRT14 (Fig. 7D and E), KRT5 (Fig. 7G and H), KRT6A (Fig. 7J and K), and p63 (Fig. 7M and N) in the uteri of *Ezh2* cKO mice. The development of stratified epithelia was accompanied by endometrial hyperplasia, evident in nulliparous *Ezh2* cKO mice at the age of 5-8 months (Fig. 7 and Appendix A-3). Histologically, cystic dilation of endometrial glands containing eosin-stained substance could be observed in *Ezh2* cKO uteri (Appendix A-3B and C). The morphologically altered glands were variable in size and some of them contained stratified epithelial layers (Fig. 7D, E, G, H, J, K, M, and N and Appendix A-3B and C), with nuclear atypia in some cases (Fig. 7E and H and Appendix A-3C and D). A minor level of gland crowding was observed in discrete regions of *Ezh2* cKO uteri, in which intervening stroma among glands was sparse (Appendix A-3B and D). Immunostaining of VIM that marks uterine stroma confirmed this observation (Appendix A-3E and F). Despite the pathological changes in the endometrium, the myometrial layers remained intact in *Ezh2* cKO mice (Appendix A-3B). Moreover, immunoreactive signals for Ki67 could be detected in some abnormal glands or cystic glandular structures in *Ezh2* cKO uteri (Appendix A-3G-L), supporting potentially altered cell proliferation in the development of endometrial hyperplasia [29]. Of note, the weight of uterine horns from *Ezh2* cKO mice (28.8 ± 5.6 mg, $n = 3$) was increased compared to controls (11.7 ± 1.1 mg; $n = 6$) even before sexual maturity (1 month; $P < 0.01$). Collectively, the endometrial pathology in *Ezh2* cKO mice resembled human endometrial hyperplasia [166, 167].

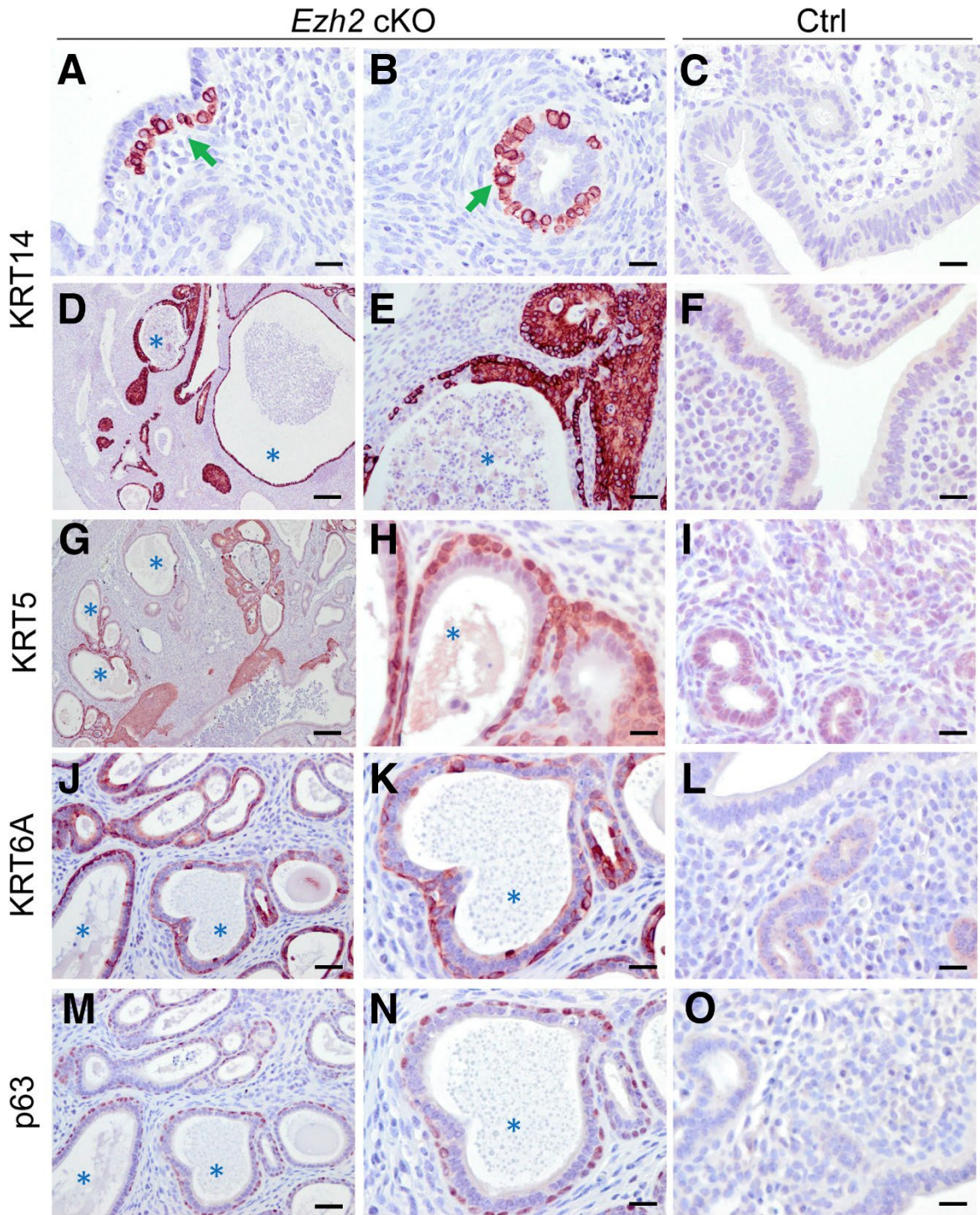


Figure 7. Epithelial stratification and endometrial hyperplasia in aged *Ezh2* cKO mice. A–F: Expression of cytokeratin 14 (KRT14) in the uteri from control (Ctrl) and *Ezh2* cKO mice at 2 (A–C) and 8 (D–F) months of age. More extensive immunoreactive signals of KRT14 were found in the uteri of 8-month-old mice (D and E) versus 2-month-old mice (A and B). Panel E shows a higher-magnification image of D. Arrows indicate KRT14-positive cells. G–O: Expression of KRT5, KRT6A, and tumor protein 63 (p63) in 8-month-old *Ezh2* cKO and control mice. G, H, J, K, M, and N: Higher-magnification images (H, K, and N) for G, J, and M,

respectively. J, K, M, and N: Adjacent sections (M and N) for J and K, respectively. At least three independent samples per group were examined. Asterisks indicate cyst-like structures. Scale bars: 20 μm (A–C, F, H, I, K, L, N, and O); 40 μm (E, J, and M); 200 μm (D and G).

To determine whether the observed epithelial abnormalities in the EZH2-ablated uterus were associated with dysregulation of genes known to regulate uterine epithelial stratification, we examined the transcript levels of *Fgfr2* [30], wingless-type MMTV integration site family member 4 (*Wnt4*) [168], *Wnt7a* [169], and phosphatase and tensin homolog (*Pten*) [170], using both uterine tissues and isolated uterine epithelia from *Ezh2* cKO mice. Significant differences were not detected in the expression of these genes in uterine tissues or epithelial preparations between control and *Ezh2* cKO mice (Appendix A-4).

2.3 Altered FOXA2 expression in EZH2-depleted uterus

A recent study has shown that altered expression of FOXA2 is associated with epithelial stratification [171]. Therefore, we determined if dysregulation of FOXA2 contributed to the formation of stratified epithelia in *Ezh2* cKO uteri. At 2 months of age, glandular epithelia were identified by FOXA2 staining in control uteri (Fig. 8A and B). However, we observed sporadic/partial loss of FOXA2 immunostaining in the glandular epithelia of *Ezh2* cKO mice (arrows; Fig. 8C-F). This result is in agreement with the finding that *Foxa2* mRNA levels were decreased in uterine epithelia of *Ezh2* cKO mice at 1 month of age (Fig. 8G). In addition, double immunofluorescence staining of KRT14 and FOXA2 showed no FOXA2 expression in KRT14-positive epithelial cells lining the luminal/glandular epithelia of *Ezh2* cKO uteri (Fig. 9B, D, and F), in contrast to controls lacking specific KRT14 staining (Fig. 9A, C, and E). Negative controls are shown in Figure 9G and H. Because FOXA2 regulates the expression of genes involved in

uterine gland development and function [172], these results suggest that conditional deletion of *Ezh2* may impair uterine function.

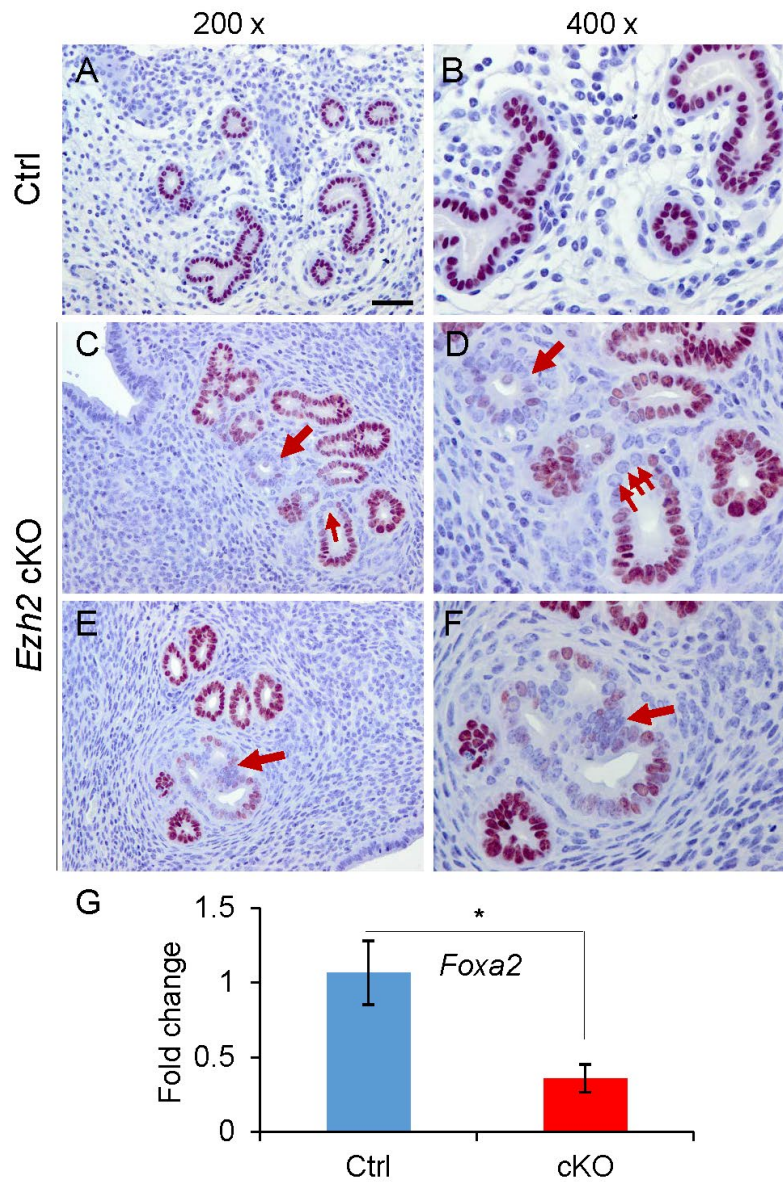


Figure 8. Dysregulation of forkhead box A2 (FOXA2) in the uteri of *Ezh2* cKO mice. A–F: Immunohistochemical analysis of FOXA2 distribution in the uteri of control (Ctrl) and *Ezh2* cKO mice at the age of 2 months. A, C, and E are shown at higher magnification in B, D, and F, respectively. Note the reduction or partial loss of FOXA2 signals in some uterine glands of *Ezh2* cKO mice versus controls (arrows). Three independent samples per group were examined. G: Real-time PCR analysis of expression of *Foxa2* mRNA in uterine epithelia isolated from control and *Ezh2* cKO mice. Data are expressed as means \pm SEM (G). $n = 4$ (G). * $P < 0.05$. Scale bars:

50 μm (A, C, and E); 25 μm (B, D, and F). Original magnification: $\times 200$ (A, C, and E); $\times 400$ (B, D, and F).

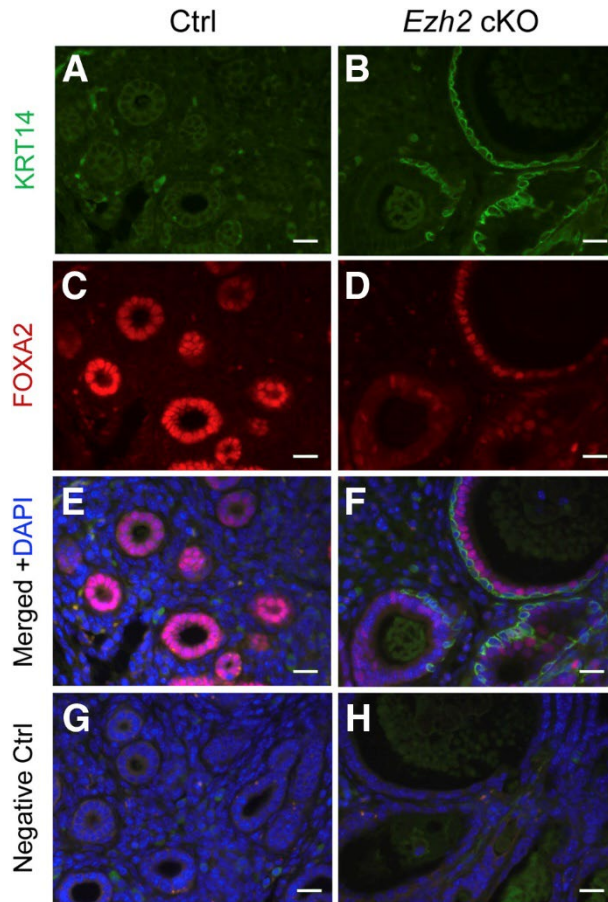


Figure 9. Minimal forkhead box A2 (FOXA2) expression in cytokeratin 14 (KRT14)-positive cells. A–F: Double-immunofluorescence staining of KRT14 and FOXA2 in the uteri of control (Ctrl; A, C, and E) and *Ezh2* cKO (B, D, and F) mice at the age of 8 months. KRT14-positive cells (green) did not express FOXA2 (red). G and H: Negative controls, using isotype-matched IgGs to replace primary antibodies, are shown. At least three independent samples per group were examined. Scale bars = 20 μm (A–H).

2.4 Conditional deletion of EZH2 in the mouse uterus gives rise to basal-like epithelial cells and upregulates genes associated with basal cell phenotype

Double indirect immunofluorescence of KRT8 and KRT14 demonstrated the presence of basal-like epithelial cells (KRT14-positive but KRT8-negative) lining some KRT8-positive epithelial cells in the uteri of *Ezh2* cKO mice (Fig. 10E–H), in contrast to the controls where epithelia were only stained for KRT8 (Fig. 10A–D). To understand the molecular underpinnings of the observed

basal-like cell phenotype, we examined whether ablation of EZH2 promoted the expression of basal cell-related genes including *Krt5*, *Krt14*, *Krt17*, and *TAp63* and $\Delta Np63$ that encode p63 isoforms using 1-month-old mice. Results showed that transcript levels of *Krt5*, *Krt14*, and *Krt17* were significantly elevated in *Ezh2* cKO uteri compared with those in age-matched controls (Fig. 10I-K). In contrast, mRNA levels of *Krt8* were not significantly altered between *Ezh2* cKO and control uteri (Fig. 10L). Interestingly, the mRNA expression of $\Delta Np63$, but not *TAp63*, was dramatically increased in the uteri of *Ezh2* cKO mice (Fig. 10M and N). A marked reduction of *Ezh2*, but not *Ezh1*, transcript levels was found in *Ezh2* cKO mice (Fig. 5C and Fig. 10O), confirming *Ezh2*-specific deletion in the uterus. To further demonstrate dysregulation of basal cell-related genes in the epithelial compartment, we isolated uterine epithelia from both control and *Ezh2* cKO uteri at 1 month of age and performed real-time PCR analysis. In line with results obtained using uterine tissues, increased expression of $\Delta Np63$, *Krt5*, and *Krt14* was found in uterine epithelia of *Ezh2* cKO mice compared with controls (Appendix A-5). Thus, loss of EZH2 gives rise to basal-like epithelial cells or a cell population expressing basal markers.

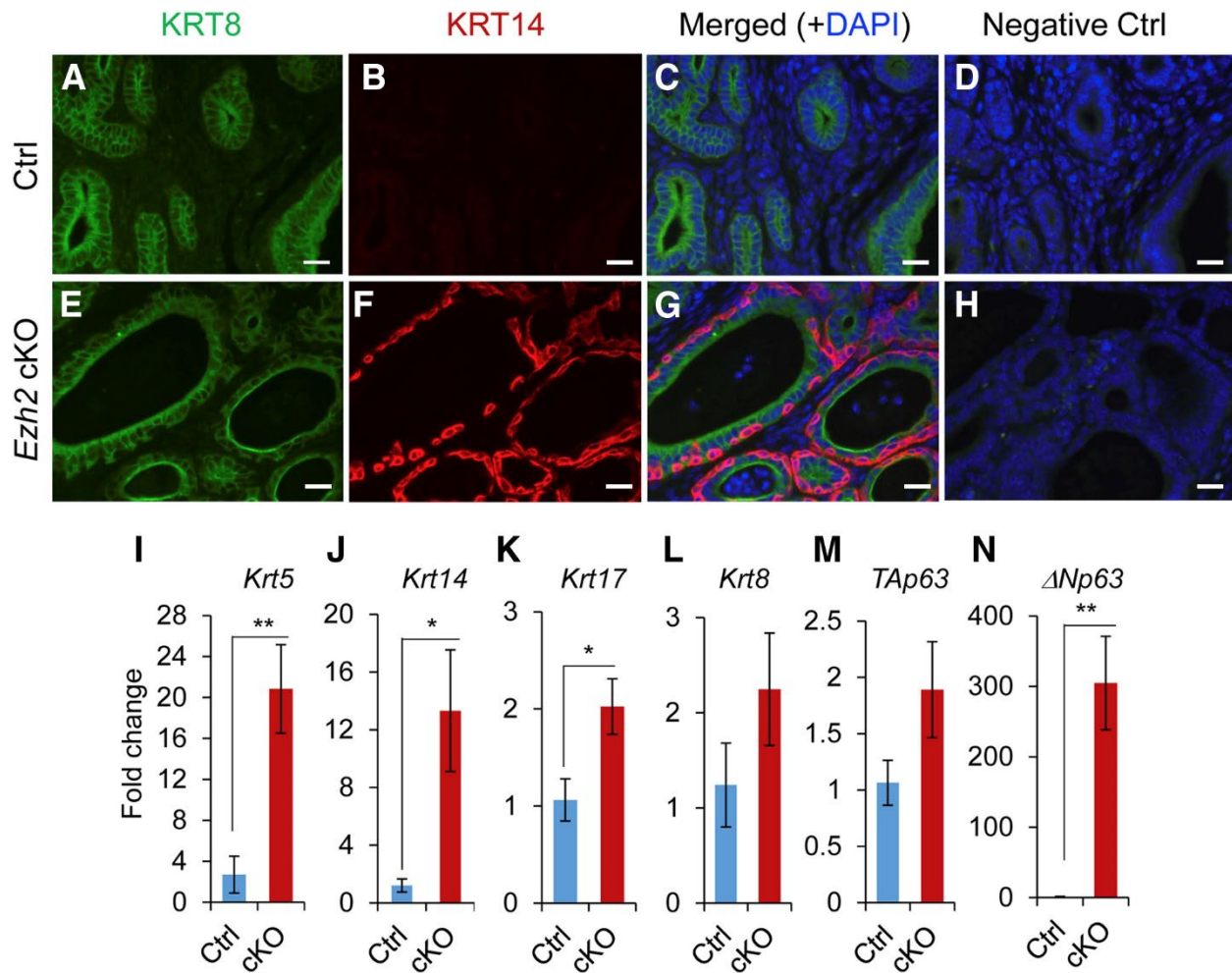


Figure 10. Ablation of EZH2 produces basal-like cell types with up-regulation of basal cell makers. A–H: Double-immunofluorescence staining of cytokeratin 8 (KRT8) and KRT14 in the uteri of control (Ctrl; A–D) and *Ezh2* cKO (E–H) mice at the age of 8 months. D and H: Negative controls using IgGs are shown. At least three independent samples per group were examined. I–N: Real-time PCR analysis of *Krt5*, *Krt14*, *Krt17*, *Krt8*, *TAp63*, and $\Delta Np63$ transcript levels in the uteri of control and *Ezh2* cKO mice at the age of 1 month. Data are expressed as means ± SEM (I–N). *n* = 4 (I–N, Ctrl mice); *n* = 5 (I–N, cKO mice). **P* < 0.05, ***P* < 0.01. Scale bars = 20 μm (A–H).

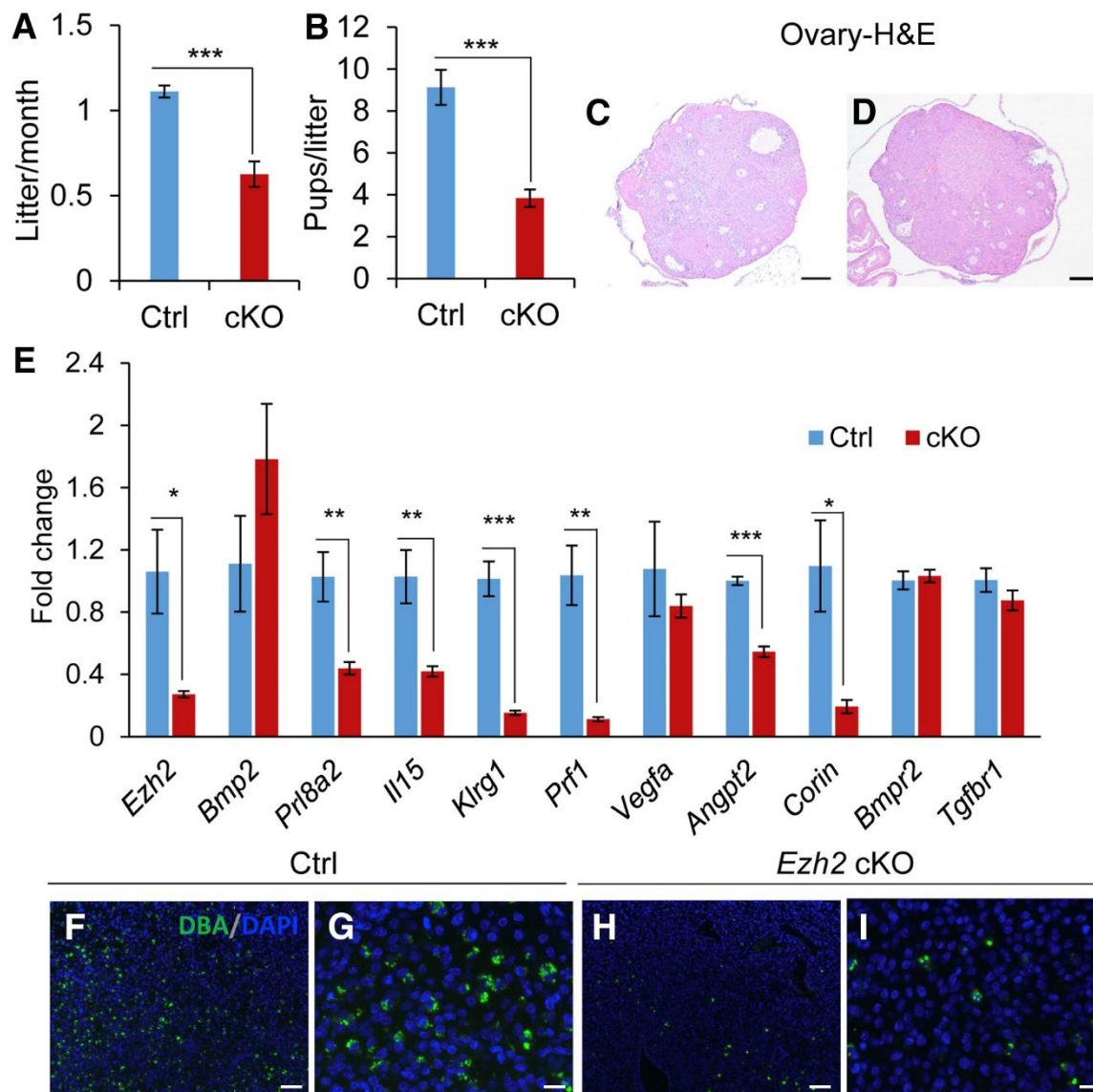


Figure 11. Reproductive defects in *Ezh2* cKO mice. A and B: Reduced number of litters and litter size during a 6-month fertility test. Approximately 64% of *Ezh2* cKO mice, but not controls (Ctrls), developed signs of dystocia or difficulty in labor during the fertility test. In that case, fertility parameters were calculated on the basis of data collected before mice developed the labor complication. C and D: Hematoxylin and eosin staining of ovaries from control and *Ezh2* cKO mice at 2 months of age. E: Real-time PCR analysis of expression of genes associated with decidual differentiation, uterine natural killer (uNK) cells, and transforming growth factor- β family signaling in embryonic day 8.5 (E8.5) decidual tissues from control and *Ezh2* cKO mice. F–I: Reduction of uNK cells in E8.5 decidual basalis of *Ezh2* cKO mice, evidenced by dolichos biflorus agglutinin (DBA) staining. F–I: F and H are shown at higher magnification in G and I, respectively. Data are expressed as means \pm SEM (A, B, and E). $n = 11$ (A and B, cKO mice); $n = 6$ (A and B, Ctrl mice); $n = 3$ (C, D, E, Ctrl mice, and F–I); $n = 4$ (E, cKO mice). * $P < 0.05$, ** $P < 0.01$, and *** $P < 0.001$. Scale bars: 250 μm (C and D); 100 μm (F and H); 25 μm (G and I).

I). Original magnification: ×40 (C and D); ×100 (F and H); ×400 (G and I). H&E, hematoxylin and eosin staining.

2.5 Ablation of EZH2 impairs female fertility

To examine whether EZH2 depletion in the uterus impacted female fertility, *Ezh2* cKO mice and controls were continuously mated with fertile male mice for a period of 6 months. During the fertility test, *Ezh2* cKO mice showed reduced number of litters and smaller litter size compared with controls (Fig. 11A and B). It was noteworthy that while all control mice delivered normally, approximately 64% of *Ezh2* cKO mice exhibited signs of dystocia or difficulty in labor during the testing period. Histological analysis of the ovary showed normal follicular development in *Ezh2* cKO mice (Fig. 11C and D). Furthermore, blastocysts could be retrieved from *Ezh2* cKO uteri at embryonic day 3.5 (E3.5; data not shown). Our findings indicate that the reduced reproductive potential of *Ezh2* cKO mice is likely caused by impaired uterine function.

To explore potential effect of *Ezh2* deletion on uterine decidual function, we first verified that *Ezh2* expression was reduced in E8.5 decidual tissues collected from *Ezh2* cKO mice (Fig. 11E). Implantation sites could be found in *Ezh2* cKO mice at E8.5 (Appendix A-6A), suggesting that decidualization occurred in these mice. Further analysis revealed potential defects in decidual differentiation evidenced by impaired expression of prolactin family 8 subfamily a member 2 (*Prl8a2*), a decidual marker, in *Ezh2* cKO decidual tissues (Fig. 11E). However, mRNA expression of another key regulator of decidualization, bone morphogenetic protein 2 (*Bmp2*), was not significantly altered (Fig. 11E). We extended the analysis to additional genes involved in decidualization including *Wnt4*, *Wnt6*, secreted frizzled-related protein 4 (*Sfrp4*), dishevelled-binding antagonist of beta-catenin 1 (*Dact1*), mechanistic target of rapamycin kinase (*Mtor*, also

known as *Frap1*), prostaglandin-endoperoxide synthase 2 (*Ptgs2*), homeobox A10 (*Hoxa10*), FK-506-binding proteins 3 (*Fkbp3*), *Fkbp4*, and *Fkbp5* [168, 173-175]. None of these genes were significantly altered except *Fkbp4*, which was upregulated in *Ezh2* cKO uteri (Appendix A-6B). Because decidualization is accompanied by active angiogenesis and vascular remodeling [176, 177], we next examined the expression of angiogenic factors including vascular endothelial growth factor A (*Vegfa*) and angiopoietins (*Angpts*) 1, 2, and 4 and *Corin*, a gene critical for uterine spiral artery remodeling [178]. Our results showed that the transcript levels of *Angpt2* and *Corin* were significantly reduced in E8.5 deciduae from *Ezh2* cKO mice (Fig. 11E). Interestingly, we also found dysregulation of genes associated with the recruitment/differentiation of uterine natural killer (uNK) cells, including interleukin 15 (*Il-15*), killer cell lectin-like receptor subfamily G member 1 (*Klrg1*), and perforin 1 (*Prf1*) (Fig. 11E). DBA lectin staining showed that the number of uNK cells was reduced in E8.5 decidual basalis of *Ezh2* cKO mice versus controls (Fig. 11F-I). Because defects in uNK cell recruitment/differentiation were found in mice with conditional deletion of BMP receptor 2 (BMPR2) or transforming growth factor β receptor 1 (TGFBR1) [148, 179], we examined the expression of both genes in the deciduae of *Ezh2* cKO mice. Results showed comparable expression levels of *Bmpr2* and *Tgfb1* mRNA in decidual tissues between *Ezh2* cKO mice and controls (Fig. 11E), suggesting that EZH2 may act independently or upstream/downstream of BMPR2 and TGFBR1. The findings of dysregulation of genes involved in angiogenesis and vascular remodeling, together with the observed reduction of the number of uNK cells in *Ezh2* cKO mice, indicate potentially impaired decidual function during pregnancy.

3 Discussion

Numerous reports highlight the involvement of EZH2 in multiple stages of cancer development including initiation, formation, progression, and metastasis [180]. As a core member of the PRC2 group, EZH2 promotes the proliferation and invasion of endometrial carcinoma [53], drives epithelial to mesenchymal transition in endometriosis [181] and hampers the expression of DNA damage repair genes in uterine fibroids [4]. In contrast, the physiological function of EZH2 in the uterus remains largely unknown. One study using *in vitro* cultured human endometrial stromal cells indicates that decidualization is accompanied by a downregulation of EZH2 expression to allow for epigenetic programming [36]. Treatment of mice with DNA demethylating agent, 5-aza-2'-deoxycytidine, impairs embryo implantation [182]. These studies indicate that modifications of chromatin and DNA are important for normal uterine function. Global deletion of *Ezh2* leads to embryonic lethality during early development [183], precluding further characterization of the function of EZH2 during postnatal uterine development. We circumvented this issue by using Cre-LoxP approach to delete *Ezh2* in the uterus. Our results suggest that EZH2 plays important roles in maintaining endometrial homeostasis and integrity.

The inner surface of the uterus is lined by a single layer of simple columnar epithelial cells, which extend into the endometrium to form uterine glands. Stratification of uterine epithelial cells is a pathological event and has been observed in several genetically modified mouse models described below. Conditional deletion of *Fgfr2* in the mouse uterus leads to the formation of stratified luminal epithelium, with the occurrence of p63 and KRT14-positive basal cells [30]. Despite the normal appearance of uterine stromal cells and the myometrium layer, these mice show fertility defects due to pregnancy loss during peri-implantation period [30]. Loss of PTEN

in the mouse uterus using *Pgr*-Cre promotes tumorigenesis, epithelial stratification, and squamous differentiation, characterized by the presence of KRT5 and p63-positive epithelial cells [170]. In contrast, deletion of *Pten* specifically in the epithelium using lactoferrin-Cre does not cause stratification but results in apoptosis of epithelial cells, suggesting a potential role of PTEN-mediated epithelial-mesenchymal communication in epithelial stratification [170].

Dysregulation of the WNT pathway is also associated with epithelial stratification. Deletion of *Wnt4* in the mouse uterus causes the formation of stratified luminal epithelium and glandular defects, accompanied by defective embryo implantation and stromal cell function [168]. *Wnt7a* null mice also show stratified epithelium and defective adenogenesis in the uterus [169].

Interestingly, conditional deletion of *Wnt7a* in the mouse uterus postnatally does not induce stratification of uterine epithelium, suggesting that the timing of WNT7A loss may contribute to the phenotypic difference observed between the ubiquitous deletion and conditional knockout models [184]. Further supporting the role of WNT pathway in maintaining epithelial integrity, dysregulation of CTNNB1 induces epithelial stratification [185]. Recently, it was shown that conditional overexpression of FOXA2 in the mouse uterus results in the development of stratified luminal/glandular epithelium [171]. Of note, in the stratified luminal epithelium of adult transgenic mice, FOXA2 was expressed in the nuclei of cells within the upper non-basal layer [171]. These results indicate that dysregulation of FOXA2 may cause epithelial stratification [171]. The observation that decreased FOXA2 expression in the uteri of adult *Ezh2* cKO females was not accompanied by depletion of uterine glands suggests a stage-specific function of FOXA2 in uterine gland development. Indeed, a recent study showed that adenogenic defects in *Foxa2* conditional knockout mice are dependent on the stage of FOXA2 depletion; and ablation of FOXA2 in the uteri of adult mice does not affect uterine gland formation [35]. As

FOXA2 is a key regulator of the function of uterine glands [35], reduced FOXA2 expression in *Ezh2* cKO mice likely leads to impaired glandular function.

Despite these findings, little is known about how dysregulation of the aforementioned genes leads to epithelial stratification. Our results did not reveal a direct link between EZH2 and dysregulation of *Fgfr2*, *Wnt4*, *Wnt7a*, and *Pten* in the formation of stratified uterine epithelium. Instead, our data suggest that EZH2 is required for uterine epithelial integrity via suppressing the expression of p63, which is consistent with a role of EZH2 in restricting the basal cell lineage in the development of the lung [186, 187]. *p63* is a key gene implicated in the stratification of epithelium, as stratification is impaired and differentiation markers are absent in the skin of p63-deficient mice [188]. In the mammary gland, overexpression of p63 in luminal cells reprograms them to basal type [189]. Due to the existence of alternative promoters, two classes of p63 proteins are translated, one containing an N-terminal transactivation (TA) domain and the other not (i.e., TAp63 and Δ Np63) [190]. In addition, the alternative splicing at the C-terminus produces at least three isoforms (α , β , and γ) [190]. The exact function of p63 isoforms in epithelial stratification remains controversial. In the epidermis, TAp63 has been found to drive the stratification and expression of KRT5 and KRT14 [191]. However, other reports indicate that Δ Np63 may initiate stratification or expansion of the basal layer [192-194]. In the uterus, the role of p63 isoforms in epithelial stratification remains unknown. Our data support the involvement of Δ Np63 in uterine epithelial stratification in the absence of EZH2. Based on these findings, it is tempting to speculate that *p63* and other basal cell genes are upregulated as a result of decreased H3K27 methylation upon loss of EZH2, leading to the differentiation of basal-like cells in the uterus. However, the function of these cells in *Ezh2* cKO mice remains unclear. Because uterine

epithelia generally do not contain basal cells, the appearance of this cell type and the expression of basal cell-associated keratins in EZH2-depleted uteri may indicate altered differentiation of epithelial cells that normally form a simple epithelium in the uterus. As basal-like cells in the uterus are associated with uterine dysfunction and tumor progression [30, 170], it is conceivable that epithelial stratification in *Ezh2* cKO mice may link to the development of endometrial hyperplasia and/or reproductive deficiency.

Of note, limitations exist for the current study. Since *Pgr*-Cre deletes genes in both epithelial and mesenchymal compartments, a potential contribution of epithelial-stromal interaction to the observed phenotype in *Ezh2* cKO uteri should be considered. Future studies are needed to define how loss of EZH2 alters uterine growth and differentiation pathways and uncover the contribution of epithelial versus stromal EZH2 to the observed basal-like cell phenotype.

Generation of *Ezh2* conditional knockout mice using an epithelial- or stromal-specific Cre driver may help clarify this question. Of note, *Ezh2* cKO female mice showed defects in parturition, the cause of which is unclear. Further investigations are warranted to gain mechanistic insights into this defect and determine whether EZH2 plays a role in the myometrium or cervix. It is also important to further define the epithelial versus stromal/decidual contribution to the observed reproductive defects. In addition, the methylation status of H3K27 of stratification-related genes (e.g., *p63*, *Krt14*, and *Krt5*) in uterine epithelial cells of *Ezh2* cKO mice versus controls was not determined, due to technical challenges of chromatin immunoprecipitation (CHIP)-qPCR assays using low amounts of uterine epithelial cells isolated from mice at an early developmental stage or using uterine tissues which contain multiple cell types. Nevertheless, the current findings reveal a novel role for uterine EZH2 in reproductive development and function.

Understanding of the role of EZH2 and EZH1 and their potential redundancy in establishing H3K27 methylation and gene silencing is incomplete. Our results clearly showed an EZH1-independent role of EZH2 in the regulation of endometrial homeostasis and integrity and uterine function, supporting that EZH1 and EZH2 may play distinct roles in maintaining the repressive chromatin [195]. However, a number of studies indicate that EZH2 is not the only histone methyltransferase that establishes the H3K27 methylation mark [146, 196, 197]. Instead, EZH1 and EZH2 function redundantly in regulating the methylation status of H3K27 during development [146, 196, 197]. Generation and characterization of mice with compound loss of EZH2 and EZH1 in the uterus will help determine the functional overlap between the two genes, if any, and elucidate the role of histone modifications in the uterus.

In summary, results from the current study suggest that EZH2 maintains uterine epithelial integrity partially through preventing the differentiation of basal-like cells and the development of endometrial hyperplasia. Importantly, the altered uterine growth and impaired fertility in the *Ezh2* cKO mouse make it a useful model to understand mechanisms regulating endometrial homeostasis and uterine function. Our findings support the concept that manipulation of epigenetic regulators could offer an exquisite approach to treat reproductive diseases and fertility issues related to epigenetic changes or epigenetic drift caused by environmental or intrinsic cues.

Aim 2. EZH2 AND ENDOMETRIAL CANCER DEVELOPMENT: INSIGHTS FROM A MOUSE MODEL *

1 Materials and Methods

1.1 Animals and Ethics

Protocols involving the use of mice were approved by Texas A&M University Institutional Animal Care and Use Committee. Mice were on a mixed C57BL/6/129SvEv background and handled according to NIH guideline for the Care and Use of Laboratory Animals. The reporting of experiments followed the ARRIVE guidelines. Mice were housed in the Laboratory Animal Resources and Research (LARR) facility under a 12-h light: 12-h dark cycle. *Pgr*-Cre mice were generated previously [198]. *Ezh2*^{lox/lox} mice (# 022616) and *Pten*^{lox/lox} mice (# 006440) were purchased from the Jackson Laboratory.

1.2. Genotyping and DNA Recombination Analysis

Genotyping was conducted using genomic DNA isolated from mouse tails. Recombination of the *Ezh2* and *Pten* conditional alleles at the DNA level was analyzed using uterine DNA samples. Primer information for *Ezh2* and *Pten* was obtained from the Jackson Laboratory. Gene-specific primers were used to detect *Ezh2* (5'-CATGTG-CAGCTTTCTGTTCA-3' and 5'-CACAGCCTTTCTGCTCACTG-3'; wild-type band = 203 bp and flox band = ~300 bp), *Pten* (5'-CAAGCACTCTGCGAACTGAG-3' and 5'-AAGTTTTTGAAGGCAAGATGC-3'; wild-type band = 156 bp and flox band = 328 bp), *Ezh2* recombination (5'-

* Reprinted in slight modified form with permission from 'EZH2 and Endometrial Cancer Development: Insights from a Mouse Model.' by Fang X, Ni N, Wang X, Tian Y, Ivanov I, Rijnkels M, Bayless KJ, Lydon JP, Li Q. *Cells*. 2022 Mar 7;11(5):909.

CCCATGTTTAAGGGCATAGTGACATG-3' and 5'-
TCGAGGGACCTAATAACTCGTATAGCA-3') [146], and *Pten* recombination (5'-
ACTCAAGGCAGGGATGAGC -3' and 5'- AATCTAGGGCCTCTTGTGCC -3') [71].

1.3 Histology, Immunohistochemistry, and Immunofluorescence

Uterine samples were fixed in 10% (v/v) neutral-buffered formalin (MilliporeSigma, Burlington, MA, USA), embedded in paraffin, and processed using the Texas A&M College of Veterinary Medicine & Biomedical Sciences Core Histology Laboratory. Sections (5 µm) were subjected to hematoxylin and eosin (H.E.) staining and Periodic Acid Schiff (PAS) staining to determine the histopathological features of the uterus/endometrial cancer. Immunohistochemistry and immunofluorescence procedures were detailed elsewhere [89]. Briefly, slides were deparaffinized, rehydrated, and boiled in sodium citrate buffer (pH = 6) to restore antigenicity. Sections were then blocked and incubated sequentially with primary antibodies (Table 6) overnight at 4 °C and biotinylated secondary antibodies (immunohistochemistry) or fluorescent secondary antibodies (immunofluorescence). For immunohistochemistry, avidin-biotin complex (# PK-6100; Vector Laboratories, Burlingame, CA, USA) and NovaRed (#SK-4800; Vector Laboratories) were used to amplify the signal and develop the slides, respectively. For immunohistochemistry, slides were mounted with Fisher mounting medium. In contrast, slides from immunofluorescence experiment were directly mounted using DAPI-containing medium to counterstain the nuclei.

Vector Laboratories, Burlingame, CA, USA) and NovaRed (#SK-4800; Vector Laboratories) were used to amplify the signal and develop the slides, respectively. For immunohistochemistry,

slides were mounted with Fisher mounting medium. In contrast, slides from immunofluorescence experiment were directly mounted using DAPI-containing medium to counterstain the nuclei. Vector Laboratories, Burlingame, CA, USA) and NovaRed (#SK-4800; Vector Laboratories) were used to amplify the signal and develop the slides, respectively. For immunohistochemistry, slides were mounted with Fisher mounting medium. In contrast, slides from immunofluorescence experiment were directly mounted using DAPI-containing medium to counterstain the nuclei.

Table 6. Information of primary antibodies (Aim2).

Name	Manufacturer	Cat. #	Species	IHC/IF	WB
EZH2	Cell Signaling	5246	Rabbit	1:400	1:1000
pAKT	Cell Signaling	4060	Rabbit	1:50	1:2000
Ki67	Cell Signaling	12202	Rabbit	1:500	
ECAD	Cell Signaling	3195	Rabbit	1:400	
KRT14	Thermo Fisher Scientific	PA5-16722	Rabbit	1:400	
Δ Np63	BioLegend (San Diego, CA, USA)	619001	Rabbit	1:200	
F4/80	Cell Signaling	70076	Rabbit	1:250	
LY6G	BioLegend	127601	Rat	1:500	
PTEN	Cell Signaling	9188	Rabbit		1:1000
AKT	Cell Signaling	4691	Rabbit		1:1000
H3K27me3	Cell Signaling	9733	Rabbit		1:1000
Histone H3	Cell Signaling	4499	Rabbit		1:5000
ACTB	MilliporeSigma	A3854	Mouse		1:50,000

IHC, immunohistochemistry; IF, immunofluorescence; WB, western blot.

1.4 Western Blot

Western blot was performed as described elsewhere [89]. Uterine tissue homogenates were prepared from mice at 14 days of age, and 30 μg of protein samples were subject to electrophoresis. Incubation of primary antibodies (Table 6) was carried out overnight at 4 °C. Western blot images were quantified using NIH Image J (version 1.52p, Bethesda, MD, USA).

1.5 Hypoxia Staining

Hypoxia staining was performed using Hypoxyprobe Plus Kit (# HP2-100Kit, Hypoxyprobe, Burlington, MA, USA) based on the manufacturer's protocol. Briefly, hypoxyprobe-1 (pimonidazole) was administered prior to sample collection. Slides were incubated at 60 °C for 20 min, deparaffinized, and then rehydrated. The slides were then treated with H_2O_2 to inactivate endogenous peroxidase activity. The antigenicity was restored by boiling the sides in sodium citrate buffer (pH = 6). After being blocked with non-immune sera, slides were incubated with FITC-MAb1 (1:50) at 4 °C overnight. In hypoxic cells/tissues, pimonidazole is bioreductively activated to form stable adducts (PIM) detectable by immunostaining. The next day, slides were washed and then mounted with DAPI-containing medium and examined under a fluorescence microscope (Olympus, Waltham, MA, USA).

1.6 Enzyme-Linked Immunosorbent Assay (ELISA)

The levels of mouse neutrophil elastase/ELA2 or tumor necrosis factor α ($\text{TNF}\alpha$) in the serum/uterine tissue homogenates were measured using Quantikine ELISA kit (R&D, Minneapolis, MN, USA) based on manufacturer's instructions. Serum samples were diluted (1:5-1:100) to meet the detection range, with at least three biological replicates per experimental

group and two technical replicates per sample. Tissue homogenates were prepared and then treated with repeated freezing and thawing cycles. The optical density (OD) values were measured using a microplate reader (Bio-Rad, Hercules, CA, USA) at dual wavelengths (450 nm and 540 nm). OD values were corrected by subtracting readings at 540 nm from those at 450 nm. The concentration of ELA2 or TNF α was calculated using an online tool (<http://elisaanalysis.com> (accessed on 19 December 2019)).

1.7 Hormone Assays

Serum estradiol and progesterone levels from nine-week-old *Pten*^{d/d} and *Pten*^{d/d}; *Ezh2*^{d/d} mice were determined using the Ligand Assay and Analysis Core (Center for Research in Reproduction, University of Virginia). Assay details are available at <https://med.virginia.edu/research-in-reproduction/ligand-assay-analysis-core/> (accessed on 2 July 2021).

1.8 Quantitative Reverse Transcription-PCR

Total RNA was isolated from uterine tissues using RNeasy Mini Kit (Qiagen, Germantown, MD). Reverse transcription (RT) was performed using a SuperScript III reverse transcriptase (ThermoFisher Scientific, Waltham, MA, USA) in the presence of 500 ng total RNA.

Quantitative RT-PCR (qRT-PCR) was conducted using gene-specific primers as described [89].

At least three biological replicates per group and two technical replicates per sample were included. Relative levels of gene expression were determined as described elsewhere [163], with ribosomal protein L19 (*Rpl19*) as an internal control. Primers include cellular retinoic acid binding protein II (*Crabp2*) (5'-ATGCCTAACTTTTCTGGCAACT-3' and 5'-

GCACAGTGGTGGAGGTTTTGA-3'; PrimerBank ID 33469075a1), dehydrogenase/reductase (SDR family) member 9 (*Dhrs9*) (5'-ATGCTGTTTTGGTTGTTGGCT-3' and 5'-GTTCTGGCTGCTAAGTTTCCA-3'; PrimerBank ID 30425272a1), *Ezh2^{del}*, *Pten*, keratin 14 (*Krt14*), *ΔNp63*, chemokine (C-X-C motif) ligand 5 (*Cxcl5*), chemokine (C-X-C motif) receptor 2 (*Cxcr2*), and aldehyde dehydrogenase 3 family, member B2 (*Aldh3b2*) [71, 199-201] .

1.9 Statistical Analysis

Statistical analysis was conducted using GraphPad Prism 9 (San Diego, CA, USA). Unpaired two-tailed *t*-test was used to compare means between two groups. One-way analysis of variance (ANOVA) and Tukey's multiple comparison test were used to compare means among multiple groups. Kaplan–Meier survival curves were analyzed using Log-rank (Mantel-Cox) test. Data are means ± s.e.m. A *P* value of less than 0.05 was reported as statistically significant (* *p* < 0.05, ** *p* < 0.01, *** *p* < 0.001, and **** *p* < 0.0001).

2 Results

2.1 Generation of Mice with Conditional Deletion of *Ezh2* and *Pten*

Conditional ablation of PTEN using *Pgr-Cre* (*Pten^{d/d}*) in the mouse uterus leads to the development of endometrial cancer [71, 202]. *Ezh2* conditional knockout mice are free of endometrial cancer but develop stratified uterine epithelia that contain basal-like cells absent in the normal uterus [200]. To determine the role of EZH2 in endometrial cancer development, we created mice with simultaneous deletion of *Ezh2* and *Pten* (*Pten^{d/d}; Ezh2^{d/d}*) or *Pten* only (*Pten^{d/d}*) in the uterus using Cre-LoxP approach (Figure 12A). *Pten^{ff}* and *Pten^{ff}; Ezh2^{ff}* mice were included as controls. Recombination of *Pten* and *Ezh2* alleles occurred specifically in the

uteri of *Pten^{d/d}* and *Pten^{d/d}; Ezh2^{d/d}* mice but not controls (Appendix A-7A). Conditional deletion of *Ezh2* and *Pten* at the transcript levels was demonstrated using qRT-PCR (Figure 12B,C). We also verified the ablation of PTEN and EZH2 proteins by western blot (Figure 12D) and immunostaining (Appendix A-7B–G). Of note, expression of EZH2 was increased in *Pten^{d/d}* uteri compared with age-matched controls (i.e., *Pten^{ff}* and *Pten^{ff}; Ezh2^{ff}*) (Figure 12D). Loss of PTEN was expected to enhance PI3K/AKT activity, as PTEN inhibits PI3K-AKT pathway [203]. Indeed, increased expression of phospho-AKT (pAKT) was found in the uteri of *Pten^{d/d}* and *Pten^{d/d}; Ezh2^{d/d}* mice versus controls (Figures 12D and Appendix A-7H–J).

EZH2 is a histone methyltransferase that methylates H3K27 [204]. To determine if loss of EZH2 affected H3K27me3 levels, we examined the expression of H3K27me3 using uteri from controls, *Pten^{d/d}*, and *Pten^{d/d}; Ezh2^{d/d}* mice at 14 days of age. Immunostaining revealed reduced levels of H3K27me3 in *Pten^{d/d}; Ezh2^{d/d}* uteri compared with *Pten^{d/d}* uteri (Appendix A-7K–M). Although EZH2 expression was increased in *Pten^{d/d}* uteri (Figure 12D), H3K27me3 levels were not altered in *Pten^{d/d}* uteri in comparison with the control (Appendix A-7N,O). The above results indicate successful ablation of EZH2 and PTEN in the mouse uterus.

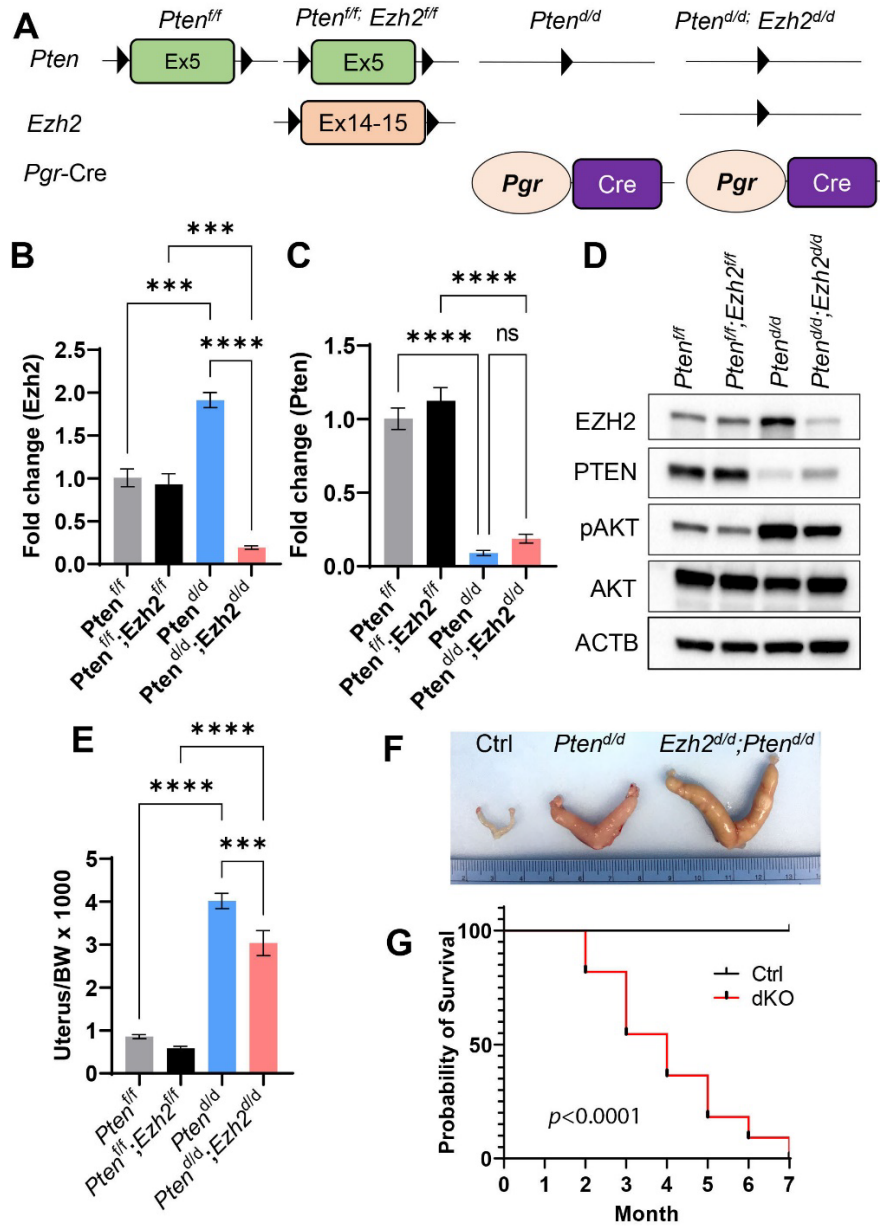


Figure 12. Generation of mice with conditional deletion of *Pten* and *Ezh2* in the uterus. **(A)** A schematic of Cre-LoxP approach to generate conditionally deleted mice. **(B,C)** Transcript levels of *Ezh2* and *Pten* in the mouse uterus at 14 days of age. $n = 3-4$. Data are mean \pm s.e.m. *** $p < 0.001$ and **** $p < 0.0001$. ns, not significant. **(D)** Western blot analysis of EZH2, PTEN, pAKT, and AKT in 14-day-old *Pten*^{fl/fl}, *Pten*^{fl/fl}; *Ezh2*^{fl/fl}, *Pten*^{d/d}, and *Pten*^{d/d}; *Ezh2*^{d/d} uteri. ACTB was used as an internal control. $n = 4$. **(E)** Ratios of the uterus/body weight (BW) in *Pten*^{fl/fl}, *Pten*^{fl/fl}; *Ezh2*^{fl/fl}, *Pten*^{d/d}, and *Pten*^{d/d}; *Ezh2*^{d/d} mice at three weeks of age. $n = 9-13$. Data are mean \pm s.e.m. *** $p < 0.001$ and **** $p < 0.0001$. **(F)** Gross image of uteri from nine-week-old *Pten*^{fl/fl} (Ctrl), *Pten*^{d/d}, and *Pten*^{d/d}; *Ezh2*^{d/d} mice. **(G)** Kaplan-Meier survival curves of *Pten*^{fl/fl}; *Ezh2*^{fl/fl} (Ctrl) and *Pten*^{d/d}; *Ezh2*^{d/d} mice. $n = 11$.

2.2 Loss of EZH2 Reduces Tumor Burden during Early Carcinogenesis but Negatively Impacts Disease Outcome

Consistent with the documented epithelial hyperplasia and endometrial cancer development resulting from loss of PTEN [70, 202], the uterine weights of *Pten*^{d/d} and *Pten*^{d/d}; *Ezh2*^{d/d} mice were significantly increased compared with controls at three weeks of age (Figure 12E).

Simultaneous loss of EZH2 and PTEN reduced the uterine weight compared with *Pten*^{d/d} mice (Figure 12E). However, the uteri of *Pten*^{d/d}; *Ezh2*^{d/d} mice were larger than those of *Pten*^{d/d} mice at the age of nine weeks (Figure 12F). To assess the outcome of endometrial cancer in mice with conditional deletion of *Pten* and *Ezh2*, we generated Kaplan–Meier survival curves, which showed that *Pten*^{d/d}; *Ezh2*^{d/d} mice succumbed to death starting around two months of age (Figure 12G). As endometrial cancer in *Pten*^{d/d} mice does not substantially affect the viability up through five months of age [71, 202], current results suggest that deletion of *Ezh2* negatively impacts the disease outcome.

As *Pten*^{d/d}; *Ezh2*^{d/d} mice showed a reduction in uterine weight compared with *Pten*^{d/d} mice during early tumor development (Figure 12E), we sought to determine the effect of *Ezh2* deletion on the proliferation of endometrial cancer cells. Immunostaining of Ki67, a cell proliferation marker, was performed using uteri from three-week-old control, *Pten*^{d/d}, and *Pten*^{d/d}; *Ezh2*^{d/d} mice.

Results showed reduced Ki67 index (i.e., number of Ki67-positive cells/number of total cells) in *Pten*^{d/d}; *Ezh2*^{d/d} uteri versus *Pten*^{d/d} uteri (Figure 13A–E). It has been reported that retinoic acid (RA) signaling inhibits endometrial cancer cell proliferation [205]. Herein, we found that several genes associated with RA synthesis were upregulated in *Pten*^{d/d}; *Ezh2*^{d/d} uteri versus *Pten*^{d/d} uteri (Figure 13F–H). These genes encode DHRS9 that is involved in RA biosynthesis from

retinaldehyde, CRABP2 that transports RA to the RA receptor, and ALDH3B2, an enzyme of the aldehyde dehydrogenase superfamily. The finding that deletion of *Ezh2* in *Pten^{d/d}* uteri reduced endometrial cell proliferation during early carcinogenesis suggests an oncogenic role of EZH2.

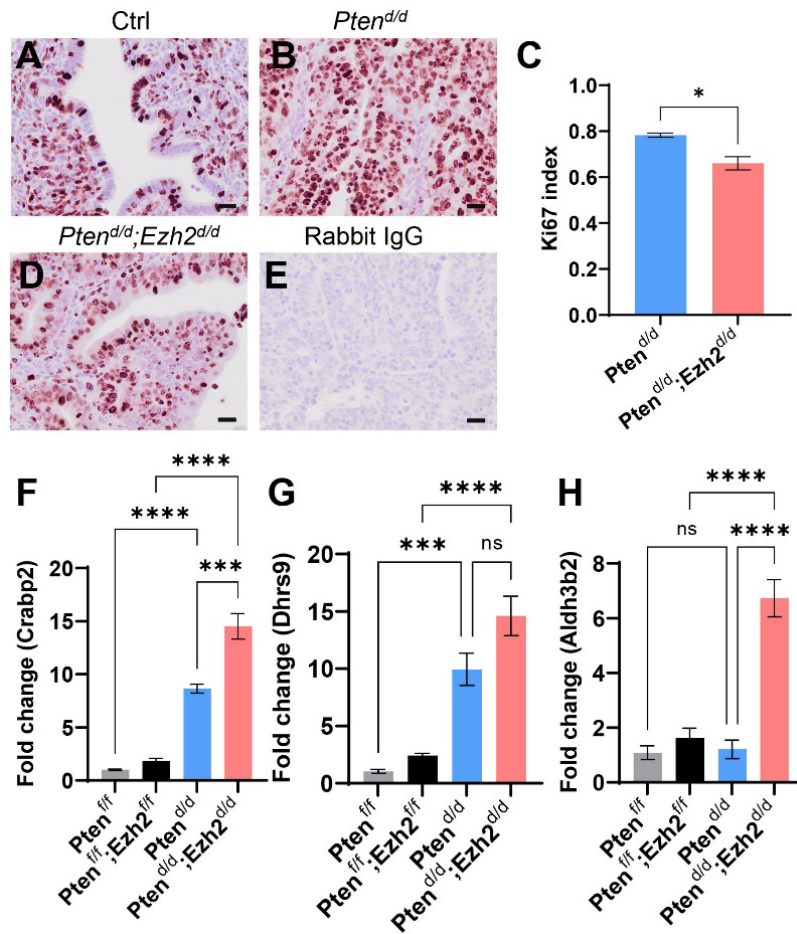


Figure 13. Reduced Ki67 index in the uteri of *Pten^{d/d}; Ezh2^{d/d}* mice compared with *Pten^{d/d}* mice. (A–E) Immunohistochemical analysis of Ki67 using three-week-old *Pten^{fl/fl}* (Ctrl), *Pten^{d/d}*, and *Pten^{d/d}; Ezh2^{d/d}* mice. Ki67 index for *Pten^{d/d}* and *Pten^{d/d}; Ezh2^{d/d}* mice is shown in panel (C). $n = 3$. Data are mean \pm s.e.m. * $p < 0.05$. Scale bar = 20 μ m (A,B,D,E). (F–H) Transcript levels of *Crabp2*, *Dhhrs9*, and *Aldh3b2* in uterine tissues from *Pten^{fl/fl}*, *Pten^{fl/fl}; Ezh2^{fl/fl}*, *Pten^{d/d}*, and *Pten^{d/d}; Ezh2^{d/d}* mice at three weeks of age. $n = 4$. Data are mean \pm s.e.m. *** $p < 0.001$ and **** $p < 0.0001$. ns, not significant.

2.3 *Ezh2* and *Pten* Deletion Enhances the Accumulation of Intraluminal Neutrophils Compared with *Pten* Deletion Alone

To begin to understand the cellular basis of altered endometrial cancer progression in *Pten*^{d/d}; *Ezh2*^{d/d} mice, we examined the morphological/histological changes of the uterus. At one month of age, H.E. staining showed that the size of the uteri was enlarged in both *Pten*^{d/d} and *Pten*^{d/d}; *Ezh2*^{d/d} mice compared with controls (Figure 14A–D). Of note, some *Pten*^{d/d}; *Ezh2*^{d/d} mice showed a ring-like uterine lumen on the cross section, with loss of uterine epithelia and massive accumulation of polymorphonuclear neutrophils and cell debris (Figure 14C,D,G,H and Appendix A-8).

Neutrophils are critical for cancer development and metastasis [206]. To determine a timeline of the observed intraluminal neutrophil accumulation, tumor development was next examined in *Pten*^{d/d}; *Ezh2*^{d/d} mice at three weeks of age. To better visualize neutrophil infiltration, we performed immunostaining of lymphocyte antigen 6 complex, locus G (LY6G), a neutrophil marker. Although neutrophil infiltration occurred in both *Pten*^{d/d}; *Ezh2*^{d/d} and *Pten*^{d/d} mice, no substantial accumulation of intraluminal neutrophils was observed in *Pten*^{d/d}; *Ezh2*^{d/d} or *Pten*^{d/d} mice at this stage (Figure 14I–N). Negative controls are shown in Figure 14K and N. CXCL5 and CXCR2 are critical for recruiting neutrophils to endometrial cancer lesions [70]. To determine whether expression of *Cxcl5* and *Cxcr2* by uterine epithelial cells was altered upon *Ezh2* deletion, we isolated uterine epithelia from *Pten*^{d/d} and *Pten*^{d/d}; *Ezh2*^{d/d} mice. Results showed that the expression levels of *Cxcl5* and *Cxcr2* were not statistically different between *Pten*^{d/d}; *Ezh2*^{d/d} and *Pten*^{d/d} mice, despite a drastic reduction of *Ezh2* expression in the epithelia from *Pten*^{d/d}; *Ezh2*^{d/d} mice (Appendix A-9).

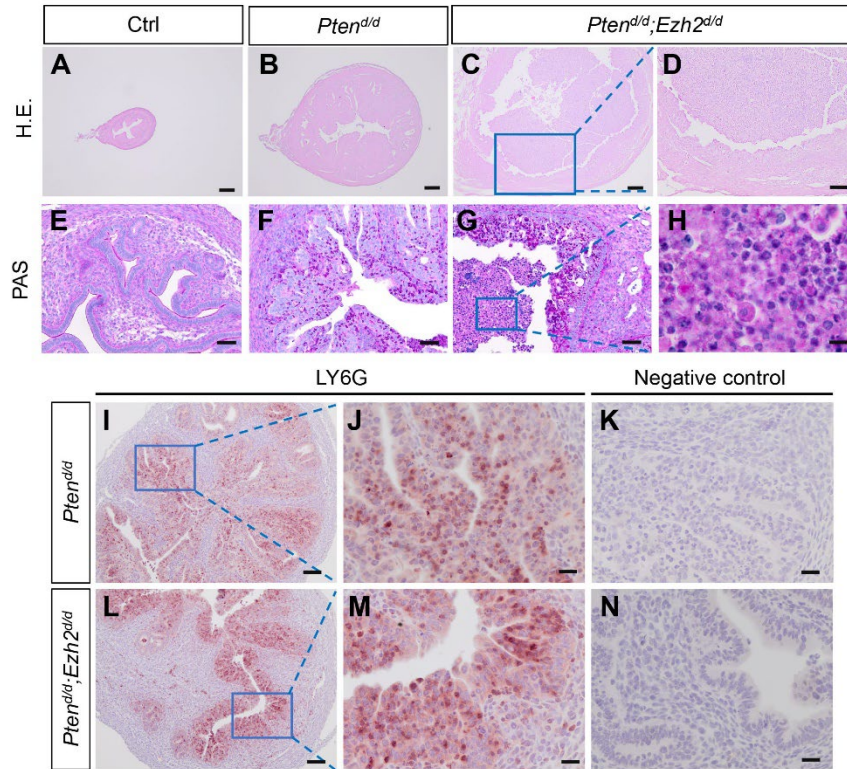


Figure 14. Deletion of *Ezh2* promotes accumulation of intraluminal neutrophils in PTEN-inactivated uteri. (A–H) Histological analyses of uteri from 1-month-old *Pten^{fl/fl}*, *Pten^{d/d}*, and *Pten^{d/d}; Ezh2^{d/d}* mice using H.E. staining (A–D) and PAS staining (E–H). Panels (D,H) are high power images of the boxed areas of panels (C,G), respectively. (I–N) Immunostaining of LY6G using uteri from three-week-old *Pten^{d/d}* and *Pten^{d/d}; Ezh2^{d/d}* mice. Panels (J,M) are high power images of the boxed areas of panels (I,L), respectively. Panels (K,N) are negative controls where the primary antibody was replaced by isotype-matched IgG. At least three independent samples per genotype were examined. Scale bar = 10 μ m (H), 20 μ m (J,K,M,N), 50 μ m (E–G), 100 μ m (D,I,L), and 200 μ m (A–C).

To further assess the extent of neutrophil accumulation during tumor progression, we examined the uteri of *Pten^{d/d}; Ezh2^{d/d}* and *Pten^{d/d}* mice at nine weeks of age. While LY6G-positive neutrophils were sparse in control uteri (Figure 15A,D), they were increased within the epithelia in *Pten^{d/d}* mice (Figure 15B,E). Strikingly, abundant neutrophils were found in *Pten^{d/d}; Ezh2^{d/d}* uteri encompassing both the stroma and epithelia, despite a substantial loss of uterine epithelia in these mice (Figures 15C,F and Appendix A-10). In addition, all *Pten^{d/d}; Ezh2^{d/d}* mice developed the aforementioned ring-like uterine lumen when cross sections were examined (Appendix A-

10C). As macrophage is involved in the clearance of cellular debris, we also examined the presence of macrophage by immunostaining of F4/80. Results showed that immunoreactive signals of F4/80 were mainly localized to the stroma of control and *Pten*^{d/d} uteri (Figure 15G,H,J,K). However, F4/80-positive macrophages were accumulated in both uterine epithelia and stroma of *Pten*^{d/d}; *Ezh2*^{d/d} mice (Figure 15I,L). Negative controls are shown in Figure 15M–O.

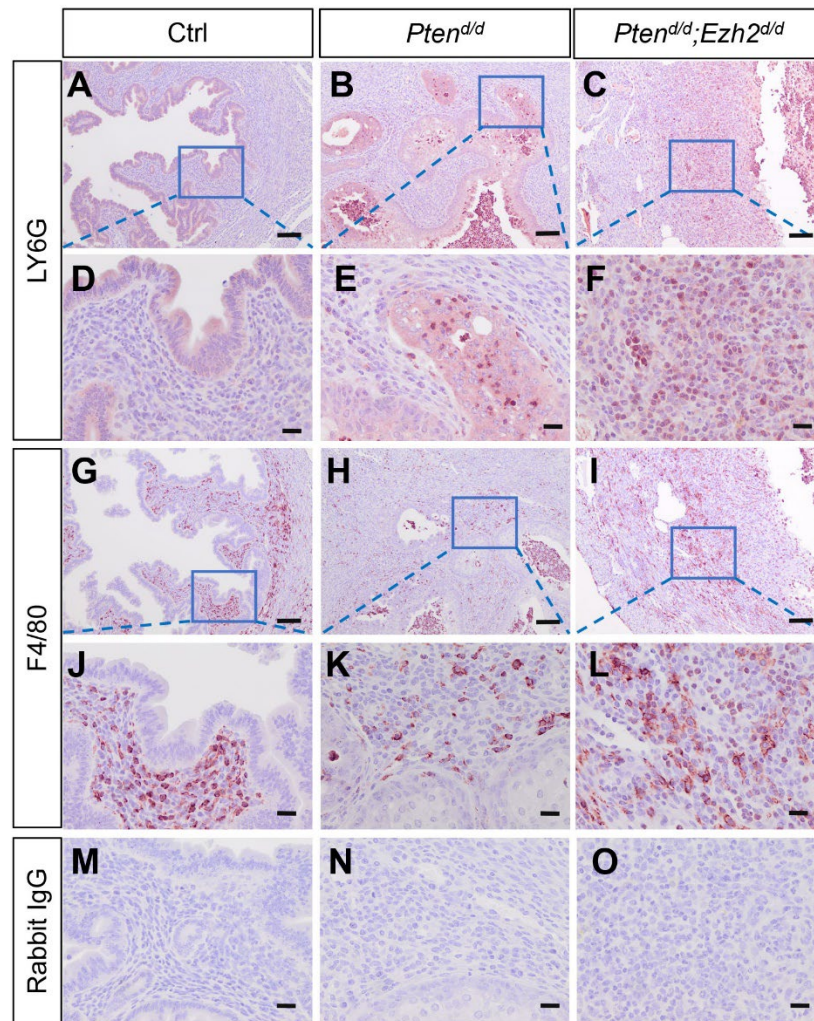


Figure 15. Deletion of *Ezh2* in PTEN-inactivated uteri causes heightened inflammation. (A–L) Immunostaining of LY6G and F4/80 in the uteri from nine-week-old *Pten*^{fl/fl}, *Pten*^{d/d}, and *Pten*^{d/d}; *Ezh2*^{d/d} mice. Panels (D–F, J–L) are high power images of the boxed areas of panels (A–C, G–I), respectively. (M–O) Negative controls where the primary antibody was replaced with isotype–

matched IgG. At least three independent mice per group were examined. Scale bar = 100 μm (A–C,G–I) and 20 μm (D–F,J–O).

To determine a potential link between the stage-dependent intraluminal accumulation of neutrophils and chronic inflammation in *Pten^{d/d}; Ezh2^{d/d}* mice, we measured the levels of serum ELA2, a serine proteinase produced by neutrophils during inflammation [207]. It was found that ELA2 levels were not statistically different between *Pten^{d/d}; Ezh2^{d/d}* and *Pten^{d/d}* mice at the age of 1 month (Figure 16A). In contrast, serum ELA2 levels were markedly elevated in *Pten^{d/d}; Ezh2^{d/d}* mice at nine weeks of age, compared with age-matched *Pten^{d/d}* mice and controls (Figure 16B). In addition, we determined the levels of another important pro-inflammatory cytokine, TNF α , in uterine tissue homogenates or the serum of control, *Pten^{d/d}*, and *Pten^{d/d}; Ezh2^{d/d}* mice. The levels of TNF α were below the limit of detection in controls. However, TNF α levels were elevated in *Pten^{d/d}* and *Pten^{d/d}; Ezh2^{d/d}* mice, although a statistical significance between *Pten^{d/d}* and *Pten^{d/d}; Ezh2^{d/d}* mice was not achieved due to sample variations (Figure 16C,D). Collectively, loss of EZH2 enhanced the accumulation of intraluminal neutrophils, leading to heightened chronic inflammation.

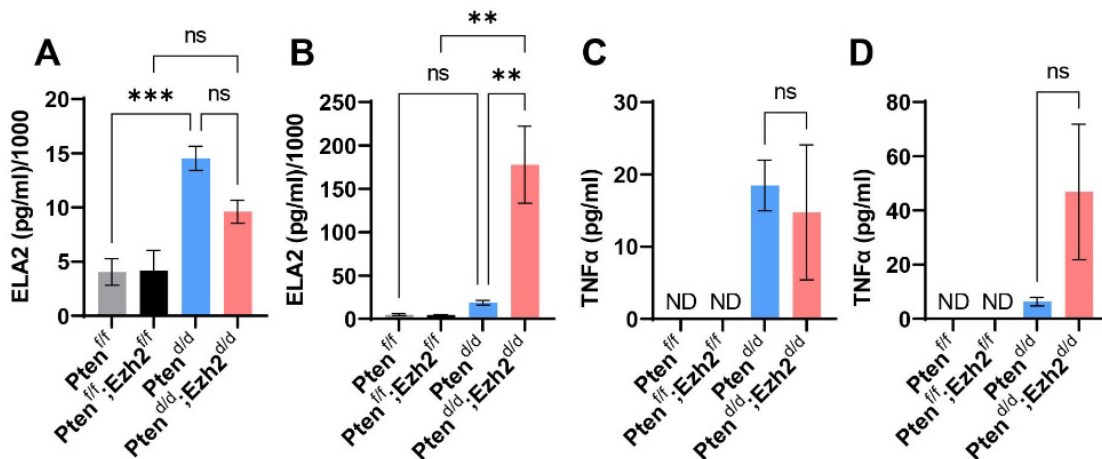


Figure 16. Analysis of ELA2 and TNF α levels using ELISA. (A and B) Serum levels of ELA2 at the age of one month (A) and nine weeks (B). (C,D) TNF α levels in uterine tissues at the age of

one month (C) and in the serum at nine weeks (D). $n = 3-4$. Data are mean \pm s.e.m. ** $p < 0.01$ and *** $p < 0.001$. ns, not significant. ND, not detected.

2.4 Factors Contributing to The Developmental Trajectory of Endometrial Cancer Lacking

PTEN and EZH2

As our previous studies showed that conditional loss of EZH2 in the uterus elicits epithelial stratification [200], we asked the question of whether uterine epithelial stratification occurred in *Pten^{d/d}; Ezh2^{d/d}* mice during tumor development. To approach this question, we first performed immunostaining of KRT14 and Δ Np63, two basal cell markers. Immunoreactive signals for both KRT14 and Δ Np63 were detectable as early as three weeks of age in *Pten^{d/d}; Ezh2^{d/d}* mice, but not in age-matched *Pten^{d/d}* mice and controls (Figure 17A–D). Supporting the immunohistochemical results, transcript levels of *Krt14* and *Δ Np63* were increased in uterine epithelia of *Pten^{d/d}; Ezh2^{d/d}* mice compared with *Pten^{d/d}* mice (Figure 17E,F). Further, *Pten^{d/d}; Ezh2^{d/d}* mice contained stratified epithelia positively stained for KRT14 and Δ Np63 at the age of one month (Figures 17I,J,M,N and Appendix A-11). In the severe case with massive accumulation of intraluminal neutrophils, nearly the entire uterine lumen was surrounded by stratified epithelia (Figures 17I,M and Appendix A-11), in sharp contrast to age-matched *Pten^{d/d}* and control mice, where minor to negligible staining of KRT14 and Δ Np63 was found (Figure 17G,H,K,L). Immunostaining of ECAD was conducted to show the epithelial components of the uterus (Figure 17O–R). Thus, conditional deletion of *Ezh2* in *Pten^{d/d}* uteri exacerbated uterine epithelial stratification that might negatively impact the disease outcome.

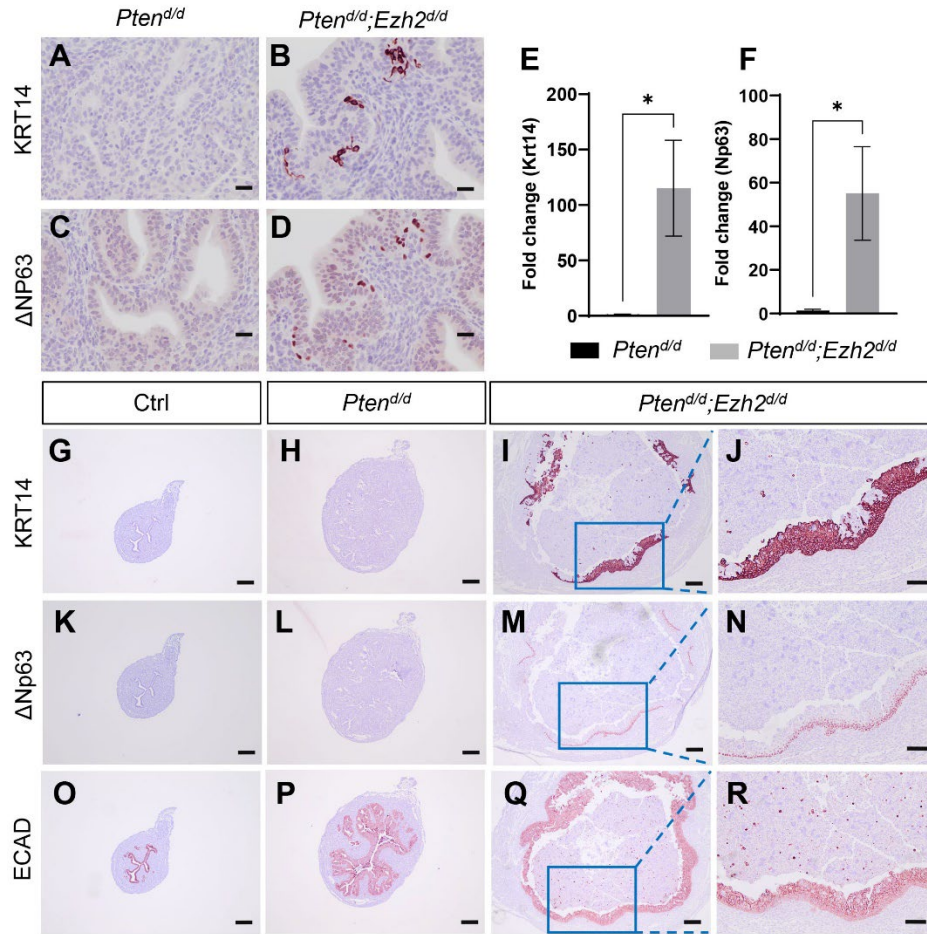


Figure 17. Deletion of *Ezh2* intensifies epithelial stratification in PTEN-depleted uteri. (A–D) Immunostaining of KRT14 and ΔNP63 using uteri from three-week-old *Pten^{d/d}* and *Pten^{d/d}; Ezh2^{d/d}* mice. (E,F) Transcript levels of *Krt14* and *ΔNp63* in uterine epithelia isolated from three-week-old *Pten^{d/d}* and *Pten^{d/d}; Ezh2^{d/d}* mice. $n = 4–5$. Data are mean \pm s.e.m. * $p < 0.05$. Note that one sample from the *Pten^{d/d}* group had undetectable *ΔNp63* expression and was not included in panel (F). (G–R) Immunostaining of KRT14 (G–J), ΔNP63 (K–N), and ECAD (O–R) in uteri from one-month-old *Pten^{f/f}* (Ctrl), *Pten^{d/d}*, and *Pten^{d/d}; Ezh2^{d/d}* mice. Panels (J,N,R) represent high power images of the boxed areas of panels (I,M,Q), respectively. At least three independent samples were examined for each genotype. Scale bar = 20 μ m (A–D), 100 μ m (J,N,R), and 200 μ m (G–I,K–M,O–Q).

Hypoxia is implicated in endometrial cancer development [70, 208]. We found that hypoxia signals were mainly localized to the epithelial compartment of the uteri from *Pten^{d/d}* and *Pten^{d/d}; Ezh2^{d/d}* mice at one month of age (Figure 18E–L), with background levels of staining in the control uteri (Figure 18A–D). Interestingly, reduced hypoxia was observed in *Pten^{d/d}; Ezh2^{d/d}*

uteri compared with *Pten*^{d/d} uteri (Figure 18E–L). As relieving tumor hypoxia enhances the tumoricidal activity of neutrophils in *Pten*^{d/d} mouse model [209], lower hypoxic levels in the *Pten*^{d/d}; *Ezh2*^{d/d} uteri may facilitate the debridement of cancer epithelia by neutrophils, resulting in increased intraluminal accumulation of cancer cells/debris.

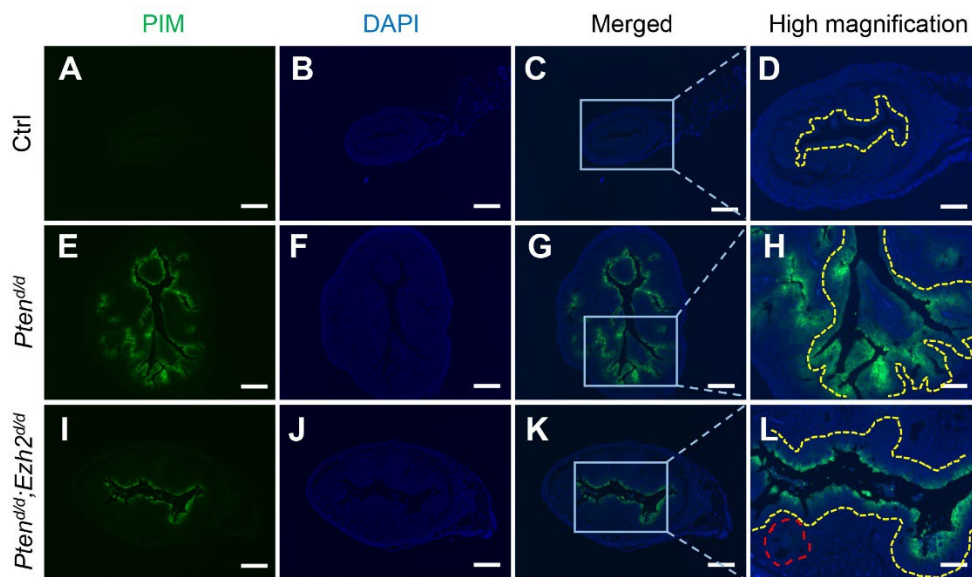


Figure 18. Reduced hypoxia in the uteri of *Pten*^{d/d}; *Ezh2*^{d/d} mice compared with *Pten*^{d/d} mice. (A–L) Immunofluorescence staining of pimonidazole protein adducts using one-month-old *Pten*^{fl/fl} (Ctrl), *Pten*^{d/d}, and *Pten*^{d/d}; *Ezh2*^{d/d} uteri. PIM, pimonidazole protein adducts. Panels (D,H,L) are high power images of the boxed areas of panels (C,G,K), respectively. Yellow dashed lines denote the luminal epithelial component or epithelia adjacent to the uterine lumen. Note the reduced extent of epithelial hypoxia and diminished hypoxia in the glandular-like component (red dashed line) in *Pten*^{d/d}; *Ezh2*^{d/d} uteri. At least three independent mice were examined for each genotype. DAPI was used to counterstain the nuclei. Scale bar = 250 μ m (A–C,E–G,I–K) and 100 μ m (D,H,L).

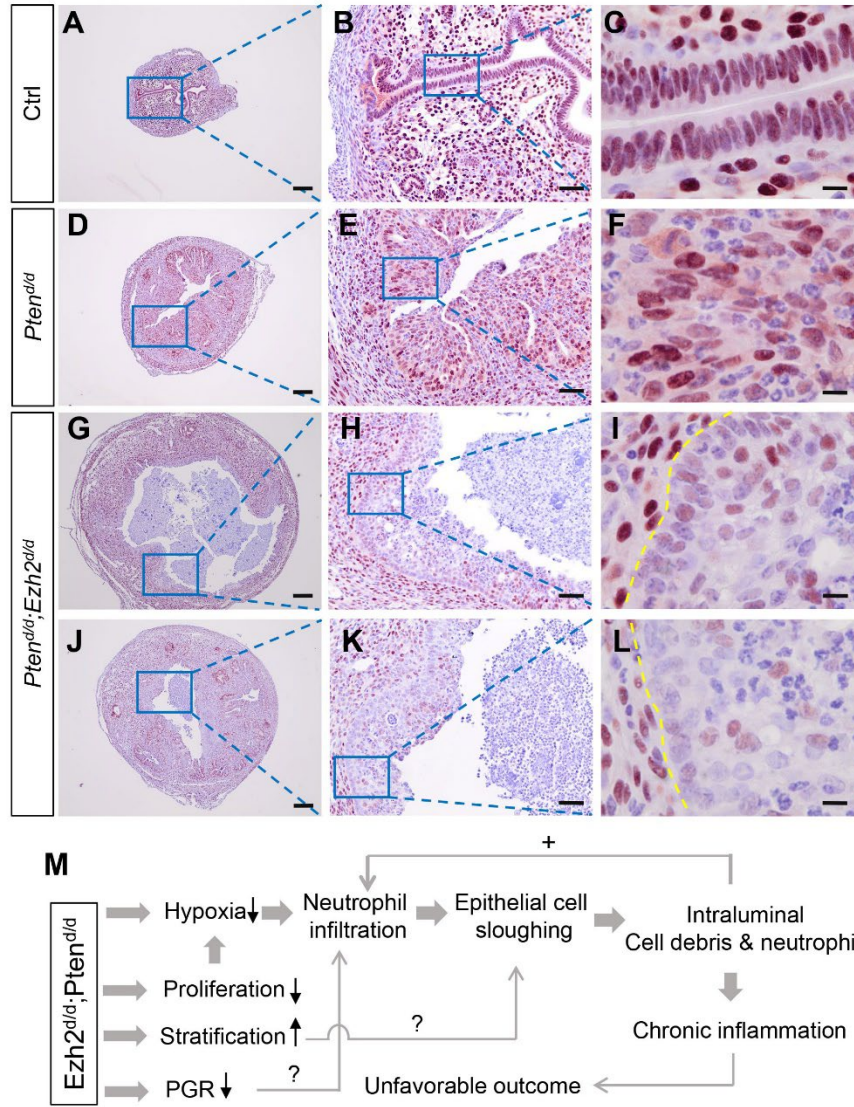


Figure 19. Expression of PGR in *Pten^{d/d}* and *Pten^{d/d}; Ezh2^{d/d}* uteri. (A–L) Immunostaining of PGR in the uteri of 1-month-old *Pten^{fl/fl}* (Ctrl), *Pten^{d/d}*, and *Pten^{d/d}; Ezh2^{d/d}* mice. Panels (G–I) and Panels (J–L) represent two independent *Pten^{d/d}; Ezh2^{d/d}* mice with different disease progression. Panels (B,E,H,K) are high power images of the boxed areas of panels (A,D,G,J), respectively. Panels (C,F,I,L) are high power images of the boxed areas of panels (B,E,H,K), respectively. At least three independent samples were examined for each genotype. Scale bar = 10 μ m (C,F,I,L), 50 μ m (B,E,H,K), and 200 μ m (A,D,G,J). Yellow dashed lines demarcate the border between uterine stroma and epithelia. (M) A hypothetical model of endometrial cancer development in mice harboring uterine deletion of both *Pten* and *Ezh2*.

Progesterone receptor signaling plays important roles in endometrial cancer development, and loss of PGR is linked to the development of aggressive endometrial cancer [210, 211].

Immunostaining was performed to examine whether PGR expression was altered in *Pten*^{d/d}; *Ezh2*^{d/d} uteri. Results showed reduced PGR expression in the luminal epithelia of 1-month-old *Pten*^{d/d}; *Ezh2*^{d/d} mice (Figure 19G–L) compared with age-matched *Pten*^{d/d} mice and controls (Figure 19A–F). Hormone assays showed that the levels of estrogen and progesterone were comparable between *Pten*^{d/d}; *Ezh2*^{d/d} mice and *Pten*^{d/d} mice (Appendix A-12), indicating that ablation of EZH2 did not affect the levels of ovarian steroid hormones. As PGR signaling interacts with estrogen signaling that promotes neutrophil recruitment [212, 213], reduced PGR expression may alter estrogen action and inflammation. Collectively, these studies identified potential contributing factors to the unfavorable outcome of endometrial cancer lacking both PTEN and EZH2 (Figure 19M).

3 Discussion

Both *PTEN* and *EZH2* play important roles in endometrial cancer. The mutation of *PTEN* gene has been identified in ~20% of human endometrial hyperplasia, suggesting its importance in early cancer development [214]. The frequency of *PTEN* mutation appears to be associated with the histotypes of endometrial cancer, as *PTEN* mutation occurs in ~40% of endometrioid cancers but only 5% of serous or clear cell endometrial cancers [215]. *EZH2* is overexpressed in endometrial cancer, and its downregulation in endometrial cancer cells inhibits cell proliferation [39, 53]. A more recent study has identified a correlation between overexpression of *EZH2* in endometrial cancer patients and disease-free and overall survival [55]. This report has further demonstrated that silencing *EZH2* in endometrial cancer cells impairs the expression of growth-

related genes such as peroxiredoxin 6 (*PRDX6*) [55]. The mechanisms underlying EZH2 action in endometrial cancer progression remain incompletely understood. However, it appears that microRNA-361/Twist axis plays an important role in mediating the role of EZH2 in driving endometrial cancer development [54]. The evidence points to the therapeutic potential of targeting EZH2. However, EZH2 may also function as a tumor suppressor in myeloma and pancreatic tumor [216, 217]. It has been shown that loss of EZH2 in the mouse uterus enhances epithelial cell proliferation [218-220] and induces epithelial stratification [200]. Herein, we found that conditional deletion of both *Ezh2* and *Pten* reduced cell proliferation and uterine growth during early carcinogenesis but exacerbated intraluminal neutrophil accumulation and chronic inflammation during tumor progression, leading to an unfavorable disease outcome. Current results revealed dual roles of EZH2 in the development of endometrial cancer lacking *Pten*, a gene frequently mutated in endometrioid carcinomas.

The uterine weights of *Pten*^{d/d}; *Ezh2*^{d/d} mice were lower than those of *Pten*^{d/d} mice at three weeks of age, accompanied by reduced cell proliferation revealed by Ki67-staining. As EZH2 inhibits uterine epithelial cell proliferation and uterine growth [200, 218-220], our results suggest that EZH2 plays distinct roles in normal uterine epithelial cells versus malignant epithelial cells. Supporting the assumption that the role of EZH2 in PTEN-depleted epithelial cells differs from that in PTEN-expressing epithelial cells, it was reported that loss of PTEN or activation of AKT switches the tumor suppressive role of EZH2 to an oncogenic function [221]. Interestingly, AKT activation is also implicated in normal and estrogen-induced uterine epithelial cell proliferation [222]. These findings support a complex, yet contextually dependent, role of EZH2 in cancer development.

Neutrophils are the first-line defenders that actively participate in host defense, tissue damage, and inflammatory disease [223]. Tumor-associated neutrophils play important roles in tumor microenvironment, where N1 neutrophils are anti-tumorigenic and N2 neutrophils are pro-tumorigenic [206, 224]. The pro-tumorigenic action of neutrophils is generally associated with their effects on cancer cell invasion, extracellular matrix remodeling, and angiogenesis [224]. Although the oncogenic role of EZH2 has been documented, some *in vivo* experiments suggest a tumor-suppressive function of EZH2. One study showed that loss of EZH2 promotes Kras^{G12D}-driven oncogenesis in pancreatic cancer [217]. In another report, deletion of *Ezh2* accelerates Kras-driven lung adenocarcinoma in a mouse model [225]. In both cases, EZH2 appears to play a role in controlling inflammatory microenvironment [217, 225]. In the present study, we found that tumor burden was reduced in *Pten*^{d/d}; *Ezh2*^{d/d} mice during early tumor development, revealing an oncogenic role of EZH2 in endometrial cancer development. However, unfavorable cancer outcomes were observed in these mice compared with *Pten*^{d/d} mice. The latter effect is likely non-cell autonomous, as dysregulation of EZH2 in cancer cells is known to alter immune response [8]. Indeed, massive accumulation of intraluminal neutrophils is a hallmark of the endometrial cancer in *Pten*^{d/d}; *Ezh2*^{d/d} mice at nine weeks of age. Our finding is also consistent with a previous report that increased levels of intratumoral neutrophils correlate with a poor cancer outcome [226].

The underlying mechanisms that promote the heightened inflammation in *Pten*^{d/d}; *Ezh2*^{d/d} mice remain unclear. However, several important contributing factors were identified by the present study. First, we found reduced hypoxia in the uteri of *Pten*^{d/d}; *Ezh2*^{d/d} mice at 1 month of age.

Elegant studies have demonstrated that hypoxia increases neutrophil recruitment in endometrial cancer induced by PTEN depletion, which serves to restrain the development of endometrial cancer by debridement of the malignant cells [70, 209]. Interestingly, reduction of hypoxia causes attenuated neutrophil infiltration. However, these neutrophils gain more efficient capability of attacking cancer cells [209]. Loss of EZH2 limited the extent of hypoxia in *Pten^{d/d}*; *Ezh2^{d/d}* mice, likely enhancing the tumoricidal effect of neutrophils [209]. Intraluminal accumulation of cancer cells/debris would in turn stimulate neutrophil influx and cause heightened immune reactions, forming a vicious cycle and resulting in chronic inflammation and/or eliciting secondary infectious event. The exact reasons of how EZH2 ablation led to reduced hypoxia is unclear. However, increased vascularization in *Pten^{d/d}*; *Ezh2^{d/d}* uteri (Fang X and Li Q, unpublished observation) may be one of the reasons. Second, conditional deletion of *Ezh2* potentiated epithelial stratification in *Pten^{d/d}* mice. The uterus contains simple columnar epithelial cells expressing KRT8 but not KRT14 and p63 [227]. Current results showed that stratified epithelial markers KRT14 and Δ Np63 were expressed earlier in *Pten^{d/d}*; *Ezh2^{d/d}* uteri than *Pten^{d/d}* uteri, consistent with our previous finding that loss of EZH2 in the uterus promotes the development of basal cells and stratified epithelia [200]. The intensified epithelial stratification in *Pten^{d/d}*; *Ezh2^{d/d}* uteri likely reflected the additive effect of loss of EZH2 and PTEN. Uterine epithelial stratification is a pathological event that alters the polarity and function of epithelial cells [30, 228]. It is possible that epithelial stratification adversely impacts the progression of endometrial cancer due to altered epithelial cell properties. The role of epithelial stratification in endometrial cancer development in our model requires further investigation. Finally, it was found that epithelia adjacent to the uterine lumen had reduced expression of PGR in *Pten^{d/d}*; *Ezh2^{d/d}* mice at one month of age, when epithelial stratification intensified and marked

accumulation of intraluminal neutrophils occurred. PGR loss has been associated with increased cell proliferation and metastasis [210, 211]. PGR signaling antagonizes estrogen signaling during tumor development [229]. Estrogen is known to promote neutrophil recruitment during mammary involution or breast cancer development [212, 213]. Thus, it is tempting to speculate that the reduction of PGR expression is associated with estrogen-directed neutrophil infiltration and heightened inflammation, which merits further investigation.

Endometrial cancer in *Pten*^{d/d} mice is not metastatic to other organs even at 25–36 weeks of age [71, 202, 230]. However, dysregulation of several key regulators/signaling pathways may trigger metastasis. We have shown that conditional deletion of transforming growth factor β type 1 receptor (*Tgfb1*) in *Pten*^{d/d} mice promotes pulmonary metastases [71]. Lung metastasis was also reported in a mouse model where PTEN-ablated and K-ras expressed endometrial cancer cells were grafted [66]. In addition, conditional deletion of both *Pten* and dicer 1, ribonuclease type III (*Dicer1*) in the mouse uterus triggers adnexal metastasis [231]. EZH2 expression has been linked to endometrial cancer cell invasion and metastasis [53]. As mice conditionally overexpressing EZH2 are available [232], future investigations are needed to determine whether conditional overexpression of EZH2 in PTEN-depleted uteri impacts metastasis.

From a systems biology perspective, the functions of cells are achieved and coordinated by numerous genes/pathways within a highly interactive network [233]. Cancer may develop when perturbations of protein-protein interactions occur due to gene mutations [234]. Studies on protein-protein interaction networks in cancer may benefit cancer treatment by gaining a holistic view of mechanisms governing tumor development and discovering novel cancer drivers as well

as therapeutic targets [235, 236]. Recent studies have begun to explore protein-protein interaction networks in female reproductive cancers including endometrial cancer using an integrative computational approach [237]. Defining the interactome of endometrial cancer remains to be one of our key goals in the future.

The current study revealed dual roles of EZH2 in endometrial cancer development. We showed that ablation of EZH2 in the PTEN-inactivated endometrium reduced tumor burden during the early pathogenesis of endometrial cancer. However, these mice progressed to unfavorable disease condition, accompanied by intensified epithelial stratification, massive accumulation of intraluminal neutrophils, and heightened inflammation. These findings point to potentially unwanted effects of EZH2-targeted therapy in cancer treatment. EZH2 has been implicated as an important cancer target in different types of cancers. Several EZH2 inhibitors have been developed and tested in clinical trials, such as GSK2816126 and tazemetostat [238, 239]. No clinical trials of EZH2 inhibitors in endometrial cancer have been reported. The attenuation of early tumor growth upon *Ezh2* deletion in the current study suggests a therapeutic benefit by targeting EZH2 in endometrial cancer. However, the heightened inflammatory response and unfavorable disease outcome during tumor development strongly suggest that caution should be taken when designing anti-endometrial cancer strategies. Thus, stage-specific role of EZH2 should be considered. It is also tempting to postulate that a combination of EZH2 inhibitors and inflammatory modulators may be a possible approach to combat this most common gynecological disease.

Aim 3. A NOVEL MOUSE MODEL OF TESTICULAR GRANULOSA CELL TUMORS *

1 Materials and methods

1.1 Ethics statement

Animal use protocol for this study was approved by the Institutional Animal Care and Use Committee (IACUC) at Texas A&M University. All animals were handled in accordance with the guidelines by the IACUC of Texas A&M University.

1.2 Animals and tissue collection

Mice harboring a latent constitutively active TGFBR1 (*TGFBR1^{CA}*) were created as described [240, 241]. The *TGFBR1^{CA flox/flox}* mice were crossed to *Amhr2-Cre* line [242] to generate mice containing constitutively active TGFBR1 in the testes (*TGFBR1^{CA flox/+}; Amhr2-Cre*). These mice were termed TGFBR1-CA^{Acre}. Mice were on a mixed C57BL/6/129 background and were maintained by controlled light/dark cycles with free access to food and water. Testis samples were collected from both control and TGFBR1-CA^{Acre} males during developmental stages for histological and immunohistochemical analysis described below. Genotyping was performed using DNA extracted from mouse tails described previously [136, 240]. PCR products were separated on 1% agarose gels containing ethidium bromide and digital images captured using a VWR Gel Imager.

* Reprinted in slight modified form with permission from ‘A novel mouse model of testicular granulosa cell tumors.’ By Fang X, Ni N, Gao Y, Vincent DF, Bartholin L, Li Q. *Mol Hum Reprod.* 2018;24(7):343-356.

1.3 Histology

Testis samples from control and experimental mice were fixed in 10% neutral buffered formalin and/or Bouin's solution for histology and immunostaining. Tissue samples were processed and embedded using the histology core lab in the Department of Veterinary Integrative Biosciences at Texas A&M University. Hematoxylin and eosin (H & E) staining was performed using standard procedures.

1.4 Immunohistochemistry and Immunofluorescence

Immunohistochemistry (IHC) and Immunofluorescence (IF) were performed as described elsewhere [136, 143]. In brief, paraffin sections (5 μm) were deparaffinized in xylene, rehydrated in graded alcohol, and boiled in 10 mM citrate buffer (pH 6.0) for 20 min to retrieve the antigen. After antigen retrieval, sections were treated with 0.3% H_2O_2 for 30 mins to quench endogenous peroxidase activity. This step was only needed for IHC. Then, sections were sequentially incubated with non-immune serum (for IHC) or bovine serum albumin (for IF), primary antibodies with indicated dilutions (Table 7) overnight at 4 °C, and secondary antibodies conjugated with horseradish peroxidase (HRP; 1:300; for IHC) or Alexa Fluor 488/594 (1:400; for IF). Intervening washes were performed using Tris-buffered saline (TBS; pH 7.4). Following secondary antibody incubation, an avidin-biotin complex (ABC; Vector Laboratories, USA) was applied to amplify immunoreactive signals, which were developed using NovaRed substrate (Vector Laboratories; USA; for IHC). The sections were counterstained using hematoxylin, mounted with Permount, and examined under BX43F microscope (Olympus; USA). For IF, sections were directly mounted with ProLong Gold Slowfade media containing 4', 6-diamidino-2-phenylindole (DAPI; Invitrogen, USA) after incubation with secondary antibody. Fluorescence

signals were visualized using IX73 microscope (Olympus, USA) interfaced with an XM10 CCD camera and cellSens Software. Isotype-matched IgG controls were included to determine the staining background of the experiment.

Table 7. Primary antibodies for immunostaining and western blotting analyses (Aim 3).

Name	Manufacturer	Catalog no.	Host	IHC	IF	WB
ACTA2	Abcam, USA	Ab76549	mouse		1:2000	
YBX2	Abcam, USA	Ab33164	rabbit	1:500		
Ki67	Abcam, USA	Ab16667	rabbit	1:200		
Ki67	BD Biosciences	550609	Mouse		1:20	
DMRT1	Gift from Dr. David Zarkower	N/A	Rabbit		1:400	
GJA1	Cell Signaling Technology, USA	3512	rabbit	1:100		
SOX9	EMD Millipore, USA	Ab5535	rabbit	1:2000	1:1000	
WT1	Abcam, USA	Ab89901	rabbit	1:200		
INHA	Bio-Rad Laboratories, USA	MCA951ST	mouse	1:300		
FOXL2	Abcam, USA	Ab5096	goat	1:1500		1:1000
FOXO1	Cell Signaling Technology, USA	2880	rabbit	1:800		
CTNNB1	Cell Signaling Technology, USA	8480	rabbit	1:100		1:1000
CTNNB1	BD	610153	Mouse	1:100		
CYP17A1	Santa Cruz Biotechnology, USA	SC-46081	Goat	1:1500		
pSMAD2	Cell Signaling Technology, USA	3101s	rabbit			1:1000
pSMAD2	EMD Millipore, USA	Ab3849I	rabbit			1:1000
pSMAD3	Abcam, USA	Ab52903	rabbit			1:1000
SMAD2	Cell Signaling Technology, USA	5339	rabbit			1:1000
SMAD3	Abcam, USA	Ab28379	rabbit			1:1000
HA	Roche, Germany	1201381900	rat			1:500
GAPDH	Cell Signaling Technology, USA	2118	Rabbit			1:1000
ACTB	Sigma-Aldrich, USA	A3854	mouse			1:100000

1.5 Western blotting

Western blotting was conducted as described [243]. Protein lysates from mouse testis tissues were prepared using radioimmunoprecipitation assay (RIPA) buffer containing both proteinase and phosphatase inhibitors. Protein quantification was performed using bicinchoninic acid reagent purchased from Thermo Scientific (USA). Approximately 30 µg of proteins were loaded on each lane and separated by electrophoresis using 12% Mini-PROTEAN TGX Precast Gels (Bio-Rad Laboratories, USA). After electrophoresis, proteins were transferred to polyvinylidene difluoride (PVDF) membranes (Bio-Rad Laboratories; USA), which were subsequently incubated with primary antibodies at 4 °C overnight (Table 7). After being washed thoroughly, membranes were further incubated with HRP-conjugated anti-rabbit/rat/goat secondary antibodies (1:20,000; Jackson ImmunoResearch, USA). Immunoreactive signals were developed using Immobilon Western Chemiluminescent HRP Substrate (EMD Millipore, USA). Signals were visualized and captured using Kodak Image Station 4000 mm PRO digital scanner or Bio-Rad ChemiDoc MP Imaging System. Membranes were stripped and reprobed with antibody directed to beta actin (ACTB) or glyceraldehyde-3-phosphate dehydrogenase (GAPDH) (Table 7). Quantification of western blotting results was performed using NIH image J (version 1.51e).

1.6 RNA preparation and reverse transcription-real-time PCR

RNA samples were isolated from testes of control and TGFBR1-CA^{Acre} males using RNeasy Mini Kit (Qiagen, USA) based on instructions provided by the supplier. Potential genomic DNA contamination was eliminated by inclusion of an additional on-column DNase digestion step. Concentrations of the RNA preparations were determined by using NanoDrop Spectrophotometer ND 1000 (NanoDrop Technologies, USA). RNA samples were then

subjected to reverse transcription for cDNA synthesis [150]. Real-time PCR was performed using a CFX Connect Real-time PCR Detection System (Bio-Rad Laboratories; USA). The 10 μ l reaction system contained iTaq Universal SYBR Green Supermix (Bio-Rad Laboratories; USA) or TaqMan Universal PCR Master Mix, cDNA, and oligo primers [136]. Assays were performed in duplicates for each sample and a mean cycle threshold (CT) value was calculated. Primers for *Ccnd2* were 5'-GAGTGGGAACTGGTAGTGTTG-3' (forward) and 5'-CGCACAGAGCGATGAAGGT-3' (reverse) (PrimerBank ID 6753310a1) [244]. *Gjal* expression was analyzed using Taqman probe (Assay ID: Mm01179639_s1). Ribosomal protein L19 (*Rpl19*) was used as an internal control to normalize gene expression [150, 163]. A Taqman probe for *Rpl19* (Assay ID: Mm02601633_g1) was included in Taqman gene expression assays.

1.7 Statistical analysis

Comparisons of means between two groups were made using unpaired two-tail *t*-test. Data are presented as mean \pm standard error of the mean (s.e.m). Statistical significance was defined when *P* value is less than 0.05 and marked as **P* < 0.05, ***P* < 0.01, and ****P* < 0.001.

2 Results

2.1 Generation of mice with constitutively active TGFBR1 in testes using *Amhr2*-Cre recombinase

We previously reported that constitutive activation of TGFBR1 in the ovary using *Amhr2*-Cre recombinase leads to the development of ovarian sex cord-stromal tumors reminiscent of GrCTs [136]. Because *Amhr2*-Cre is also expressed in Sertoli and Leydig cells of the testis [245], we examined potential effects of overactivation of TGFBR1 on the development and function of the

testis by generating a mouse model harboring constitutively active TGFBR1 in the testis (Fig. 20A). As expected, TGFBR1^{CA} proteins were readily detectable in the testes of TGFBR1-CA^{Acrc} males but not controls by western blotting using anti-hemagglutinin (HA) antibody (Fig. 20B). These findings support that *Amhr2*-Cre drives the expression of TGFBR1^{CA} in mouse testes. TGFBR1 phosphorylates and activates SMAD2/3 signal transducers. To verify activation of TGFBSignaling in TGFBR1-CA^{Acrc} testes, we performed western blotting to determine the levels of phospho-SMAD2/3 in the testes of TGFBR1-CA^{Acrc} males. Results showed that the levels of both phospho-SMAD2 and phospho-SMAD3 were elevated in TGFBR1-CA^{Acrc} testes compared with controls (Fig. 20B). SMAD2, SMAD3, and beta-actin (ACTB) were included as controls (Fig. 20B).

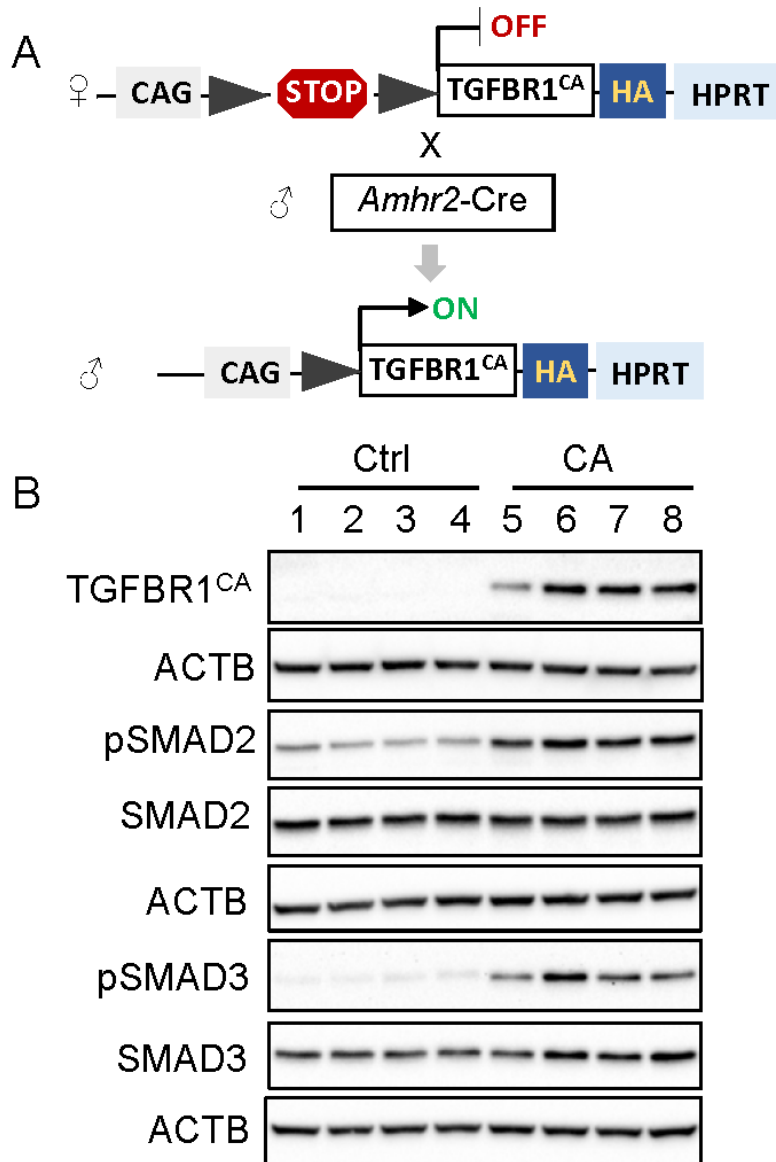


Figure 20. Constitutive activation of TGFBR1 in mouse testes. (A) A diagram depicting the generation of mice with constitutive activation of TGFBR1 using Amhr2-Cre recombinase. (B) Western blotting analysis of hemagglutinin (HA)-tagged TGFBR1^{CA}, phospho-SMAD2 and phospho-SMAD3 in the testes of control and TGFBR1-CA male mice at the age of 2 weeks. Each lane represents an independent testis sample. *n* = 4. SMAD2, SMAD3 and ACTB were included as controls.

2.2 TGFBR1-CA^{Acre} males develop testicular tumors with impaired spermatogenesis

Sterility was observed in TGFBR1-CA^{Acre} male mice when they were used as breeders. To determine the cause of sterility, we performed macroscopic and histological analyses of testes and epididymis of control and TGFBR1-CA^{Acre} males. Gross testicular tumors with hemorrhagic foci were observed in TGFBR1-CA^{Acre} mice around 2 months of age with full penetrance (Fig. 21A). In contrast, no tumors were observed in control mice (Fig. 21A). Testicular tumors progressed with age (Fig. 21B). Histological analysis of 2-month-old testes showed that while control mice had organized seminiferous tubules (Fig. 21C and E), TGFBR1-CA^{Acre} males developed testicular tumors resembling GrCTs (Fig. 21D and F), which were observed in the ovaries of TGFBR1-CA^{Acre} mice [136]. Microscopically, seminiferous tubules were displaced by circumscribed tumor nests containing poorly differentiated cells or granulosa-like cells (Fig. 21D and F and Appendix A-13B and D). Remnant seminiferous tubules lacking mature germ cells observed in control testes could be found near the edge of the testes (Appendix A-13A-D). Both histological results and immunofluorescence analyses using antibody directed to smooth muscle actin alpha (ACTA2) to mark the structure of epididymis demonstrated lack of sperm in the epididymis of TGFBR1-CA^{Acre} males (Fig. 21H and J), and this was in sharp contrast to wild type controls where abundant sperm/sperm DNA could be found within the epididymis (Fig. 21G and I). Analysis of testes from 5-6-month-old TGFBR1-CA^{Acre} males demonstrated development of more hemorrhagic tumors (Appendix A-13F and H), in contrast to control testes containing morphologically normal seminiferous tubules (Appendix A-13E and G). Thus, testicular tumors resulting from constitutive activation of TGFBR1 are detrimental to normal testis development and spermatogenesis.

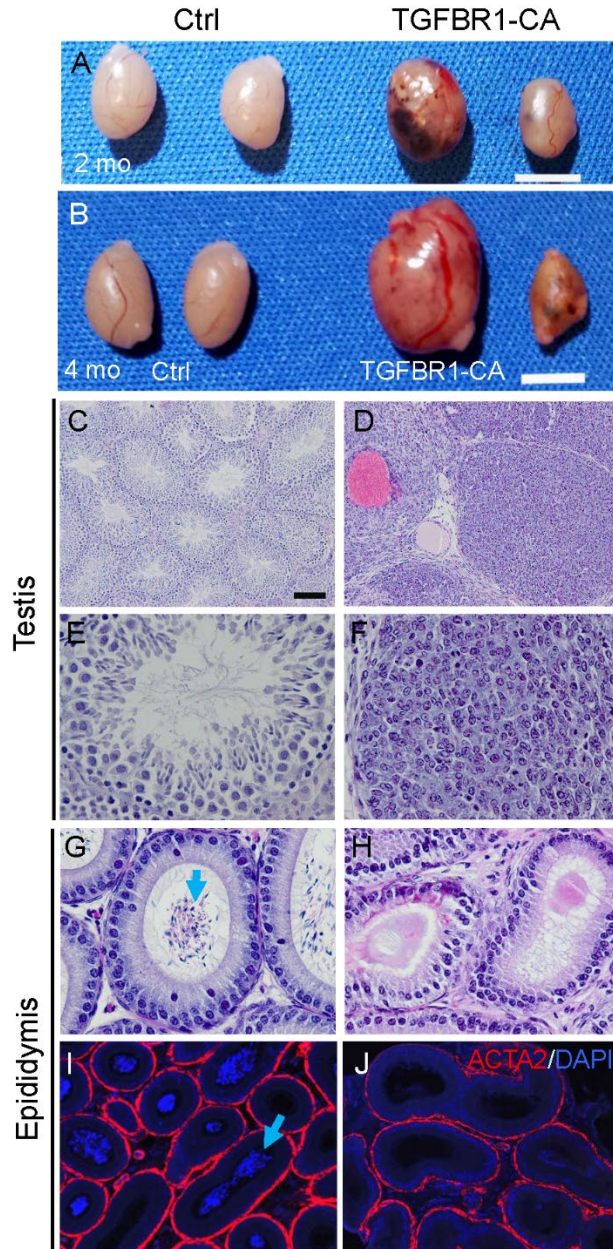


Figure 21. Sustained activation of TGFBR1 in the testis leads to sex cord-stromal tumor formation. (A, B) Development of testicular tumors in TGFBR1-CA^{Acree} males at the age of 2 and 4 months. Scale bars in panels (A and B) equal 500 μ m. Images of paired testes from two controls and two TGFBR1-CA^{Acree} mice are shown. Testes from control and TGFBR1-CA^{Acree} mice around 2 months of age were examined for testicular tumor development. Macroscopic and microscopic tumors were found in all TGFBR1-CA^{Acree} males ($n = 9$) but not controls ($n = 10$). (C–F) H and E staining of testes from control and TGFBR1-CA^{Acree} males at 2 months of age. Panels (E and F) represent higher magnification images for panels (C and D), respectively. (G–J) Loss of sperm in the epididymis of TGFBR1-CA^{Acree} mice revealed by haematoxylin and eosin

staining and immunofluorescence. Antibody directed to ACTA2 (red) was used to label seminiferous tubule structures. Note that controls had abundant sperm (G) and DNA (I) within the epididymis (blue arrows), while TGFBR1-CA^{Acre} males showed a lack of sperm/DNA in the epididymis (H and J). Scale bar is representatively shown in (C) and equals 25 μm (E–H), 50 μm (I and J) and 100 μm (C and D).

2.3 Disruption of testis development in postnatal TGFBR1-CA^{Acre} males

To define a timeline of testicular tumor development in the TGFBR1-CA^{Acre} males, we first performed histological analyses using testes from both control and TGFBR1-CA^{Acre} mice at the age of 1 week, 2 weeks, and 1 month. No histological difference was observed in the testes of TGFBR1-CA^{Acre} mice versus controls at 1 week of age (Appendix A-14A and B). Although the basic histological structure of seminiferous tubules appeared to be maintained in the TGFBR1-CA^{Acre} testes by 2 weeks of age (Appendix A-14C and D), microscopic lesions were evident within the testes of TGFBR1-CA^{Acre} mice at 1 month of age (Appendix A-14F and H). Compared with control testes consisting of highly organized seminiferous tubules (Appendix A-14E and G), loss of germ cells occurred within the seminiferous tubules of TGFBR1-CA^{Acre} testes (Appendix A-14F and H). Enrichment of Sertoli-like cells was observed in abnormal tubules of TGFBR1-CA^{Acre} mice (Appendix A-14F). Tumor nodules were readily discernible in TGFBR1-CA^{Acre} testes at this stage (Appendix A-14H). The histological findings were confirmed by immunohistochemical staining of Y box protein 2 (YBX2, also known as MSY2), a marker for germ cells [246], and Ki67 (a marker for cell proliferation). YBX2 was abundantly expressed in germ cells within seminiferous tubules in control testes (Fig. 22A). However, loss of YBX2-positive cells was pronounced in the seminiferous tubules of TGFBR1-CA^{Acre} males at 1 month of age (Fig. 22B). The adverse effect of constitutive activation of TGFBR1 on germ cell production could be observed at 2 weeks (Appendix A-14I and J). Moreover, the neoplastic tumor foci contained proliferative cells, evidenced by intense staining of Ki67 versus controls

(Fig. 22C and D). Enhanced cell proliferation of TGFBR1-CA^{Acre} testes was further supported by upregulation of cyclin D2 (CCND2) protein and transcripts (Fig. 22E and F). Interestingly, double immunofluorescence of Ki67 and SOX9 demonstrated colocalization of Ki67 and SOX9, a Sertoli cell marker, in 1-month-old TGFBR1-CA^{Acre} testes (yellow/orange labelling; Fig. 22J-L), in sharp contrast to control testes where SOX9 and Ki67 signals did not overlap (Fig. 22G-I). A similar result supporting Sertoli cell proliferation in TGFBR1-CA^{Acre} testes was found using 2-week-old mice (Appendix A-15). Since Sertoli cells stop proliferating around 2 weeks after birth in mice [247], our results indicate that sustained activation of TGFBR1 extends the proliferation of Sertoli cells. As gap junction protein alpha 1 (GJA1), also known as Connexin 43, is implicated in Sertoli cell development and conditional loss of GJA1 in Sertoli cells impedes the differentiation but extends the proliferation of Sertoli cells [248], we examined the expression of GJA1 in TGFBR1-CA^{Acre} testes to determine whether altered Sertoli cell proliferation is associated with reduced expression of GJA1. A significant change of *Gjal* mRNA abundance was not found in the testes of TGFBR1-CA^{Acre} mice at 2 weeks of age (Appendix A-16A), although localization of GJA1 proteins appeared to be increased in cells within the basal region of the seminiferous cord (Appendix A-16B and C). In contrast, *Gjal* mRNA expression was markedly elevated in the testes of 1-month-old TGFBR1-CA^{Acre} mice (Appendix A-16D), with abundant GJA1 immunoreactive signals detected in the TGFBR1-CA^{Acre} testes compared with controls (Appendix A-16E and F). These results are in concordance with reports that TGFB upregulates GJA1 expression in human granulosa cells and trophoblast cells [249, 250] and suggest that altered Sertoli cell proliferation in TGFBR1-CA^{Acre} mice is not a result of deficient production of GJA1.

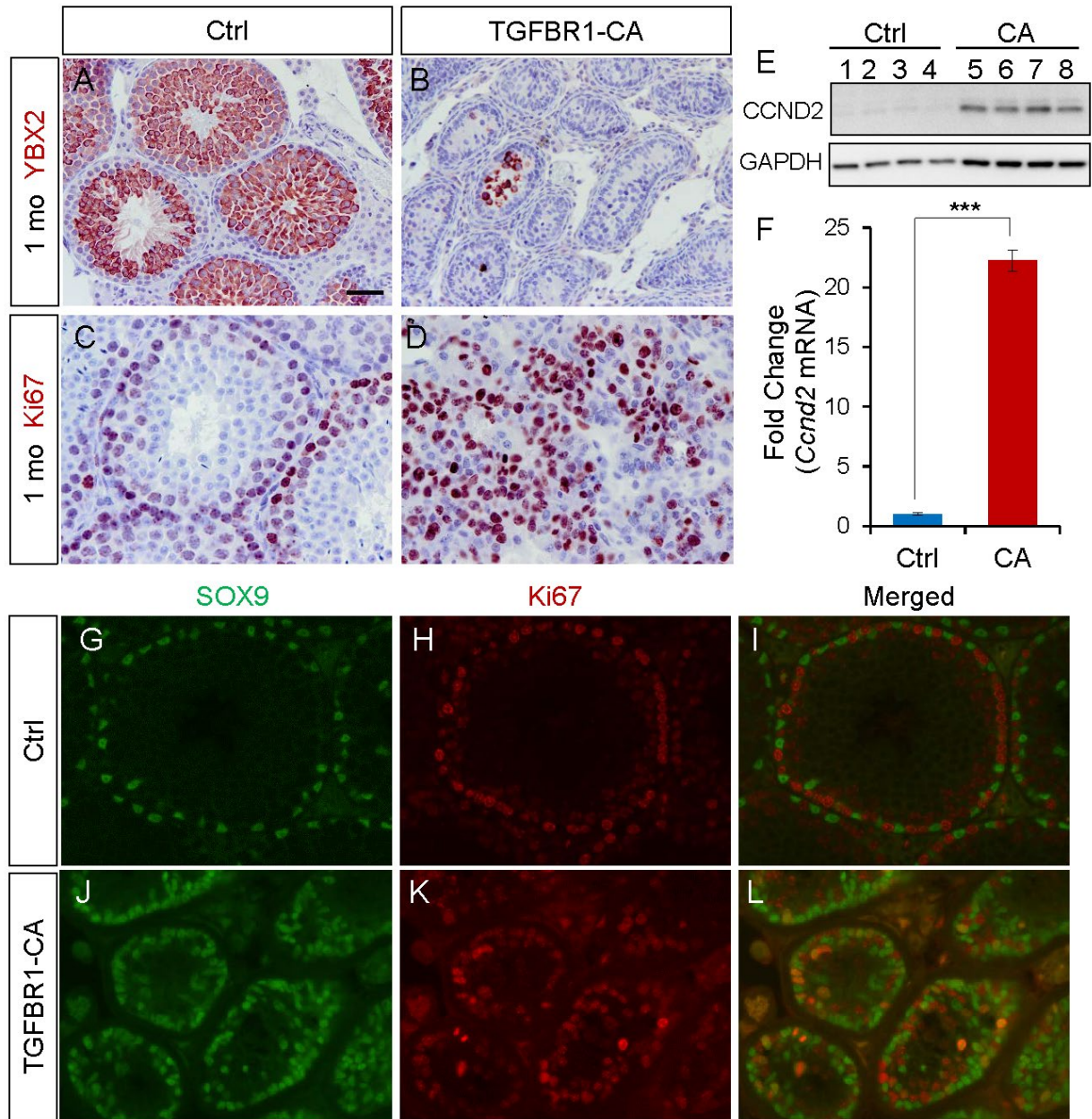


Figure 22. Depletion of germ cells and alteration of cell proliferation in the testes of TGFBR1-CA^{Acre} males. (A–D) Immunostaining of YBX2 and Ki67 in the testes of control and TGFBR1-CA^{Acre} mice at 1 month of age. Note the presence of abundant YBX2-positive germ cells within the seminiferous tubules in controls (A). However, loss of YBX2-positive cells was observed in TGFBR1-CA^{Acre} testes (B). Meanwhile, tumor foci were positively stained for Ki67 (D), indicative of cell proliferation. Three mice per group were examined. (E) Western blotting analysis of CCND2 expression in testes of 1-month-old control and TGFBR1-CA^{Acre} males. Each lane represents an independent testis sample. $n = 4$. (F) Increased expression of *Ccmd2* transcripts in TGFBR1-CA^{Acre} testes versus controls using real-time PCR. Data are presented as mean \pm SEM. $n = 5$. *** $P < 0.001$. (G–L) Immunofluorescence staining of SOX9 and Ki67

using testes from control and TGFBR1-CA^{Acrc} males at 1 month of age. Note the presence of double positive cells (yellow/orange) in TGFBR1-CA^{Acrc} testes (L) but not controls (I). Scale bar is representatively shown in (A) and equals 25 μm (C, D and G–L) and 50 μm (A and B).

To further probe the cellular and molecular alterations resulting from constitutive activation of TGFBR1 in mouse testes, we performed immunofluorescence using antibodies directed to SOX9 and ACTA2 (Fig. 23). Results showed that ACTA2-labeled seminiferous tubules (green) in the testes of TGFBR1-CA^{Acrc} were structurally comparable to those of controls at 2 weeks of age, except for disorganized arrangement of Sertoli cells labeled by SOX9 (red; Fig. 23A-F). In accordance with the histological observation of enrichment of Sertoli-like cells in the dysplastic seminiferous tubules in 1-month-old TGFBR1-CA^{Acrc} males (Appendix A-16F), markedly disorganized arrangement of SOX9-positive cells was found within these abnormal tubules (Fig. 23G-I). This result also provided indirect support for the aforementioned observation of germ cell depletion in TGFBR1-CA^{Acrc} testes. In addition, SOX9 staining was low to undetectable in tumor foci/nodules, in contrast to the strong immunoreactive signals of SOX9 observed in adjacent dysplastic tubules (Fig. 23J-L). Therefore, these studies suggest potential loss of SOX9 expression in tubule-like structures/neoplastic nodules during tumor development and progression.

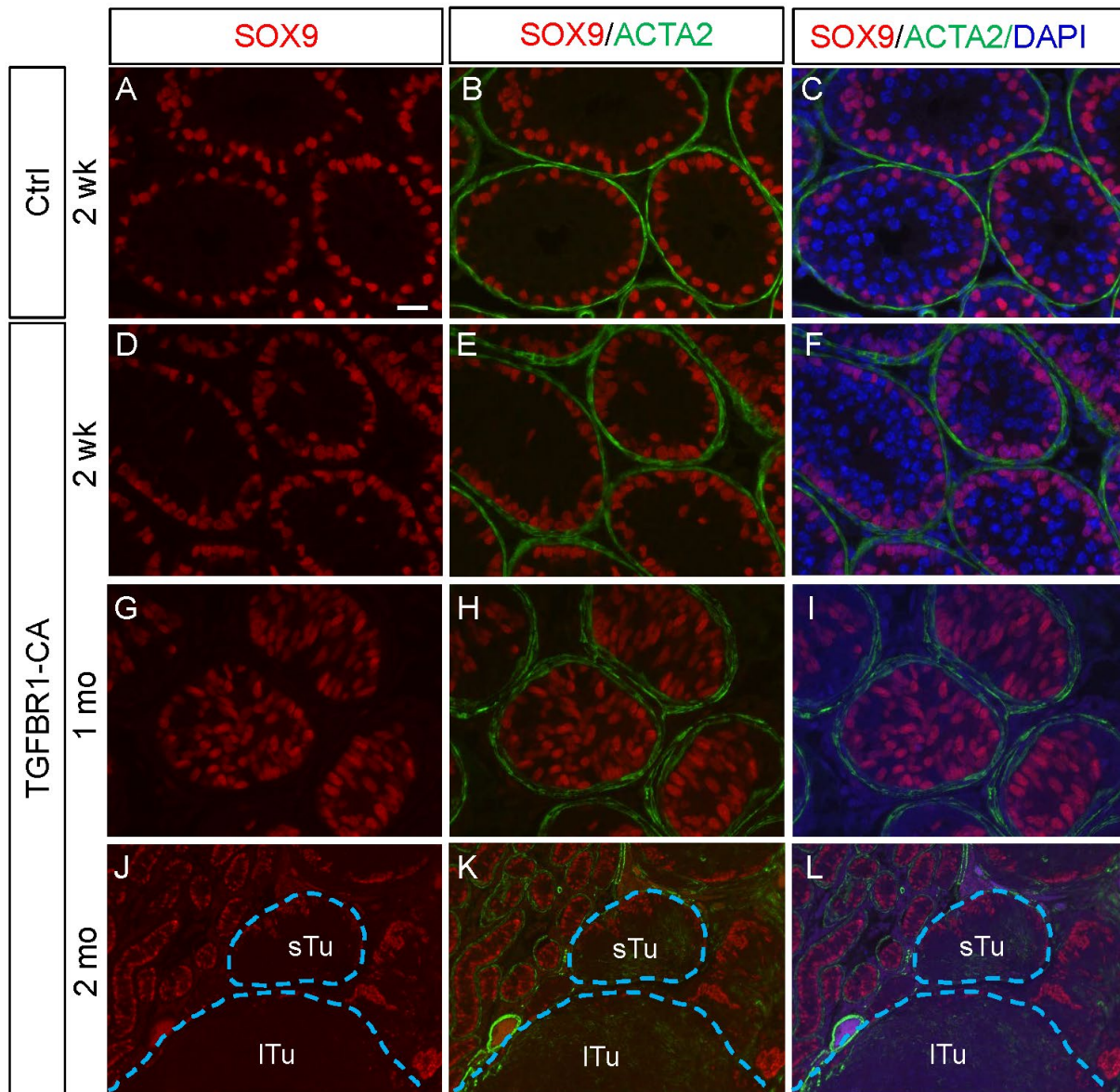


Figure 23. Immunofluorescence analysis of testicular tumor development in TGFBFR1-CA^{Acre} males. (A–L) Immunofluorescence staining of SOX9 and ACTA2 using testes from control and TGFBFR1-CA^{Acre} males at the age of 2 weeks, 1 month and 2 months. Note that seminiferous tubules in the testes of TGFBFR1-CA^{Acre} males were structurally comparable to those of controls at 2 weeks of age (A–F), except for disorganized arrangement of Sertoli cells. However, at 1 month of age, abnormal seminiferous tubules containing dramatically disorganized arrangement of SOX9-positive cells were found in TGFBFR1-CA^{Acre} testes (G–I). Minimal expression of SOX9 was observed in testicular tumor foci/nodules of TGFBFR1-CA^{Acre} mice, in sharp contrast to the adjacent abnormal tubules consisting of SOX9-positive cells. Dotted blue lines mark small and large tumor foci/nodules (sTu/ITu). Results of immunofluorescence were verified by immunohistochemical staining of SOX9, in which three independent samples per group were used. Scale bar is representatively shown in (A) and equals 20 μ m (A–I) and 80 μ m (J–L).

2.4 Testicular tumors in TGFBR1-CA^{Acre} males express markers of GrCTs

As testicular tumors in TGFBR1-CA^{Acre} mice histologically resembled ovarian GrCTs, we examined expression of several granulosa cell markers that are expressed by GrCTs including inhibin alpha (INHA), forkhead box O1 (FOXO1), and FOXL2 within the testes of TGFBR1-CA^{Acre} males. Immunohistochemistry revealed that testicular tumor nodules in 2-month-old TGFBR1-CA^{Acre} mice were positively stained for INHA (Fig. 24B and C), FOXO1 (Fig. 24E and F), and FOXL2 (Fig. 24H and I) compared with controls (Fig. 24A, D, and G). Notably, FOXL2 is a granulosa cell lineage marker expressed in the ovary but not the testis [251]. To determine the temporal expression of FOXL2 in TGFBR1-CA^{Acre} testes, we examined mice at 1 month of age, when microscopic tumor foci were detectable (Appendix A-16H). Interestingly, FOXL2 staining was found in some abnormal seminiferous tubules or tumor nodules in TGFBR1-CA^{Acre} testes (Fig. 24K and L), in stark contrast to control testes which did not express FOXL2 (Fig. 24J). Representative negative controls using isotype-matched IgGs are depicted in Appendix A-17. Supporting the immunohistochemistry findings, protein bands of FOXL2 were only detected in the testes of TGFBR1-CA^{Acre} mice but not those of controls by western blotting (Fig. 24M). These results indicate that constitutive activation of TGFBR1 in the testis may alter Sertoli cell fate.

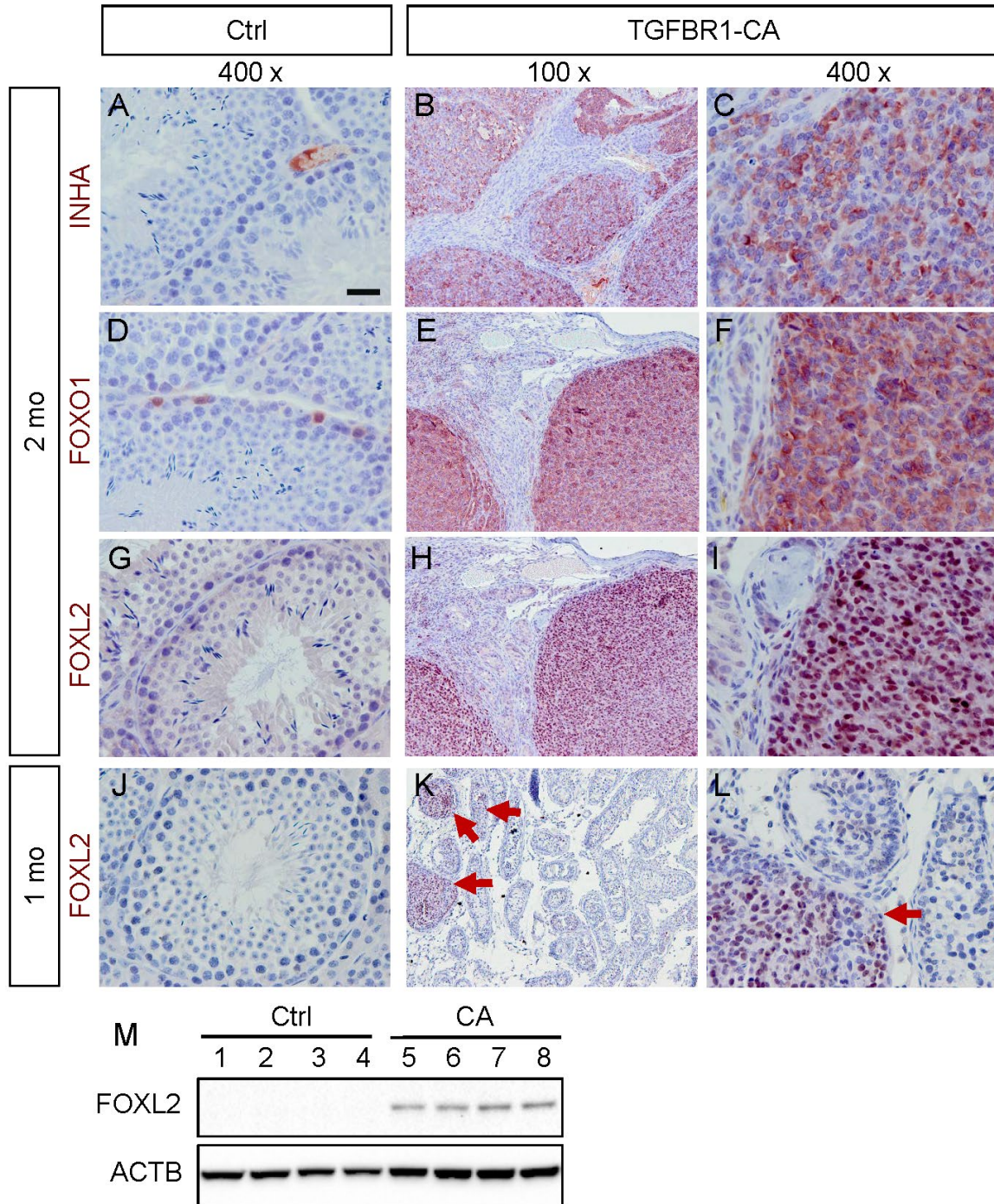


Figure 24. Testicular tumors of TGFBR1-CA^{Acre} males express granulosa cell tumor markers. (A–I) Immunostaining of INHA, FOXO1 and FOXL2 in control and TGFBR1-CA^{Acre} testes at 2 months of age. Note that intensive immunoreactive signals for INHA, FOXO1 and FOXL2 were detected in testicular tumors of TGFBR1-CA^{Acre} males compared with controls (A–I). (J–L) Immunostaining of FOXL2 in control and TGFBR1-CA^{Acre} testes at 1 month of age. Note that

FOXL2 was not expressed in control testis (J) but localized to some tumor foci (K and L; red arrows). Panels (C, F, I and L) represent higher magnification images for corresponding panels (B, E, H and K). Three mice per group were examined. Scale bar is representatively shown in (A), and equals 25 μm (A, C, D, F, G, I, J and L) and 100 μm (B, E, H and K). (M) Western blotting analysis of FOXL2 in 1-month-old control and TGFBR1-CA^{Acre} testes. Note that the FOXL2 proteins were only detected in the testes of TGFBR1-CA^{Acre} males. Each lane represents an independent testis sample. $n = 4$.

It has been well established that doublesex and mab-3 related transcription factor 1 (DMRT1) maintains testis identity; and Sertoli cells could be reprogrammed to granulosa cells in the testis upon deletion of *Dmrt1* due to activation of *Foxl2* and other female promoting genes [252, 253]. In postnatal mouse testis, DMRT1 is expressed in mitotic spermatogonia and Sertoli cells [252]. To explore whether the aberrant expression of FOXL2 in our mouse model is associated with loss of DMRT1 expression, we performed immunohistochemical analysis of DMRT1 and immunofluorescence of DMRT1 and FOXL2 using testes from control and TGFBR1-CA^{Acre} mice. DMRT1 was expressed in the testes from both control and TGFBR1-CA^{Acre} mice at 2 weeks of age (Appendix A-18A). At 1 month of age, expression of FOXL2 could be detected in a subset of DMRT1-negative cells within the seminiferous cord of TGFBR1-CA^{Acre} mice (Fig. 25B, E, H, and K) or in scattered cells within tumor nodules where many cells were positive for FOXL2 (Fig. 25C, F, I, and L). In certain tumor foci where FOXL2 positive cells prevailed, no DMRT1 was detected (data not shown). In contrast, immunoreactive signals for FOXL2 were not detected in control testes (Fig. 25A, D, G, and J). These results provide circumstantial evidence supporting a potential link between loss of DMRT1 and altered Sertoli cell fate in TGFBR1-CA^{Acre} testes.

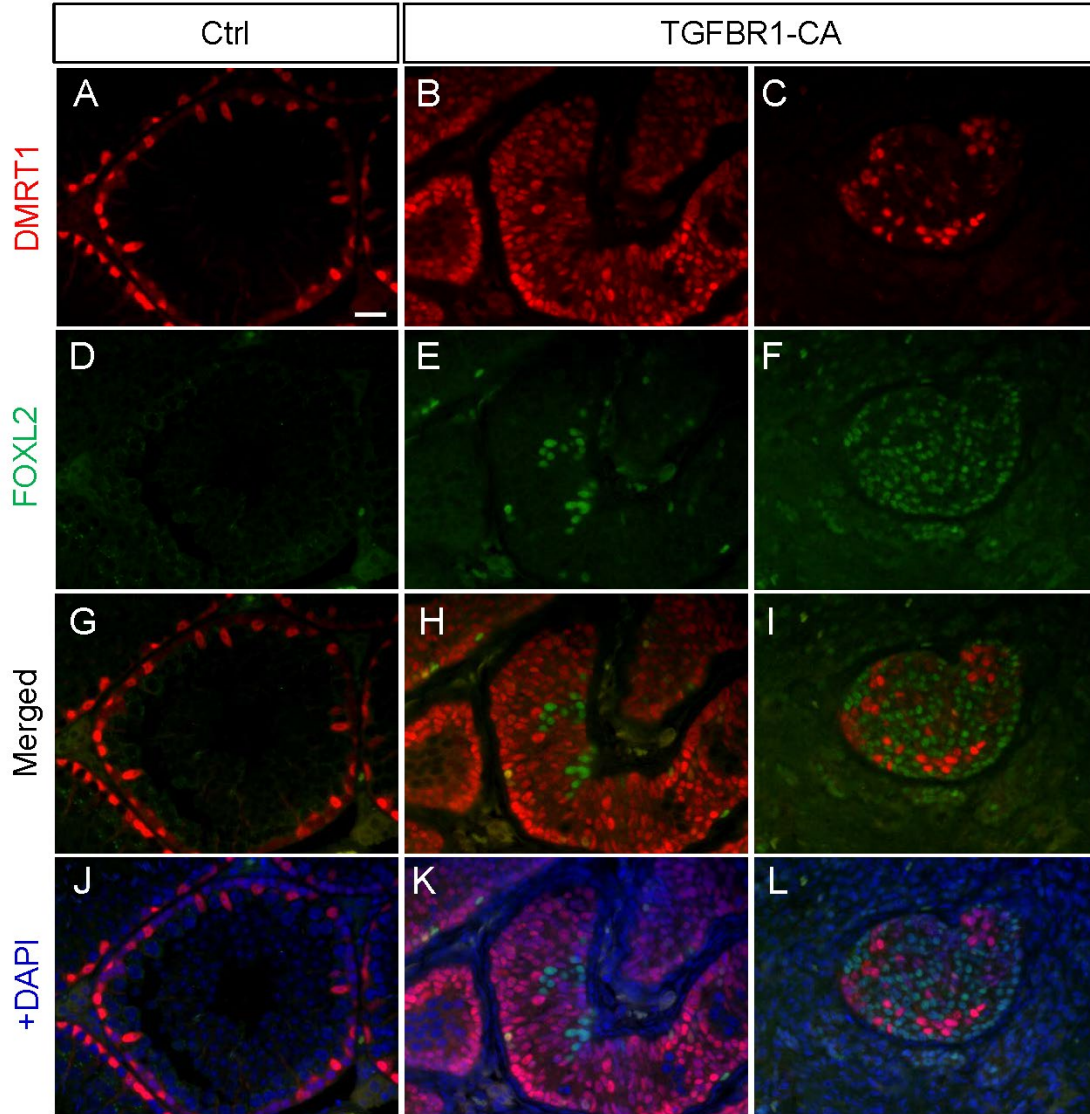


Figure 25. Immunofluorescence analysis of DMRT1 and FOXL2 distribution during testicular tumor development. (A–L) Immunofluorescence staining of DMRT1 and FOXL2 using testes from control and TGFBR1-CA^{Acre} males at the age of 1 month. Note that while DMRT1 was readily detectable in control testes, FOXL2 specific signals were not observed as expected (A, D, G and J). Scattered FOXL2-positive cells were found within some abnormal tubules in TGFBR1-CA^{Acre} testes (B, E, H and K). Panels (C, F, I and L) show a small tumor nodule in which many tumor cells were positive for FOXL2 but lacked DMRT1 expression. Three independent samples per group were used. Scale bar is representatively shown in (A) and equals 20 μ m (A–L).

As mentioned above, tumor nodules in TGFBR1-CA^{Acrc} testes expressed minimal SOX9. However, loss of SOX9 may also occur during the development of Sertoli cell tumors [254]. To further determine whether tumor cells expressed other Sertoli cell markers, we examined Wilms tumor 1 (WT1), a Sertoli cell expressed protein that is detectable in mouse Sertoli cell tumors [254]. The results showed that WT1 was expressed in Sertoli cells of control testes and abnormal seminiferous tubules (Fig. 26A-D), but not the parenchyma of the tumors at 2 months of age (Fig. 26C and D). In addition, to elucidate whether the tumors expressed Leydig cell markers, we analyzed the expression of CYP17A1 [255]. Results showed that CYP17A1 was localized to Leydig cells in control testes (Fig. 26E and F). However, only scattered CYP17A1-positive cells were observed in testicular tumors of TGFBR1-CA^{Acrc} mice (Fig. 26G and H), supporting the finding that tumors were not derived from Leydig cells. These results collectively indicate that constitutive activation of TGFBR1 in the testis leads to development of sex cord-stromal tumors resembling GrCTs.

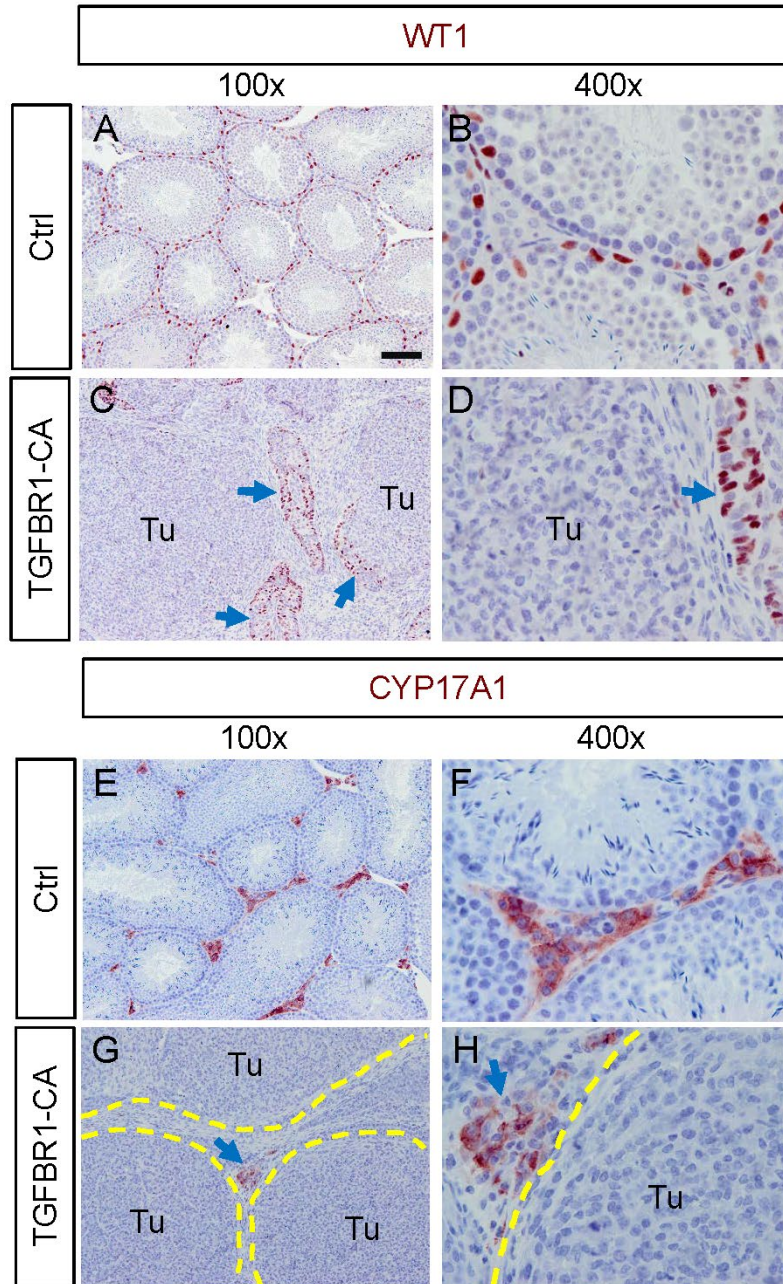


Figure 26. Analysis of Sertoli cell and Leydig cell markers in tumors from TGFBR1-CA^{Acre} males. (A–H) Immunostaining of WT1 (A–D) and CYP17A1 (E–H) in control and TGFBR1-CAAcre testes at 2 months of age. Panels (B, D, F and H) represent higher magnification images for corresponding panels (A, C, E and G). Note that tumor nodules (Tu) were not major sites for the expression of WT1 (C and D) or CYP17A1 (G and H) in TGFBR1-CA^{Acre} mice. Strong immunoreactive signals of WT1 were observed in Sertoli cells of controls (A and B) and abnormal seminiferous tubules of TGFBR1-CA^{Acre} mice (C and D; blue arrows). In contrast, expression of CYP17A1 was mainly found in Leydig cells of control testes (E and F) and inter-

nodular areas of testicular tumors (blue arrows; G and H). Dotted yellow lines in panels (G and H) mark the borders of tumor nodules. Testis samples from three mice per group were examined. Scale bar is representatively shown in (A) and equals 25 μm (B, D, F and H) and 100 μm (A, C, E and G).

2.5 WNT/CTNNB1 signaling is active in GrCTs resulting from TGFBR1 overactivation

Misregulation of WNT/ beta catenin (CTNNB1) signaling is implicated in tumorigenesis of GrCTs in multiple species including humans, horses, and mice [90, 256]. To understand how constitutive activation of TGFBR1 promoted the development of testicular tumors in TGFBR1-CA^{Acre} mice, we examined the expression of beta-catenin (CTNNB1) known to be involved in GrCT development [90, 91, 256]. Herein, we demonstrated that the levels of CTNNB1 were increased in testicular tumor tissues of TGFBR1-CA^{Acre} mice at 1 month of age compared with controls (Fig. 27A and B). Immunohistochemistry confirmed the results of western blotting by revealing extensive immunoreactive signals of CTNNB1 in testicular tumors of TGFBR1-CA^{Acre} males versus controls (Fig. 27C-E). Moreover, variable degrees of nuclear/cytoplasmic staining of CTNNB1 was observed in testicular tumor tissues (Fig. 27E). These results suggest that dysregulation of WNT/CTNNB1 signaling is potentially linked to GrCT development in TGFBR1-CA^{Acre} mice.

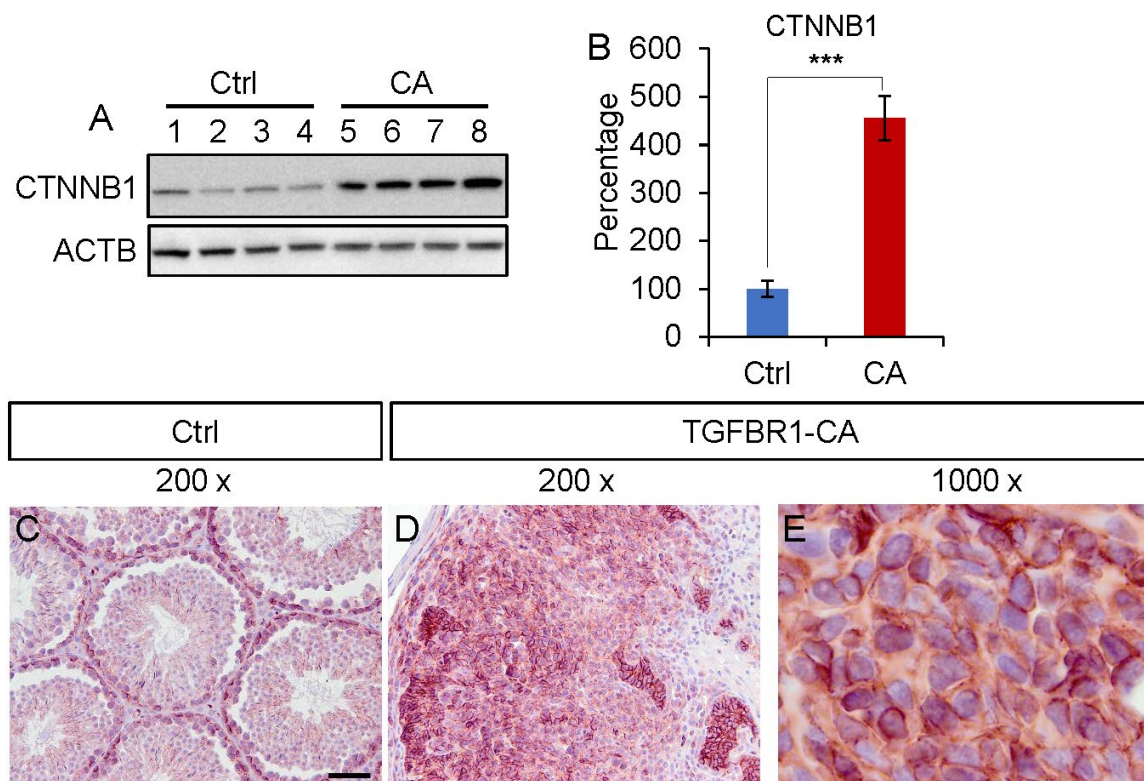


Figure 27. WNT/CTNNB1 signaling is active in GrCTs resulting from overactivation of TGFBR1. (A) Western blotting analysis of CTNNB1 expression in control and TGFBR1-CA^{Acre} testes of 1-month-old males. ACTB was included as an internal control. $n = 4$. (B) Quantification of the western blotting result shown in panel (A). Image J was used to calculate the ratio of CTNNB1 to ACTB for each sample. Results are presented as percentage, in which relative protein levels of control group are set to 100%. $n = 4$. Data are presented as mean \pm SEM. *** $P < 0.001$. (C–E) Immunostaining of CTNNB1 in tumor nodules of testes from TGFBR1-CA^{Acre} mice along with controls. Panel (E) represents a higher magnification image of panel (D). Three mice per group were examined. Scale bar is representatively shown in (C), and equals 10 μm (E) and 50 μm (C and D).

3 Discussion

GrCTs may arise from the testis with low incidence [98, 257]. The adult type GrCTs of the testis are extremely rare and occur after puberty, whereas the juvenile type GrCTs account for approximately 1-4% of total prepubertal testicular tumors and the majority of them develop

within the first 6 months [258-260]. While adult GrCTs are associated with somatic mutation [100], the juvenile type GrCTs may be associated with chromosomal abnormalities and gonadal dysgenesis [260, 261]. Animal models are useful to investigate the pathogenesis of this disease. Several mouse models are available for sex cord-stromal tumors, including but not limited to, mice with targeted deletion of *Inha* [116], *Smad1/5* [135], and BMP type 1 receptors [262], mice with overexpression of R-spondin 1 (*Rspo1*) [263], mice containing KRAS activation/*Pten* deletion and dominant-stable CTNNB1 [91], and mice with dominant-stable CTNNB1 or both dominant-stable CTNNB1 and *Pten* inactivation [90, 256]. Although it is challenging to faithfully model human GrCTs, mouse models have helped to gain significant insights into the pathobiology and signaling cascades of GrCT development.

We previously reported that overactivation of TGFBR1 using *Amhr2*-Cre to target mouse granulosa cells provokes the development of ovarian GrCTs [136]. Since *Amhr2*-Cre has been successfully used to conditionally target genes in somatic cells of the gonad in both sexes [90, 135, 137, 139, 242, 264, 265], we determined the phenotypic consequence of constitutive activation of TGFBR1 using *Amhr2*-Cre in the testis. Formation of microscopic tumor foci could be observed in testicular tubules of TGFBR1-CA^{Acree} males before puberty, suggesting balanced TGF β signaling is essential for testis development. Development of testicular tumors was accompanied by increased cell proliferation and depletion of germ cells. It was reported that TGF β superfamily signaling is active in the mouse testis, and the dosage of activin A maintains balanced numbers of Sertoli cells and germ cells [266]. As activin and TGF β signaling shares the same downstream SMADs, SMAD2/3, it appears plausible that loss of germ cells in TGFBR1-CA^{Acree} testes may be associated with altered SMAD2/3 signaling activity.

To strengthen the conclusion that testicular tumors resembled GrCTs, we examined the spatiotemporal localization of several protein markers including SOX9, CYP17A1, and FOXL2 for the respective Sertoli cells, Leydig cells, and granulosa cells. During the development of testicular GrCTs, we observed accumulation of Sertoli cells within seminiferous tubules, expression of Ki67 in Sertoli cells, and reduction of SOX9 expression but gain of FOXL2 expression in tumor nodules. The origin of testicular GrCT is poorly defined. However, based on the aforementioned findings and the observation that testicular GCTs arose within seminiferous tubules, it is tempting to postulate that Sertoli cells might transdifferentiate into granulosa tumor cells. Moreover, neither the histological feature nor the expression pattern of CYP17A1 supported that these tumors were Leydig cell tumors. Of note, the most common cell type of Leydig cell tumors is medium-sized hexagonal cell that has eosinophilic/vacuolar cytoplasm, irregular round/oval shaped nucleus, and recognizable cell border [267]. It was unclear whether gain of FOXL2 expression in TGFBR1-CA^{Acre} testes was a cause or consequence of testicular GCT development. It has been suggested that both granulosa cells and Sertoli cells share the same progenitors [140], and granulosa cells can transdifferentiate into Sertoli cells in adult female mice lacking FOXL2 [104]. Conversely, it is logic to speculate that the fate of Sertoli cells may be altered to resemble granulosa cells when FOXL2 is misregulated. Indeed, Sertoli cells could be reprogramed to granulosa cells upon conditional loss of DMRT1 due to activation of *Foxl2* and other female promoting genes [253]. Another study showed that constitutive activation of CTNNB1 in Sertoli cells promotes FOXL2 expression ectopically in the testis, resulting in the transformation of Sertoli cells into granulosa-like cells [268]. Moreover, upregulation of FOXL2 in testicular GrCTs was found in an independent mouse model, where CTNNB1 and AKT signaling was genetically enhanced [90]. Our finding is also in agreement

with the discovery that aberrant expression of FOXL2 links to the development of human juvenile GrCTs of the testis [105]. Our finding that gain of FOXL2⁺ cell population but loss of cells positive for DMRT1, a key protein that maintains Sertoli cell identity [252, 253] during tumor development in TGFBR1-CA^{Acrc} testes highlight the importance of TGFB pathway in maintaining the balance of “male-female” characteristics in the gonad. In view of the early onset of tumorigenesis, the potential of TGFBR1-CA^{Acrc} mice as a model for the juvenile GrCTs should be further explored.

Our current findings support an equally important role of TGFB signaling in the development of GrCTs in both testes and ovaries [136]. Somatic mutation of *FOXL2* has been identified as a hallmark of ovarian adult GrCTs [106]. *FOXL2* mutation was also found in testicular GrCTs [100]. Moreover, activation of TGFB signaling appears to be associated with GrCT development [131, 135, 262, 269, 270]. Interestingly, *FOXL2* mutation may impact activin/TGFβ signaling [108, 133, 271]. Previous studies indicated that unopposed activin signaling resulting from loss of inhibin promotes testicular tumor development partially through SMAD3, a critical regulator of sex cord-stromal tumor development [120]. Thus, SMAD mediated signaling likely contributes to testicular tumor development in our model system, as is supported by increased phospho-SMAD2/3 levels in the testes of TGFBR1-CA^{Acrc} males.

TGFβ signaling is complex and known to interact with other pathways. WNT pathway plays fundamental roles in normal cell functions and the development of multiple types of cancers [272]. Activation of the WNT/CTNNB1 pathway is involved in the pathogenesis of GrCTs; mice expressing a dominant-stable CTNNB1 mutant in ovarian granulosa cells develop GrCTs [256].

Simultaneous dysregulation of CTNNB1 and phosphatidylinositol 3-kinase (PI3K)/AKT pathways causes testicular GrCT formation [90]. Increased expression of phospho-AKT was found in both ovarian tumors [136] and testicular tumors (unpublished observation) from TGFBR1-CA^{Acre} mice. Moreover, the R-Spondin family proteins activate WNT signaling pathway [273]. Recent studies discovered that amplification of RSPO1 signaling leads to GrCT formation through altering the fate and properties of granulosa cells [263]. These studies collectively indicate that enhanced WNT signaling promotes GrCT development. Supporting interactions between TGF β and WNT signaling [274], we demonstrated that CTNNB1 expression was upregulated in testicular tumors. Moreover, WNT signaling appears to be active in gonadal tumors resulting from constitutive activation of TGFBR1. Of note, CTNNB1 signaling is suppressed during normal testis development, and WT1 negatively regulates CTNNB1 signaling [275]. Thus, lack of WT1 in tumor nodules of TGFBR1-CA^{Acre} testes may facilitate the expression of CTNNB1. While our studies uncovered a role of TGFBR1 activation in GrCT development, a potential regulatory mechanism of SMAD2/3-CTNNB1 activation in the pathogenesis of human GrCTs warrants further investigation. Illuminating the signaling network that underpins GrCT development will provide opportunities for designing new therapeutic interventions.

In summary, the current study created a new mouse model resembling testicular GrCTs. This mouse model may prove to be a useful addition to the mouse genetics toolkit for testicular GrCT research.

SUMMARY

The dissertation focused on two important topics in reproductive development and tumorigenesis. The first aim of dissertation was to identify the role of EZH2 in the uterus. We found Loss of EZH2 promoted stratification of uterine epithelia, an uncommon and detrimental event in the uterus. The abnormal epithelium expressed basal cell markers including p63, KRT5, KRT6A, and KRT14. These results suggest that EZH2 serves as a guardian of uterine epithelial integrity partially via inhibiting the differentiation of basal-like cells and preventing epithelial stratification. The observed epithelial abnormality was accompanied by fertility defects, altered uterine growth and function, and the development of endometrial hyperplasia. Thus, the *Ezh2* conditional knockout mouse model may be useful to explore mechanisms that regulate endometrial homeostasis and uterine function.

The second aim was to determine the impact of *Ezh2* deletion on the development of endometrial pathology induced by PTEN inactivation. Our results showed reduced tumor burden in *Pten^{d/d}; Ezh2^{d/d}* mice compared with that of *Pten^{d/d}* mice during early carcinogenesis. The decreased Ki67 index in EZH2 and PTEN-depleted uteri versus that in PTEN-depleted uteri indicated an oncogenic role of EZH2 during early tumor development. However, mice harboring uterine deletion of both *Ezh2* and *Pten* developed unfavorable disease outcome, accompanied by exacerbated epithelial stratification and heightened inflammatory response. The observed effect was non-cell autonomous and mediated by altered immune response evidenced by massive accumulation of intraluminal neutrophils, a hallmark of endometrial carcinoma in *Pten^{d/d}; Ezh2^{d/d}*

mice during disease progression. Hence, these results reveal dual roles of EZH2 in endometrial cancer development.

The third aim was to define the role of TGF β signaling activation in the pathogenesis of TGCTs. The premise was built on the importance of TGF β signaling in the pathogenesis of sex cord-stromal tumors. Mice harboring constitutively active TGFBR1 in the testes developed tumors resembling TGCT, a type of extremely rare tumor in the testis. The formation of testicular tumors led to altered cell proliferation, loss of germ cells, and defective spermatogenesis. Immunohistochemically, these tumors were positive for INHA, FOXO1, and more importantly, FOXL2, a protein specifically expressed in the ovary and required for normal granulosa cell differentiation and function. Consistent with the immunohistochemical findings, FOXL2 proteins were only detectable in testes of TGFBR1-CA^{Acrc} mice but not those of controls, suggesting potential alteration of Sertoli cell fate. To explore mechanisms underlying the tumor promoting effect of TGFBR1 overactivation, we examined the expression of CTNNB1. The results revealed increased expression of CTNNB1 in testicular tumors in TGFBR1-CA^{Acrc} mice. Collectively, this study uncovered tumorigenic function of enhanced TGF β signaling in the testis. This mouse model may prove to be a useful addition to the mouse genetics toolkit for TGCT research. The finding that dysregulation of TGF β signaling results in the development of TGCT supports a common origin between Sertoli cells and granulosa cells, and highlights the paramount importance of balanced TGF β signaling in reproduction and development.

Overall, results have identified mechanisms underlying reproductive development and tumorigenesis, opening new doors for the treatment of pregnancy failure and tumors in the reproductive system.

REFERENCES

1. Sauvageau, M. and G. Sauvageau, *Polycomb group proteins: multi-faceted regulators of somatic stem cells and cancer*. Cell Stem Cell, 2010. **7**(3): p. 299-313.
2. Vire, E., et al., *The Polycomb group protein EZH2 directly controls DNA methylation*. Nature, 2006. **439**(7078): p. 871-4.
3. Cao, R. and Y. Zhang, *The functions of E(Z)/EZH2-mediated methylation of lysine 27 in histone H3*. Curr Opin Genet Dev, 2004. **14**(2): p. 155-64.
4. Yang, Q.W., et al., *The polycomb group protein EZH2 impairs DNA damage repair gene expression in human uterine fibroids*. Biol Reprod, 2016. **94**(3): p. 69.
5. Wei, Y., et al., *CDK1-dependent phosphorylation of EZH2 suppresses methylation of H3K27 and promotes osteogenic differentiation of human mesenchymal stem cells*. Nat Cell Biol, 2011. **13**(1): p. 87-94.
6. Beguelin, W., et al., *EZH2 enables germinal centre formation through epigenetic silencing of CDKN1A and an Rb-E2F1 feedback loop*. Nat Commun, 2017. **8**(1): p. 877.
7. Wen, Y., et al., *Role of EZH2 in cancer stem cells: from biological insight to a therapeutic target*. Oncotarget, 2017. **8**(23): p. 37974-37990.
8. Gan, L., et al., *Epigenetic regulation of cancer progression by EZH2: from biological insights to therapeutic potential*. Biomark Res, 2018. **6**: p. 10.
9. Schwartz, Y.B. and V. Pirrotta, *Polycomb silencing mechanisms and the management of genomic programmes*. Nat Rev Genet, 2007. **8**(1): p. 9-22.
10. Gao, Z., et al., *PCGF homologs, CBX proteins, and RYBP define functionally distinct PRC1 family complexes*. Mol Cell, 2012. **45**(3): p. 344-56.

11. Geng, Z. and Z. Gao, *Mammalian PRC1 Complexes: Compositional Complexity and Diverse Molecular Mechanisms*. Int J Mol Sci, 2020. **21**(22).
12. Di Croce, L. and K. Helin, *Transcriptional regulation by Polycomb group proteins*. Nat Struct Mol Biol, 2013. **20**(10): p. 1147-55.
13. de Napoles, M., et al., *Polycomb group proteins Ring1A/B link ubiquitylation of histone H2A to heritable gene silencing and X inactivation*. Dev Cell, 2004. **7**(5): p. 663-76.
14. Wang, L., et al., *Hierarchical recruitment of polycomb group silencing complexes*. Mol Cell, 2004. **14**(5): p. 637-46.
15. Sugishita, H., et al., *Variant PCGF1-PRC1 links PRC2 recruitment with differentiation-associated transcriptional inactivation at target genes*. Nat Commun, 2021. **12**(1): p. 5341.
16. Cao, R., Y. Tsukada, and Y. Zhang, *Role of Bmi-1 and Ring1A in H2A ubiquitylation and Hox gene silencing*. Mol Cell, 2005. **20**(6): p. 845-54.
17. Kalb, R., et al., *Histone H2A monoubiquitination promotes histone H3 methylation in Polycomb repression*. Nat Struct Mol Biol, 2014. **21**(6): p. 569-71.
18. Maezawa, S., et al., *Polycomb directs timely activation of germline genes in spermatogenesis*. Genes Dev, 2017. **31**(16): p. 1693-1703.
19. Cohen, I., C. Bar, and E. Ezhkova, *Activity of PRC1 and Histone H2AK119 Monoubiquitination: Revising Popular Misconceptions*. Bioessays, 2020. **42**(5): p. e1900192.
20. Frangini, A., et al., *The aurora B kinase and the polycomb protein ring1B combine to regulate active promoters in quiescent lymphocytes*. Mol Cell, 2013. **51**(5): p. 647-61.

21. Gao, Z., et al., *An AUTS2-Polycomb complex activates gene expression in the CNS*. Nature, 2014. **516**(7531): p. 349-54.
22. Fischer, S., L.M. Weber, and R. Liefke, *Evolutionary adaptation of the Polycomb repressive complex 2*. Epigenetics Chromatin, 2022. **15**(1): p. 7.
23. Smits, A.H., et al., *Stoichiometry of chromatin-associated protein complexes revealed by label-free quantitative mass spectrometry-based proteomics*. Nucleic Acids Res, 2013. **41**(1): p. e28.
24. Glancy, E., C. Ciferri, and A.P. Bracken, *Structural basis for PRC2 engagement with chromatin*. Curr Opin Struct Biol, 2021. **67**: p. 135-144.
25. Conway, E., E. Healy, and A.P. Bracken, *PRC2 mediated H3K27 methylations in cellular identity and cancer*. Curr Opin Cell Biol, 2015. **37**: p. 42-8.
26. Hojfeldt, J.W., et al., *Accurate H3K27 methylation can be established de novo by SUZ12-directed PRC2*. Nat Struct Mol Biol, 2018. **25**(3): p. 225-232.
27. Margueron, R., et al., *Ezh1 and Ezh2 maintain repressive chromatin through different mechanisms*. Mol Cell, 2008. **32**(4): p. 503-18.
28. Li, Q., et al., *The antiproliferative action of progesterone in uterine epithelium is mediated by Hand2*. Science, 2011. **331**(6019): p. 912-6.
29. Gao, Y., S. Li, and Q. Li, *Uterine epithelial cell proliferation and endometrial hyperplasia: evidence from a mouse model*. Mol Hum Reprod, 2014. **20**(8): p. 776-86.
30. Filant, J., et al., *Fibroblast growth factor receptor two (FGFR2) regulates uterine epithelial integrity and fertility in mice*. Biol Reprod, 2014. **90**(1): p. 7.
31. Spencer, T.E., *Biological roles of uterine glands in pregnancy*. Semin Reprod Med, 2014. **32**(5): p. 346-57.

32. Filant, J. and T.E. Spencer, *Endometrial glands are essential for blastocyst implantation and decidualization in the mouse uterus*. Biol Reprod, 2013. **88**(4): p. 93.
33. Kelleher, A.M., et al., *Uterine glands impact uterine receptivity, luminal fluid homeostasis and blastocyst implantation*. Sci Rep, 2016. **6**: p. 38078.
34. Gray, C.A., et al., *Endometrial glands are required for preimplantation conceptus elongation and survival*. Biol Reprod, 2001. **64**(6): p. 1608-13.
35. Kelleher, A.M., et al., *Forkhead box a2 (FOXA2) is essential for uterine function and fertility*. Proc Natl Acad Sci U S A, 2017. **114**(6): p. E1018-E1026.
36. Grimaldi, G., et al., *Down-regulation of the histone methyltransferase EZH2 contributes to the epigenetic programming of decidualizing human endometrial stromal cells*. Mol Endocrinol, 2011. **25**(11): p. 1892-903.
37. Greathouse, K.L., et al., *Environmental estrogens differentially engage the histone methyltransferase EZH2 to increase risk of uterine tumorigenesis*. Mol Cancer Res, 2012. **10**(4): p. 546-57.
38. Colon-Caraballo, M., J.B. Monteiro, and I. Flores, *H3K27me3 is an Epigenetic Mark of Relevance in Endometriosis*. Reprod Sci, 2015. **22**(9): p. 1134-42.
39. Oki, S., et al., *Oncogenic histone methyltransferase EZH2: A novel prognostic marker with therapeutic potential in endometrial cancer*. Oncotarget, 2017. **8**(25): p. 40402-40411.
40. Siegel, R.L., et al., *Cancer Statistics, 2021*. CA Cancer J Clin, 2021. **71**(1): p. 7-33.
41. Di Cristofano, A. and L.H. Ellenson, *Endometrial carcinoma*. Annu Rev Pathol, 2007. **2**: p. 57-85.

42. Malik, T.Y., et al., *Comparison of Risk Factors and survival of Type I and Type II Endometrial Cancers*. Pak J Med Sci, 2016. **32**(4): p. 886-90.
43. Moore, K.N. and A.N. Fader, *Uterine papillary serous carcinoma*. Clin Obstet Gynecol, 2011. **54**(2): p. 278-91.
44. Lobo, F.D. and E. Thomas, *Type II endometrial cancers: A case series*. J Midlife Health, 2016. **7**(2): p. 69-72.
45. Horn, L.C., et al., *Histopathology of endometrial hyperplasia and endometrial carcinoma: an update*. Ann Diagn Pathol, 2007. **11**(4): p. 297-311.
46. Sherman, M.E., et al., *Risk factors and hormone levels in patients with serous and endometrioid uterine carcinomas*. Mod Pathol, 1997. **10**(10): p. 963-8.
47. Network, C.G.A.R., et al., *Integrated genomic characterization of endometrial carcinoma*. Nature, 2013. **497**(7447): p. 67-73.
48. Talhouk, A., et al., *A clinically applicable molecular-based classification for endometrial cancers*. Br J Cancer, 2015. **113**(2): p. 299-310.
49. Talhouk, A., et al., *Confirmation of ProMisE: A simple, genomics-based clinical classifier for endometrial cancer*. Cancer, 2017. **123**(5): p. 802-813.
50. Kommos, S., et al., *Final validation of the ProMisE molecular classifier for endometrial carcinoma in a large population-based case series*. Ann Oncol, 2018. **29**(5): p. 1180-1188.
51. Raffone, A., et al., *Tumor-infiltrating lymphocytes and POLE mutation in endometrial carcinoma*. Gynecol Oncol, 2021. **161**(2): p. 621-628.

52. Huvila, J., et al., *Molecular subtype diagnosis of endometrial carcinoma: comparison of the next-generation sequencing panel and Proactive Molecular Risk Classifier for Endometrial Cancer classifier*. Hum Pathol, 2021. **111**: p. 98-109.
53. Gu, Y., J. Zhang, and H. Guan, *Expression of EZH2 in endometrial carcinoma and its effects on proliferation and invasion of endometrial carcinoma cells*. Oncol Lett, 2017. **14**(6): p. 7191-7196.
54. Ihira, K., et al., *EZH2 inhibition suppresses endometrial cancer progression via miR-361/Twist axis*. Oncotarget, 2017. **8**(8): p. 13509-13520.
55. Roh, J.W., et al., *Clinical and biological significance of EZH2 expression in endometrial cancer*. Cancer Biol Ther, 2020. **21**(2): p. 147-156.
56. Alldredge, J.K. and R.N. Eskander, *EZH2 inhibition in ARID1A mutated clear cell and endometrioid ovarian and endometrioid endometrial cancers*. Gynecol Oncol Res Pract, 2017. **4**: p. 17.
57. Takeda, T., et al., *ARID1A gene mutation in ovarian and endometrial cancers (Review)*. Oncol Rep, 2016. **35**(2): p. 607-13.
58. Jia, N., et al., *Enhancer of zeste homolog 2 is involved in the proliferation of endometrial carcinoma*. Oncol Lett, 2014. **8**(5): p. 2049-2054.
59. Zhou, J., et al., *Overexpression of enhancer of zeste homolog 2 (EZH2) and focal adhesion kinase (FAK) in high grade endometrial carcinoma*. Gynecol Oncol, 2013. **128**(2): p. 344-8.
60. Gui, T., et al., *TCF3 is epigenetically silenced by EZH2 and DNMT3B and functions as a tumor suppressor in endometrial cancer*. Cell Death Differ, 2021. **28**(12): p. 3316-3328.

61. Eskander, R.N., et al., *Inhibition of enhancer of zeste homolog 2 (EZH2) expression is associated with decreased tumor cell proliferation, migration, and invasion in endometrial cancer cell lines*. Int J Gynecol Cancer, 2013. **23**(6): p. 997-1005.
62. Urick, M.E. and D.W. Bell, *Clinical actionability of molecular targets in endometrial cancer*. Nat Rev Cancer, 2019. **19**(9): p. 510-521.
63. Soumerai, T.E., et al., *Clinical Utility of Prospective Molecular Characterization in Advanced Endometrial Cancer*. Clin Cancer Res, 2018. **24**(23): p. 5939-5947.
64. Tsimberidou, A.M., et al., *Personalized medicine in a phase I clinical trials program: the MD Anderson Cancer Center initiative*. Clin Cancer Res, 2012. **18**(22): p. 6373-83.
65. Kim, T.H., J.Y. Yoo, and J.W. Jeong, *Mig-6 Mouse Model of Endometrial Cancer*. Adv Exp Med Biol, 2017. **943**: p. 243-259.
66. Fedorko, A.M., et al., *An immune competent orthotopic model of endometrial cancer with metastasis*. Heliyon, 2020. **6**(5): p. e04075.
67. Li, H.D., et al., *A PoleP286R mouse model of endometrial cancer recapitulates high mutational burden and immunotherapy response*. JCI Insight, 2020. **5**(14).
68. Contreras, C.M., et al., *Lkb1 inactivation is sufficient to drive endometrial cancers that are aggressive yet highly responsive to mTOR inhibitor monotherapy*. Dis Model Mech, 2010. **3**(3-4): p. 181-93.
69. Wild, P.J., et al., *p53 suppresses type II endometrial carcinomas in mice and governs endometrial tumour aggressiveness in humans*. EMBO Mol Med, 2012. **4**(8): p. 808-24.
70. Blaisdell, A., et al., *Neutrophils Oppose Uterine Epithelial Carcinogenesis via Debridement of Hypoxic Tumor Cells*. Cancer Cell, 2015. **28**(6): p. 785-799.

71. Gao, Y., et al., *Conditional abrogation of transforming growth factor-beta receptor 1 in PTEN-inactivated endometrium promotes endometrial cancer progression in mice.* J Pathol, 2017. **243**(1): p. 89-99.
72. Yoshida, A., et al., *Non-phosphorylatable cyclin D1 mutant potentiates endometrial hyperplasia and drives carcinoma with Pten loss.* Oncogene, 2022. **41**(15): p. 2187-2195.
73. Scully, R.E., *Ovarian tumors. A review.* Am J Pathol, 1977. **87**(3): p. 686-720.
74. Sakr, S., et al., *Granulosa cell tumors: novel predictors of recurrence in early-stage patients.* Int J Gynecol Pathol, 2017. **36**(3): p. 240-252.
75. Colombo, N., et al., *Management of ovarian stromal cell tumors.* J Clin Oncol, 2007. **25**(20): p. 2944-51.
76. Jamieson, S. and P.J. Fuller, *Molecular pathogenesis of granulosa cell tumors of the ovary.* Endocr Rev, 2012. **33**(1): p. 109-44.
77. Vassal, G., et al., *Juvenile granulosa cell tumor of the ovary in children: a clinical study of 15 cases.* J Clin Oncol, 1988. **6**(6): p. 990-5.
78. Nasu, K., et al., *Granulosa cell tumor associated with secondary amenorrhea and serum luteinizing hormone elevation.* Int J Clin Oncol, 2007. **12**(3): p. 228-30.
79. Szewczuk, W., et al., *Ovarian adult-type granulosa cell tumor concomitant with simple endometrial hyperplasia: a case study with selected immunohistochemistry.* J Int Med Res, 2019: p. 300060519886984.
80. Levin, G., et al., *Granulosa cell tumor of ovary: A systematic review of recent evidence.* Eur J Obstet Gynecol Reprod Biol, 2018. **225**: p. 57-61.
81. Schumer, S.T. and S.A. Cannistra, *Granulosa cell tumor of the ovary.* J Clin Oncol, 2003. **21**(6): p. 1180-9.

82. Roth, L.M., B. Lyu, and L. Cheng, *Perspectives on testicular sex cord-stromal tumors and those composed of both germ cells and sex cord-stromal derivatives with a comparison to corresponding ovarian neoplasms*. Hum Pathol, 2017. **65**: p. 1-14.
83. Cheng, L., et al., *Testicular cancer*. Nat Rev Dis Primers, 2018. **4**(1): p. 29.
84. Moch, H., et al., *The 2016 WHO Classification of Tumours of the Urinary System and Male Genital Organs-Part A: Renal, Penile, and Testicular Tumours*. Eur Urol, 2016. **70**(1): p. 93-105.
85. Idrees, M.T., et al., *The World Health Organization 2016 classification of testicular non-germ cell tumours: a review and update from the International Society of Urological Pathology Testis Consultation Panel*. Histopathology, 2017. **70**(4): p. 513-521.
86. Al-Agha, O.M. and C.A. Axiotis, *An in-depth look at Leydig cell tumor of the testis*. Arch Pathol Lab Med, 2007. **131**(2): p. 311-7.
87. Kim, I., R.H. Young, and R.E. Scully, *Leydig cell tumors of the testis. A clinicopathological analysis of 40 cases and review of the literature*. Am J Surg Pathol, 1985. **9**(3): p. 177-92.
88. Young, R.H., *Sex cord-stromal tumors of the ovary and testis: their similarities and differences with consideration of selected problems*. Mod Pathol, 2005. **18**(Suppl 2): p. S81-98.
89. Fang, X., et al., *A novel mouse model of testicular granulosa cell tumors*. Mol Hum Reprod, 2018. **24**(7): p. 343-356.
90. Boyer, A., et al., *Dysregulation of WNT/CTNNB1 and PI3K/AKT signaling in testicular stromal cells causes granulosa cell tumor of the testis*. Carcinogenesis, 2009. **30**(5): p. 869-78.

91. Richards, J.S., et al., *Either Kras activation or Pten loss similarly enhance the dominant-stable CTNNB1-induced genetic program to promote granulosa cell tumor development in the ovary and testis*. *Oncogene*, 2012. **31**(12): p. 1504-20.
92. Zugor, V., et al., *Congenital juvenile granulosa cell tumor of the testis in newborns*. *Anticancer Res*, 2010. **30**(5): p. 1731-4.
93. Kao, C.S., et al., *Juvenile granulosa cell tumors of the testis: a clinicopathologic study of 70 cases with emphasis on its wide morphologic spectrum*. *Am J Surg Pathol*, 2015. **39**(9): p. 1159-69.
94. Raju, U., et al., *Congenital testicular juvenile granulosa cell tumor in a neonate with X/XY mosaicism*. *Am J Surg Pathol*, 1986. **10**(8): p. 577-83.
95. Young, R.H., W.D. Lawrence, and R.E. Scully, *Juvenile granulosa cell tumor--another neoplasm associated with abnormal chromosomes and ambiguous genitalia. A report of three cases*. *Am J Surg Pathol*, 1985. **9**(10): p. 737-43.
96. Wu, J.T., L. Book, and K. Sudar, *Serum alpha fetoprotein (AFP) levels in normal infants*. *Pediatr Res*, 1981. **15**(1): p. 50-2.
97. Dieckmann, K.P., J. Bertolini, and C. Wulfing, *Adult Granulosa Cell Tumor of the Testis: A Case Report with a Review of the Literature*. *Case Rep Urol*, 2019. **2019**: p. 7156154.
98. Jimenez-Quintero, L.P., et al., *Granulosa cell tumor of the adult testis: a clinicopathologic study of seven cases and a review of the literature*. *Hum Pathol*, 1993. **24**(10): p. 1120-5.
99. Cornejo, K.M. and R.H. Young, *Adult granulosa cell tumors of the testis: a report of 32 cases*. *Am J Surg Pathol*, 2014. **38**(9): p. 1242-50.

100. Lima, J.F., et al., *FOXL2 mutations in granulosa cell tumors occurring in males*. Arch Pathol Lab Med, 2012. **136**(7): p. 825-8.
101. Suppiah, A., et al., *Adult granulosa cell tumour of the testis and bony metastasis. A report of the first case of granulosa cell tumour of the testicle metastasising to bone*. Urol Int, 2005. **75**(1): p. 91-3.
102. Hanson, J.A. and A.B. Ambaye, *Adult testicular granulosa cell tumor: a review of the literature for clinicopathologic predictors of malignancy*. Arch Pathol Lab Med, 2011. **135**(1): p. 143-6.
103. Pisarska, M.D., G. Barlow, and F.T. Kuo, *Minireview: roles of the forkhead transcription factor FOXL2 in granulosa cell biology and pathology*. Endocrinology, 2011. **152**(4): p. 1199-208.
104. Uhlenhaut, N.H., et al., *Somatic sex reprogramming of adult ovaries to testes by FOXL2 ablation*. Cell, 2009. **139**(6): p. 1130-42.
105. Kalfa, N., et al., *Aberrant expression of ovary determining gene FOXL2 in the testis and juvenile granulosa cell tumor in children*. J Urol, 2008. **180**(4 Suppl): p. 1810-3.
106. Shah, S.P., et al., *Mutation of FOXL2 in granulosa-cell tumors of the ovary*. N Engl J Med, 2009. **360**(26): p. 2719-29.
107. Nonis, D., K.J. McTavish, and S. Shimasaki, *Essential but differential role of FOXL2(wt) and FOXL2(C134W) in GDF-9 stimulation of follistatin transcription in co-operation with Smad3 in the human granulosa cell line COV434*. Mol Cell Endocrinol, 2013. **372**(1-2): p. 42-48.

108. Cheng, J.C., et al., *FOXL2-induced follistatin attenuates activin A-stimulated cell proliferation in human granulosa cell tumors*. *Biochem Biophys Res Commun*, 2014. **443**(2): p. 537-42.
109. Leung, D.T.H., P.J. Fuller, and S. Chu, *Impact of FOXL2 mutations on signaling in ovarian granulosa cell tumors*. *Int J Biochem Cell Biol*, 2016. **72**: p. 51-54.
110. Kim, J.H., et al., *Differential apoptotic activities of wild-type FOXL2 and the adult-type granulosa cell tumor-associated mutant FOXL2 (C134W)*. *Oncogene*, 2011. **30**(14): p. 1653-1663.
111. Fleming, N.I., et al., *Aromatase is a direct target of FOXL2: C134W in granulosa cell tumors via a single highly conserved binding site in the ovarian specific promoter*. *PLoS One*, 2010. **5**(12): p. e14389.
112. Fuller, P.J., et al., *Molecular pathogenesis of granulosa cell tumours*. *Mol Cell Endocrinol*, 2002. **191**(1): p. 89-96.
113. Kim, S.Y., *Insights into granulosa cell tumors using spontaneous or genetically engineered mouse models*. *Clin Exp Reprod Med*, 2016. **43**(1): p. 1-8.
114. Ying, S.Y., *Inhibins, activins, and follistatins: gonadal proteins modulating the secretion of follicle-stimulating hormone*. *Endocr Rev*, 1988. **9**(2): p. 267-93.
115. O'Connor, A.E. and D.M. De Kretser, *Inhibins in normal male physiology*. *Semin Reprod Med*, 2004. **22**(3): p. 177-85.
116. Matzuk, M.M., et al., *Alpha-inhibin is a tumour-suppressor gene with gonadal specificity in mice*. *Nature*, 1992. **360**(6402): p. 313-9.

117. Kumar, T.R., Y. Wang, and M.M. Matzuk, *Gonadotropins are essential modifier factors for gonadal tumor development in inhibin-deficient mice*. *Endocrinology*, 1996. **137**(10): p. 4210-6.
118. Cipriano, S.C., et al., *Inhibin and p27 interact to regulate gonadal tumorigenesis*. *Mol Endocrinol*, 2001. **15**(6): p. 985-96.
119. Burns, K.H., et al., *Cyclin D2 and p27 are tissue-specific regulators of tumorigenesis in inhibin alpha knockout mice*. *Mol Endocrinol*, 2003. **17**(10): p. 2053-69.
120. Li, Q., et al., *SMAD3 regulates gonadal tumorigenesis*. *Mol Endocrinol*, 2007. **21**(10): p. 2472-86.
121. Klaus, A. and W. Birchmeier, *Wnt signalling and its impact on development and cancer*. *Nat Rev Cancer*, 2008. **8**(5): p. 387-98.
122. Boerboom, D., et al., *Misregulated Wnt/beta-catenin signaling leads to ovarian granulosa cell tumor development*. *Cancer Res*, 2005. **65**(20): p. 9206-15.
123. Mitsiades, C.S., N. Mitsiades, and M. Koutsilieris, *The Akt pathway: molecular targets for anti-cancer drug development*. *Curr Cancer Drug Targets*, 2004. **4**(3): p. 235-56.
124. Hay, N., *The Akt-mTOR tango and its relevance to cancer*. *Cancer Cell*, 2005. **8**(3): p. 179-83.
125. Li, Y., et al., *beta-Catenin directs the transformation of testis Sertoli cells to ovarian granulosa-like cells by inducing Foxl2 expression*. *J Biol Chem*, 2017. **292**(43): p. 17577-17586.
126. Haigis, K.M., *KRAS Alleles: The Devil Is in the Detail*. *Trends Cancer*, 2017. **3**(10): p. 686-697.

127. Fan, H.Y., et al., *Selective expression of KrasG12D in granulosa cells of the mouse ovary causes defects in follicle development and ovulation*. *Development*, 2008. **135**(12): p. 2127-37.
128. Hannenhalli, S. and K.H. Kaestner, *The evolution of Fox genes and their role in development and disease*. *Nat Rev Genet*, 2009. **10**(4): p. 233-40.
129. Uhlenhaut, N.H. and M. Treier, *Forkhead transcription factors in ovarian function*. *Reproduction*, 2011. **142**(4): p. 489-95.
130. Belli, M., et al., *FOXO1 Negates the Cooperative Action of FOXL2(C134W) and SMAD3 in CYP19 Expression in HGrC1 Cells by Sequestering SMAD3*. *J Endocr Soc*, 2019. **3**(11): p. 2064-2081.
131. Liu, Z., et al., *FOXO1/3 and PTEN Depletion in Granulosa Cells Promotes Ovarian Granulosa Cell Tumor Development*. *Mol Endocrinol*, 2015. **29**(7): p. 1006-24.
132. Massague, J., *TGF-beta signal transduction*. *Annu Rev Biochem*, 1998. **67**: p. 753-91.
133. Fang, X., Y. Gao, and Q. Li, *SMAD3 Activation: A Converging Point of Dysregulated TGF-Beta Superfamily Signaling and Genetic Aberrations in Granulosa Cell Tumor Development?* *Biol Reprod*, 2016. **95**(5): p. 105.
134. Massague, J., *TGFbeta in Cancer*. *Cell*, 2008. **134**(2): p. 215-30.
135. Pangas, S.A., et al., *Conditional deletion of Smad1 and Smad5 in somatic cells of male and female gonads leads to metastatic tumor development in mice*. *Mol Cell Biol*, 2008. **28**(1): p. 248-57.
136. Gao, Y., et al., *Constitutively active transforming growth factor beta receptor 1 in the mouse ovary promotes tumorigenesis*. *Oncotarget*, 2016. **7**(27): p. 40904-40918.

137. Boyer, A., et al., *Seminiferous tubule degeneration and infertility in mice with sustained activation of WNT/CTNNB1 signaling in sertoli cells*. Biol Reprod, 2008. **79**(3): p. 475-85.
138. Jamin, S.P., et al., *Requirement of Bmpr1a for Mullerian duct regression during male sexual development*. Nat Genet, 2002. **32**(3): p. 408-10.
139. Tanwar, P.S., et al., *Constitutive WNT/beta-catenin signaling in murine Sertoli cells disrupts their differentiation and ability to support spermatogenesis*. Biol Reprod, 2010. **82**(2): p. 422-432.
140. Albrecht, K.H. and E.M. Eicher, *Evidence that Sry is expressed in pre-Sertoli cells and Sertoli and granulosa cells have a common precursor*. Dev Biol, 2001. **240**(1): p. 92-107.
141. Muzumdar, M.D., et al., *A global double-fluorescent Cre reporter mouse*. Genesis, 2007. **45**(9): p. 593-605.
142. Snyder, C.S., et al., *A dual-color genetically engineered mouse model for multispectral imaging of the pancreatic microenvironment*. Pancreas, 2013. **42**(6): p. 952-8.
143. Gao, Y., et al., *Constitutive activation of transforming growth factor Beta receptor 1 in the mouse uterus impairs uterine morphology and function*. Biol Reprod, 2015. **92**(2): p. 34.
144. Li, Q., et al., *Transforming growth factor beta receptor type 1 is essential for female reproductive tract integrity and function*. PLoS Genet, 2011. **7**(10): p. e1002320.
145. Soyak, S.M., et al., *Cre-mediated recombination in cell lineages that express the progesterone receptor*. Genesis, 2005. **41**(2): p. 58-66.

146. Shen, X., et al., *EZH1 mediates methylation on histone H3 lysine 27 and complements EZH2 in maintaining stem cell identity and executing pluripotency*. Mol Cell, 2008. **32**(4): p. 491-502.
147. Bigsby, R.M., P.S. Cooke, and G.R. Cunha, *A simple efficient method for separating murine uterine epithelial and mesenchymal cells*. Am J Physiol, 1986. **251**(5): p. E630-E636.
148. Nagashima, T., et al., *BMPR2 is required for postimplantation uterine function and pregnancy maintenance*. J Clin Invest, 2013. **123**(6): p. 2539-50.
149. Paffaro, V.A., Jr., et al., *Subset classification of mouse uterine natural killer cells by DBA lectin reactivity*. Placenta, 2003. **24**(5): p. 479-88.
150. Gao, Y., K.J. Bayless, and Q. Li, *TGFBR1 is required for mouse myometrial development*. Mol Endocrinol, 2014. **28**(3): p. 380-94.
151. Guo, C., et al., *Stage- and subunit-specific functions of polycomb repressive complex 2 in bladder urothelial formation and regeneration*. Development, 2017. **144**(3): p. 400-408.
152. Gu, J., et al., *Mouse p63 variants and chondrogenesis*. Int J Clin Exp Pathol, 2013. **6**(12): p. 2872-9.
153. Reardon, S.N., et al., *Cdh1 is essential for endometrial differentiation, gland development, and adult function in the mouse uterus*. Biol Reprod, 2012. **86**(5): p. 141.
154. Ni, N., et al., *Glandular defects in the mouse uterus with sustained activation of TGF-beta signaling is associated with altered differentiation of endometrial stromal cells and formation of stromal compartment*. Plos One, 2018. **13**(12): p. e0209417.
155. Guenzl, P.M., et al., *Insulin hypersensitivity induced by hepatic PTEN gene ablation protects from murine endotoxemia*. PLoS One, 2013. **8**(6): p. e67013.

156. Cawthorn, W.P., et al., *Wnt6, Wnt10a and Wnt10b inhibit adipogenesis and stimulate osteoblastogenesis through a beta-catenin-dependent mechanism*. Bone, 2012. **50**(2): p. 477-489.
157. Mori, H., et al., *Secreted frizzled-related protein 5 suppresses adipocyte mitochondrial metabolism through WNT inhibition*. J Clin Invest, 2012. **122**(7): p. 2405-16.
158. Fisher, D.A., et al., *Three Dact gene family members are expressed during embryonic development and in the adult brains of mice*. Dev Dyn, 2006. **235**(9): p. 2620-30.
159. Gao, Y., et al., *SMAD7 antagonizes key TGFbeta superfamily signaling in mouse granulosa cells in vitro*. Reproduction, 2013. **146**(1): p. 1-11.
160. Spandidos, A., et al., *PrimerBank: a resource of human and mouse PCR primer pairs for gene expression detection and quantification*. Nucleic Acids Res, 2010. **38**: p. D792-799.
161. Song, G.A., et al., *Molecular consequences of the ACVR1(R206H) mutation of fibrodysplasia ossificans progressiva*. J Biol Chem, 2010. **285**(29): p. 22542-53.
162. Segers, I., et al., *Gene expression differences induced by equimolar low doses of LH or hCG in combination with FSH in cultured mouse antral follicles*. J Endocrinol, 2012. **215**(2): p. 269-80.
163. Livak, K.J. and T.D. Schmittgen, *Analysis of relative gene expression data using real-time quantitative PCR and the 2^{(-Delta Delta C(T))} Method*. Methods, 2001. **25**(4): p. 402-8.
164. Gan, L., et al., *The polycomb group protein EZH2 induces epithelial-mesenchymal transition and pluripotent phenotype of gastric cancer cells by binding to PTEN promoter*. J Hematol Oncol, 2018. **11**(1): p. 9.

165. Bragulla, H.H. and D.G. Homberger, *Structure and functions of keratin proteins in simple, stratified, keratinized and cornified epithelia*. J Anat, 2009. **214**(4): p. 516-59.
166. Silverberg, S.G., *Problems in the differential diagnosis of endometrial hyperplasia and carcinoma*. Mod Pathol, 2000. **13**(3): p. 309-27.
167. Sanderson, P.A., et al., *New concepts for an old problem: the diagnosis of endometrial hyperplasia*. Hum Reprod Update, 2017. **23**(2): p. 232-254.
168. Franco, H.L., et al., *WNT4 is a key regulator of normal postnatal uterine development and progesterone signaling during embryo implantation and decidualization in the mouse*. FASEB. J., 2011. **25**(4): p. 1176-87.
169. Miller, C. and D.A. Sassoon, *Wnt-7a maintains appropriate uterine patterning during the development of the mouse female reproductive tract*. Development, 1998. **125**(16): p. 3201-11.
170. Liang, X.H., et al., *The uterine epithelial loss of Pten is inefficient to induce endometrial cancer with intact stromal Pten*. PLoS Genet, 2018. **14**(8): p. e1007630.
171. Wang, P., et al., *Generation of mouse for conditional expression of forkhead box A2*. Endocrinology, 2018. **159**(4): p. 1897-1909.
172. Filant, J., J.P. Lydon, and T.E. Spencer, *Integrated chromatin immunoprecipitation sequencing and microarray analysis identifies FOXA2 target genes in the glands of the mouse uterus*. FASEB. J., 2014. **28**(1): p. 230-43.
173. Lee, K.Y., et al., *Bmp2 is critical for the murine uterine decidual response*. Mol Cell Biol, 2007. **27**(15): p. 5468-78.
174. Ramathal, C.Y., et al., *Endometrial decidualization: of mice and men*. Semin Reprod Med, 2010. **28**(1): p. 17-26.

175. Benson, G.V., et al., *Mechanisms of reduced fertility in Hoxa-10 mutant mice: uterine homeosis and loss of maternal Hoxa-10 expression*. *Development*, 1996. **122**(9): p. 2687-96.
176. Matsumoto, H. and E. Sato, *Uterine angiogenesis during implantation and decidualization in mice*. *Reprod Med Biol*, 2006. **5**(2): p. 81-86.
177. Gellersen, B., I.A. Brosens, and J.J. Brosens, *Decidualization of the human endometrium: mechanisms, functions, and clinical perspectives*. *Semin Reprod Med*, 2007. **25**(6): p. 445-53.
178. Cui, Y., et al., *Role of corin in trophoblast invasion and uterine spiral artery remodelling in pregnancy*. *Nature*, 2012. **484**(7393): p. 246-50.
179. Peng, J., et al., *Uterine activin receptor-like kinase 5 is crucial for blastocyst implantation and placental development*. *Proceedings of the National Academy of Sciences of the United States of America*, 2015. **112**(36): p. E5098-107.
180. Yamaguchi, H. and M.C. Hung, *Regulation and Role of EZH2 in Cancer*. *Cancer Res Treat*, 2014. **46**(3): p. 209-22.
181. Zhang, Q., et al., *Enhancer of Zeste homolog 2 (EZH2) induces epithelial-mesenchymal transition in endometriosis*. *Sci Rep*, 2017. **7**(1): p. 6804.
182. Ding, Y.B., et al., *5-aza-2'-deoxycytidine leads to reduced embryo implantation and reduced expression of DNA methyltransferases and essential endometrial genes*. *PLoS One*, 2012. **7**(9): p. e45364.
183. O'Carroll, D., et al., *The Polycomb-group gene Ezh2 is required for early mouse development*. *Molecular and Cellular Biology*, 2001. **21**(13): p. 4330-4336.

184. Dunlap, K.A., et al., *Postnatal deletion of Wnt7a inhibits uterine gland morphogenesis and compromises adult fertility in mice*. Biol Reprod, 2011. **85**(2): p. 386-96.
185. Jeong, J.W., et al., *beta-catenin mediates glandular formation and dysregulation of beta-catenin induces hyperplasia formation in the murine uterus*. Oncogene, 2009. **28**(1): p. 31-40.
186. Snitow, M.E., et al., *Ezh2 represses the basal cell lineage during lung endoderm development*. Development, 2015. **142**(1): p. 108-17.
187. Galvis, L.A., et al., *Repression of Igf1 expression by Ezh2 prevents basal cell differentiation in the developing lung*. Development, 2015. **142**(8): p. 1458-69.
188. Mills, A.A., et al., *p63 is a p53 homologue required for limb and epidermal morphogenesis*. Nature, 1999. **398**(6729): p. 708-713.
189. Yalcin-Ozuysal, O., et al., *Antagonistic roles of Notch and p63 in controlling mammary epithelial cell fates*. Cell Death Differ, 2010. **17**(10): p. 1600-12.
190. Murray-Zmijewski, F., D.P. Lane, and J.C. Bourdon, *p53/p63/p73 isoforms: an orchestra of isoforms to harmonise cell differentiation and response to stress*. Cell Death Differ, 2006. **13**(6): p. 962-72.
191. Koster, M.I., et al., *p63 is the molecular switch for initiation of an epithelial stratification program*. Genes & Development, 2004. **18**(2): p. 126-131.
192. Candi, E., et al., *Differential roles of p63 isoforms in epidermal development: selective genetic complementation in p63 null mice*. Cell Death Differ, 2006. **13**(6): p. 1037-47.
193. Laurikkala, J., et al., *p63 regulates multiple signalling pathways required for ectodermal organogenesis and differentiation*. Development, 2006. **133**(8): p. 1553-1563.

194. Romano, R.A., et al., *An active role of the DeltaN isoform of p63 in regulating basal keratin genes K5 and K14 and directing epidermal cell fate*. PLoS One, 2009. **4**(5): p. e5623.
195. Margueron, R., et al., *Ezh1 and Ezh2 maintain repressive chromatin through different mechanisms*. Molecular Cell, 2008. **32**(4): p. 503-518.
196. Ezhkova, E., et al., *EZH1 and EZH2 cogovern histone H3K27 trimethylation and are essential for hair follicle homeostasis and wound repair*. Genes & development, 2011. **25**(5): p. 485-498.
197. Ezhkova, E., et al., *Ezh2 orchestrates gene expression for the stepwise differentiation of tissue-specific stem cells*. Cell, 2009. **136**(6): p. 1122-35.
198. Soyak, S.M., et al., *Cre-mediated recombination in cell lineages that express the progesterone receptor*. Genesis, 2005. **41**(2): p. 58-66.
199. Wang, X., et al., *PrimerBank: a PCR primer database for quantitative gene expression analysis, 2012 update*. Nucleic Acids Res, 2012. **40**(Database issue): p. D1144-9.
200. Fang, X., et al., *Enhancer of Zeste 2 Polycomb Repressive Complex 2 Subunit Is Required for Uterine Epithelial Integrity*. Am J Pathol, 2019. **189**(6): p. 1212-1225.
201. Naganuma, T., et al., *Disruption of the Sjogren-Larsson Syndrome Gene Aldh3a2 in Mice Increases Keratinocyte Growth and Retards Skin Barrier Recovery*. J Biol Chem, 2016. **291**(22): p. 11676-88.
202. Daikoku, T., et al., *Conditional loss of uterine Pten unfailingly and rapidly induces endometrial cancer in mice*. Cancer Res, 2008. **68**(14): p. 5619-27.
203. Blanco-Aparicio, C., et al., *PTEN, more than the AKT pathway*. Carcinogenesis, 2007. **28**(7): p. 1379-1386.

204. Kim, K.H. and C.W. Roberts, *Targeting EZH2 in cancer*. Nat Med, 2016. **22**(2): p. 128-34.
205. Cheng, Y.H., et al., *Retinoic acid inhibits endometrial cancer cell growth via multiple genomic mechanisms*. J Mol Endocrinol, 2011. **46**(2): p. 139-53.
206. Wu, L., et al., *Tumor-Associated Neutrophils in Cancer: Going Pro*. Cancers (Basel), 2019. **11**(4): p. 564.
207. Korkmaz, B., et al., *Neutrophil elastase, proteinase 3, and cathepsin G as therapeutic targets in human diseases*. Pharmacol Rev, 2010. **62**(4): p. 726-59.
208. Pijnenborg, J.M.A., et al., *Hypoxia contributes to development of recurrent endometrial carcinoma*. Int J Gynecol Cancer, 2007. **17**(4): p. 897-904.
209. Mahiddine, K., et al., *Relief of tumor hypoxia unleashes the tumoricidal potential of neutrophils*. J Clin Invest, 2020. **130**(1): p. 389-403.
210. Tangen, I.L., et al., *Loss of progesterone receptor links to high proliferation and increases from primary to metastatic endometrial cancer lesions*. Eur J Cancer, 2014. **50**(17): p. 3003-10.
211. Kim, J.J. and E. Chapman-Davis, *Role of progesterone in endometrial cancer*. Semin Reprod Med, 2010. **28**(1): p. 81-90.
212. Chung, H.H., et al., *Estrogen reprograms the activity of neutrophils to foster protumoral microenvironment during mammary involution*. Sci Rep, 2017. **7**: p. 46485.
213. Vazquez Rodriguez, G., et al., *Estradiol Promotes Breast Cancer Cell Migration via Recruitment and Activation of Neutrophils*. Cancer Immunol Res, 2017. **5**(3): p. 234-247.
214. Maxwell, G.L., et al., *Mutation of the PTEN tumor suppressor gene in endometrial hyperplasias*. Cancer Res, 1998. **58**(12): p. 2500-3.

215. Risinger, J.I., et al., *PTEN mutation in endometrial cancers is associated with favorable clinical and pathologic characteristics*. Clin Cancer Res, 1998. **4**(12): p. 3005-10.
216. Kikuchi, J., et al., *Phosphorylation-mediated EZH2 inactivation promotes drug resistance in multiple myeloma*. J Clin Invest, 2015. **125**(12): p. 4375-90.
217. Mallen-St Clair, J., et al., *EZH2 couples pancreatic regeneration to neoplastic progression*. Genes Dev, 2012. **26**(5): p. 439-44.
218. Nanjappa, M.K., et al., *The histone methyltransferase EZH2 is required for normal uterine development and function in mice*. Biol Reprod, 2019. **101**(2): p. 306-317.
219. Mesa, A.M., et al., *Mice lacking uterine enhancer of zeste homolog 2 have transcriptomic changes associated with uterine epithelial proliferation*. Physiol Genomics, 2020. **52**(2): p. 81-95.
220. Mesa, A.M., et al., *Spatial transcriptomics analysis of uterine gene expression in enhancer of zeste homolog 2 conditional knockout micedagger*. Biol Reprod, 2021. **105**(5): p. 1126-1139.
221. Xie, Y., et al., *Power of PTEN/AKT: Molecular switch between tumor suppressors and oncogenes*. Oncol Lett, 2016. **12**(1): p. 375-378.
222. Sirohi, V.K., et al., *Regulation of AKT Signaling in Mouse Uterus*. Endocrinology, 2022. **163**(1).
223. Kruger, P., et al., *Neutrophils: Between host defence, immune modulation, and tissue injury*. PLoS Pathog, 2015. **11**(3): p. e1004651.
224. Masucci, M.T., M. Minopoli, and M.V. Carriero, *Tumor Associated Neutrophils. Their Role in Tumorigenesis, Metastasis, Prognosis and Therapy*. Front Oncol, 2019. **9**: p. 1146.

225. Wang, Y., et al., *Ezh2 Acts as a Tumor Suppressor in Kras-driven Lung Adenocarcinoma*. Int J Biol Sci, 2017. **13**(5): p. 652-659.
226. Shen, M., et al., *Tumor-associated neutrophils as a new prognostic factor in cancer: a systematic review and meta-analysis*. PLoS One, 2014. **9**(6): p. e98259.
227. Cunha, G.R., et al., *Molecular mechanisms of development of the human fetal female reproductive tract*. Differentiation, 2017. **97**: p. 54-72.
228. McCaffrey, L.M. and I.G. Macara, *Epithelial organization, cell polarity and tumorigenesis*. Trends Cell Biol, 2011. **21**(12): p. 727-35.
229. Rodriguez, A.C., et al., *Estrogen Signaling in Endometrial Cancer: a Key Oncogenic Pathway with Several Open Questions*. Horm Cancer, 2019. **10**(2-3): p. 51-63.
230. Lindberg, M.E., et al., *Loss of CDH1 and Pten accelerates cellular invasiveness and angiogenesis in the mouse uterus*. Biol Reprod, 2013. **89**(1): p. 8.
231. Wang, X., et al., *Pten and Dicer1 loss in the mouse uterus causes poorly differentiated endometrial adenocarcinoma*. Oncogene, 2020. **39**(40): p. 6286-6299.
232. Koppens, M.A., et al., *A new transgenic mouse model for conditional overexpression of the Polycomb Group protein EZH2*. Transgenic Res, 2017. **26**(2): p. 187-196.
233. Ideker, T., T. Galitski, and L. Hood, *A new approach to decoding life: systems biology*. Annu Rev Genomics Hum Genet, 2001. **2**: p. 343-72.
234. Qiu, J., et al., *Network-based protein-protein interaction prediction method maps perturbations of cancer interactome*. PLoS Genet, 2021. **17**(11): p. e1009869.
235. Kim, M., et al., *A protein interaction landscape of breast cancer*. Science, 2021. **374**(6563): p. eabf3066.

236. Pilot-Storck, F., et al., *Interactome mapping of the phosphatidylinositol 3-kinase-mammalian target of rapamycin pathway identifies deformed epidermal autoregulatory factor-1 as a new glycogen synthase kinase-3 interactor*. *Mol Cell Proteomics*, 2010. **9**(7): p. 1578-93.
237. Pane, K., et al., *An Integrative Computational Approach Based on Expression Similarity Signatures to Identify Protein-Protein Interaction Networks in Female-Specific Cancers*. *Front Genet*, 2020. **11**: p. 612521.
238. Yap, T.A., et al., *Phase I Study of the Novel Enhancer of Zeste Homolog 2 (EZH2) Inhibitor GSK2816126 in Patients with Advanced Hematologic and Solid Tumors*. *Clin Cancer Res*, 2019. **25**(24): p. 7331-7339.
239. Italiano, A., et al., *Tazemetostat, an EZH2 inhibitor, in relapsed or refractory B-cell non-Hodgkin lymphoma and advanced solid tumours: a first-in-human, open-label, phase 1 study*. *Lancet Oncol*, 2018. **19**(5): p. 649-659.
240. Bartholin, L., et al., *Generation of mice with conditionally activated transforming growth factor Beta signaling through the T beta RI/ALK5 receptor*. *Genesis*, 2008. **46**(12): p. 724-731.
241. Vincent, D.F., et al., *A rapid strategy to detect the recombined allele in LSL-TbetaR1CA transgenic mice*. *Genesis*, 2010. **48**(9): p. 559-62.
242. Jamin, S.P., et al., *Requirement of Bmpr1a for Mullerian duct regression during male sexual development*. *Nat Genet*, 2002. **32**(3): p. 408-410.
243. Li, Q., et al., *Redundant roles of SMAD2 and SMAD3 in ovarian granulosa cells in vivo*. *Mol Cell Biol*, 2008. **28**(23): p. 7001-11.

244. Spandidos, A., et al., *A comprehensive collection of experimentally validated primers for Polymerase Chain Reaction quantitation of murine transcript abundance*. BMC genomics, 2008. **9**: p. 633.
245. Jeyasuria, P., et al., *Cell-specific knockout of steroidogenic factor 1 reveals its essential roles in gonadal function*. Mol Endocrinol, 2004. **18**(7): p. 1610-9.
246. Yu, J., N.B. Hecht, and R.M. Schultz, *Expression of MSY2 in mouse oocytes and preimplantation embryos*. Biol Reprod, 2001. **65**(4): p. 1260-70.
247. Vergouwen, R.P., et al., *Proliferative activity of gonocytes, Sertoli cells and interstitial cells during testicular development in mice*. J Reprod Fertil, 1991. **93**(1): p. 233-43.
248. Sridharan, S., et al., *Proliferation of adult sertoli cells following conditional knockout of the Gap junctional protein GJA1 (connexin 43) in mice*. Biol Reprod, 2007. **76**(5): p. 804-12.
249. Chen, Y.C., et al., *Transforming growth factor-beta 1 up-regulates connexin43 expression in human granulosa cells*. Human Reproduction, 2015. **30**(9): p. 2190-2201.
250. Cheng, J.C., et al., *TGF-beta 1 Up-Regulates Connexin43 Expression: A Potential Mechanism for Human Trophoblast Cell Differentiation*. Journal of Cellular Physiology, 2015. **230**(7): p. 1558-1566.
251. Wilhelm, D., et al., *Antagonism of the testis- and ovary-determining pathways during ovotestis development in mice*. Mech Dev, 2009. **126**(5-6): p. 324-36.
252. Matson, C.K., et al., *DMRT1 prevents female reprogramming in the postnatal mammalian testis*. Nature, 2011. **476**(7358): p. 101-4.

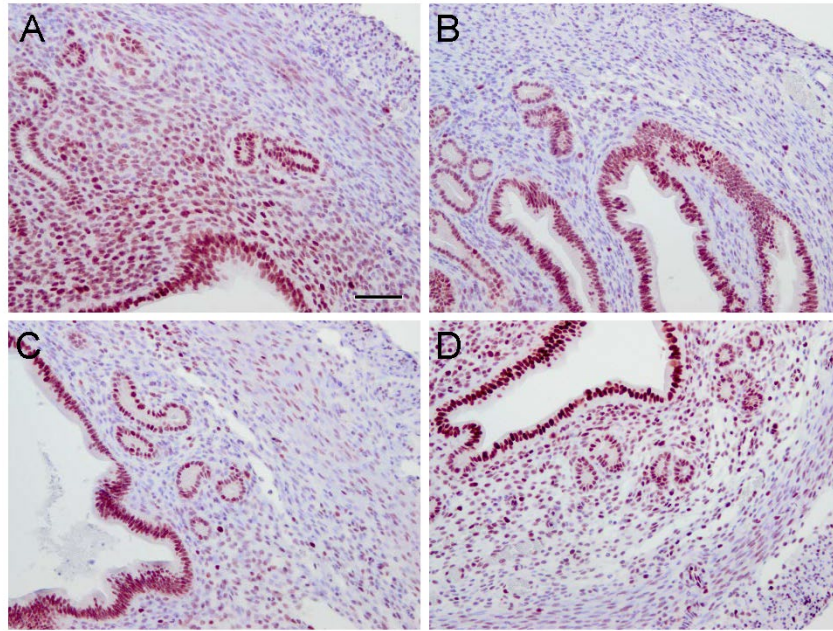
253. Raymond, C.S., et al., *Dmrt1, a gene related to worm and fly sexual regulators, is required for mammalian testis differentiation*. Genes & Development, 2000. **14**(20): p. 2587-2595.
254. Chang, H., et al., *Overactive beta-catenin signaling causes testicular sertoli cell tumor development in the mouse*. Biol Reprod, 2009. **81**(5): p. 842-9.
255. Liu, C., K. Rodriguez, and H.H. Yao, *Mapping lineage progression of somatic progenitor cells in the mouse fetal testis*. Development, 2016. **143**(20): p. 3700-3710.
256. Boerboom, D., et al., *Misregulated Wnt/beta-Catenin signaling leads to ovarian granulosa cell tumor development*. Cancer Res, 2005. **65**(20): p. 9206-9215.
257. Wang, B.Y., et al., *Gonadal tumor with granulosa cell tumor features in an adult testis*. Ann Diagn Pathol, 2002. **6**(1): p. 56-60.
258. Shukla, A.R., et al., *Juvenile granulosa cell tumor of the testis: Contemporary clinical management and pathological diagnosis*. Journal of Urology, 2003. **169**(4): p. 127-127.
259. Lawrence, W.D., R.H. Young, and R.E. Scully, *Juvenile Granulosa-Cell Tumor of the Infantile Testis - a Report of 14 Cases*. American Journal of Surgical Pathology, 1985. **9**(2): p. 87-94.
260. Dudani, R., et al., *Juvenile Granulosa Cell Tumor of Testis: Case Report and Review of Literature*. Amer J Perinatol, 2008. **25**(04): p. 229-231.
261. Lawrence, W.D. and R.E. Scully, *Juvenile granulosa cell tumor—Another neoplasm associated with abnormal chromosomes and ambiguous genitalia: A report of three cases*. The American Journal of Surgical Pathology, 1985. **9**(10): p. 737-740.

262. Edson, M.A., et al., *Granulosa cell-expressed BMPRIA and BMPR1B have unique functions in regulating fertility but act redundantly to suppress ovarian tumor development*. Mol Endocrinol, 2010. **24**(6): p. 1251-66.
263. De Cian, M.C., et al., *Amplification of R-spondin1 signaling induces granulosa cell fate defects and cancers in mouse adult ovary*. Oncogene, 2017. **36**(2): p. 208-218.
264. Kyronlahti, A., et al., *GATA4 regulates Sertoli cell function and fertility in adult male mice*. Mol Cell Endocrinol, 2011. **333**(1): p. 85-95.
265. Papaioannou, M.D., et al., *Sertoli cell Dicer is essential for spermatogenesis in mice*. Developmental Biology, 2009. **326**(1): p. 250-259.
266. Mendis, S.H., et al., *Activin A balances Sertoli and germ cell proliferation in the fetal mouse testis*. Biol Reprod, 2011. **84**(2): p. 379-91.
267. Mostofi, F.K., *Proceedings: Testicular tumors. Epidemiologic, etiologic, and pathologic features*. Cancer, 1973. **32**(5): p. 1186-201.
268. Li, Y., et al., *Beta-catenin directs the transformation of testis Sertoli cells to ovarian granulosa-like cells by inducing Foxl2 expression*. J Biol Chem, 2017. **292**: p. 17577-17586.
269. Middlebrook, B.S., et al., *Smad1-Smad5 ovarian conditional knockout mice develop a disease profile similar to the juvenile form of human granulosa cell tumors*. Endocrinology, 2009. **150**(12): p. 5208-17.
270. Kim, S.Y., et al., *Constitutive activation of PI3K in oocytes induces ovarian granulosa cell tumors*. Cancer Res, 2016. **76**(13): p. 3851-61.
271. Rosario, R., et al., *The transcriptional targets of mutant FOXL2 in granulosa cell tumours*. PLoS One, 2012. **7**(9): p. e46270.

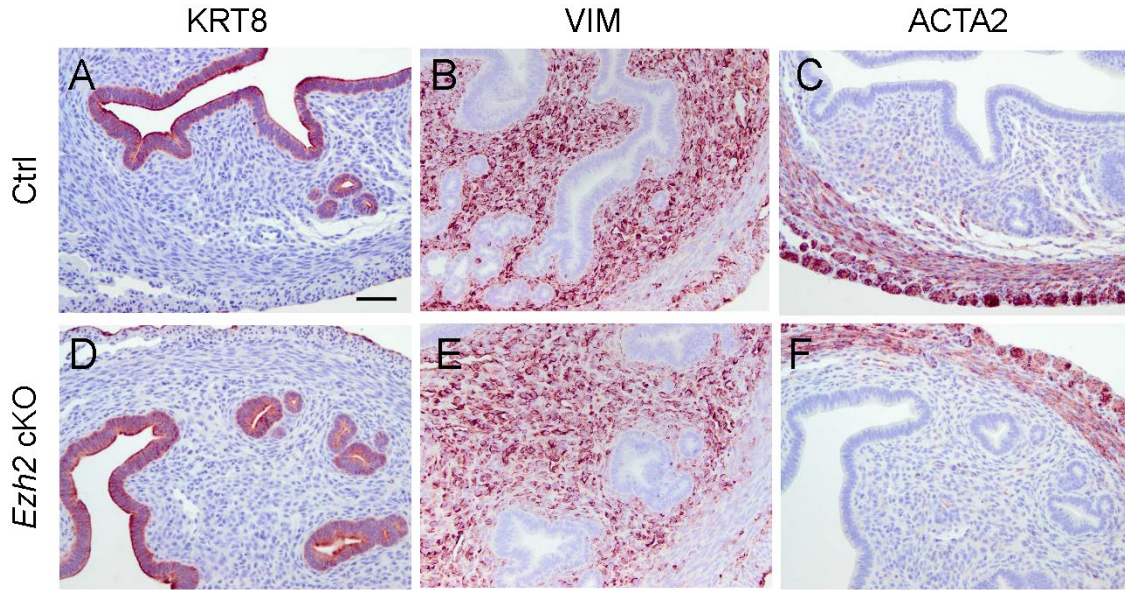
272. Giles, R.H., J.H. van Es, and H. Clevers, *Caught up in a Wnt storm: Wnt signaling in cancer*. *Biochim Biophys Acta*, 2003. **1653**(1): p. 1-24.
273. Kim, K.A., et al., *R-Spondin family members regulate the Wnt pathway by a common mechanism*. *Mol Biol Cell*, 2008. **19**(6): p. 2588-96.
274. Akhmetshina, A., et al., *Activation of canonical Wnt signalling is required for TGF-beta-mediated fibrosis*. *Nature Communications*, 2012. **3**: p. 735.
275. Chang, H., et al., *Wt1 negatively regulates beta-catenin signaling during testis development*. *Development*, 2008. **135**(10): p. 1875-85.

APPENDIX A

FIGURES

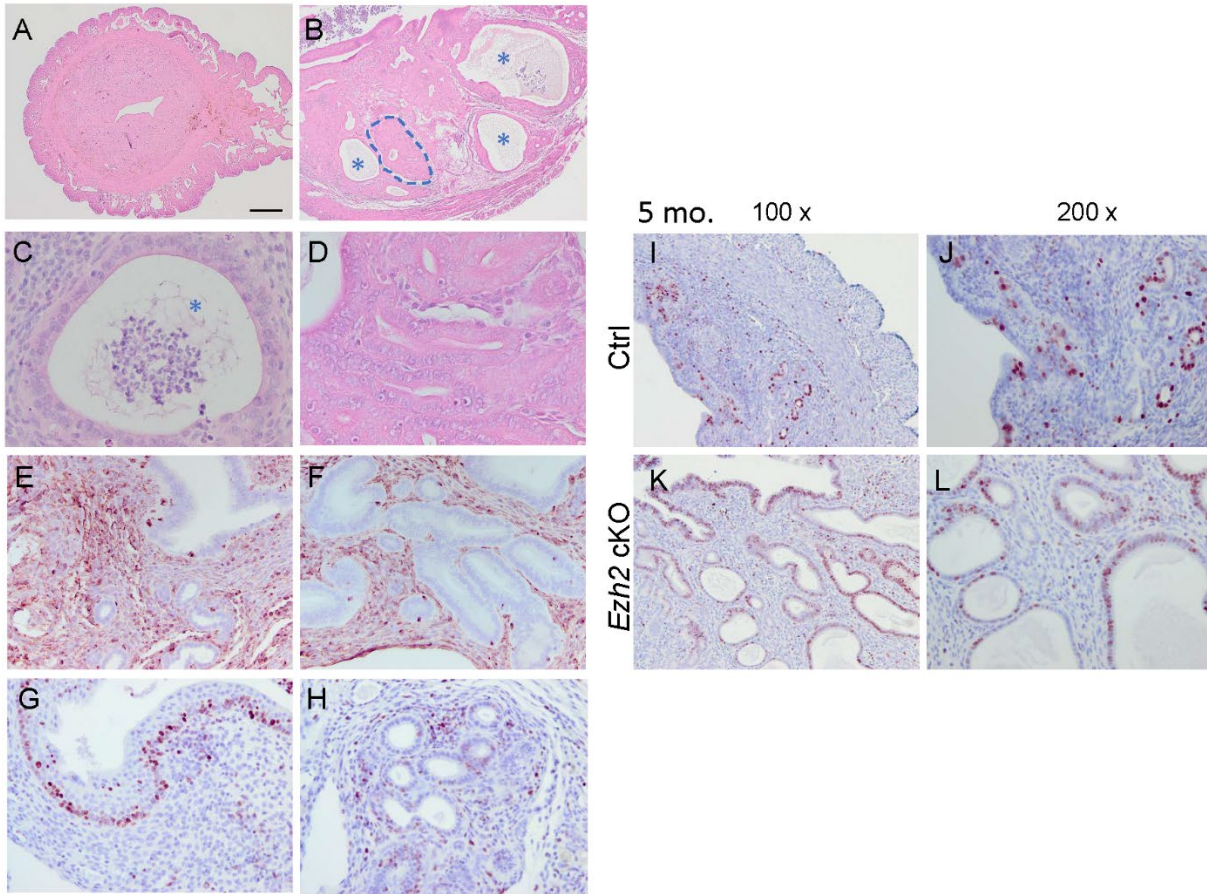


A-1. Localization of EZH2 in the mouse uterus during the estrous cycle. Immunohistochemical staining of EZH2 using uterine samples from wild-type mice at diestrus (A), proestrus (B), estrus (C), and metestrus (D) stages. $n = 3$ (A–D). Scale bar = 50 μm (A–D).

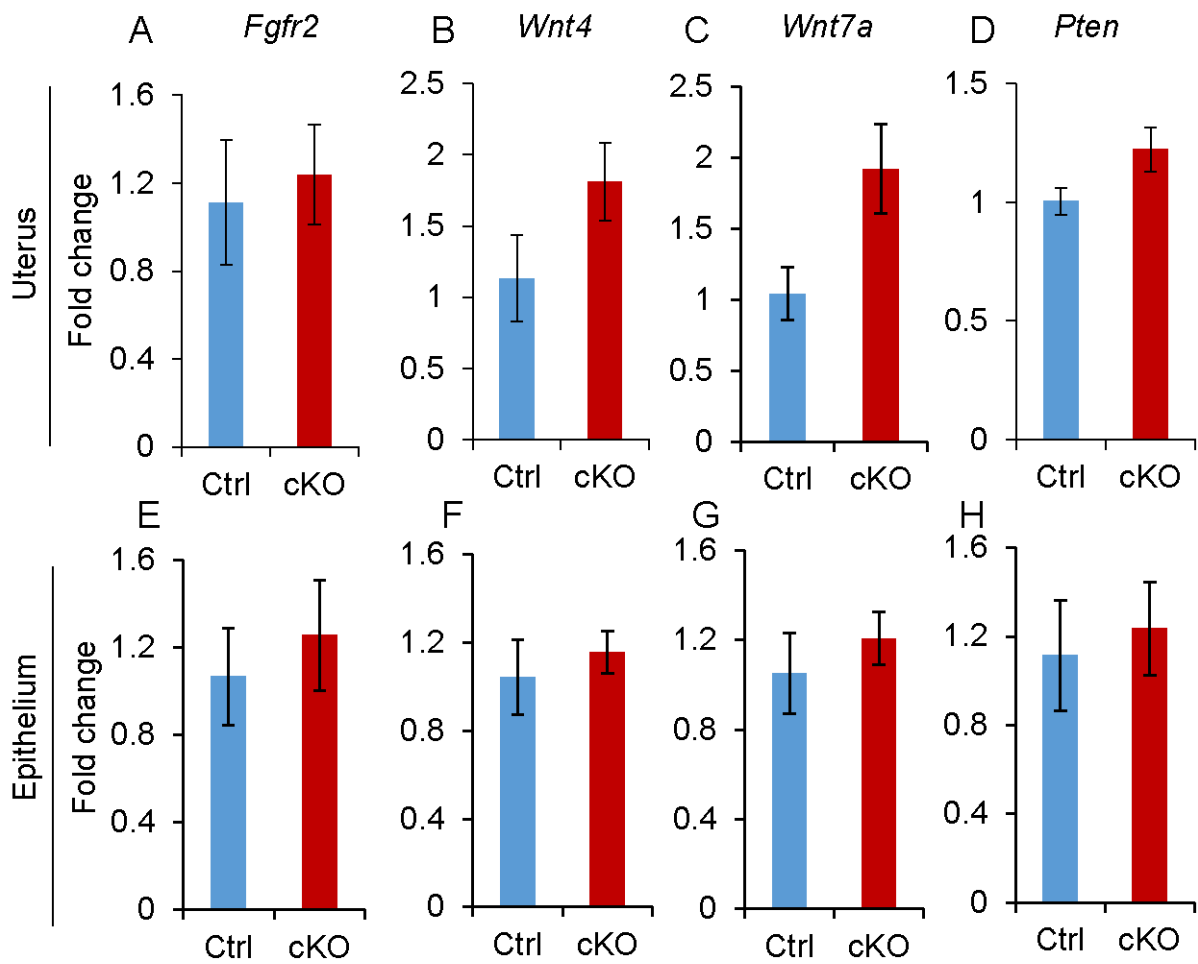


A-2. Immunohistochemical staining of epithelial, stromal, and myometrial compartments in *Ezh2* cKO uteri. Immunostaining of cytokeratin 8 (KRT8), vimentin (VIM), and α -smooth muscle actin (ACTA2) in 1-month-old control (Ctrl) and *Ezh2* cKO uteri. $n = 3$ (A–F). Scale bar = 50 μm (A–F).

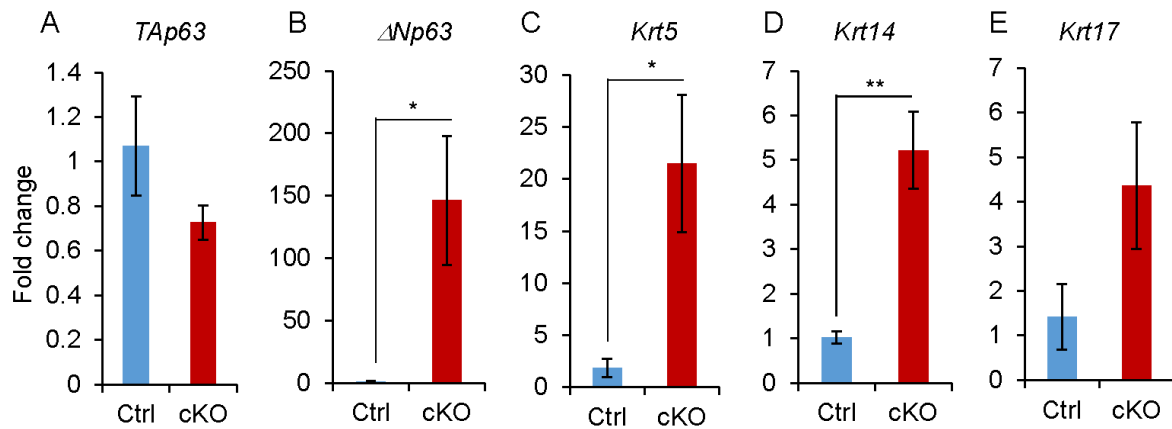
8 mo.



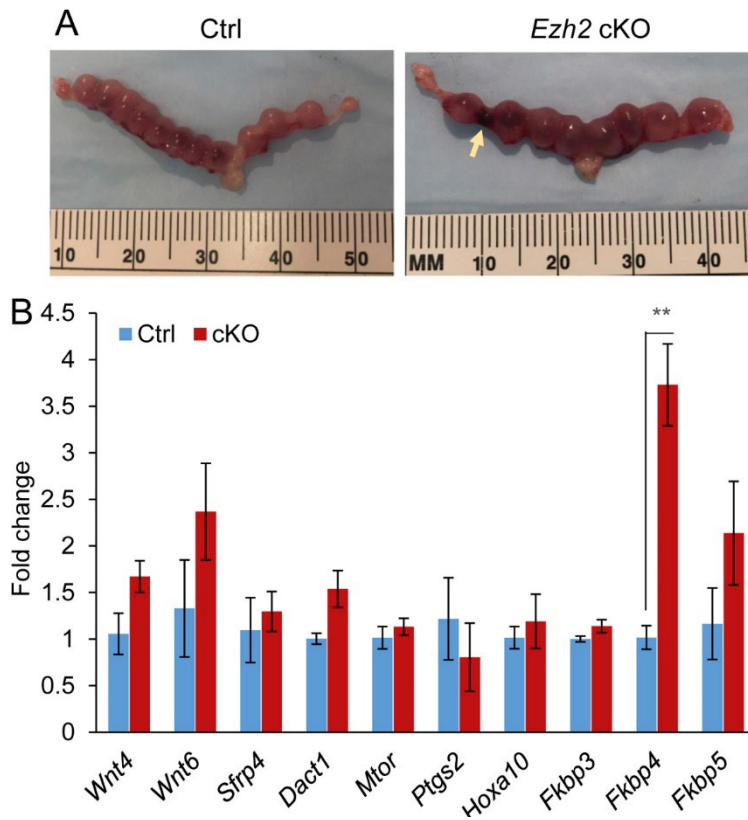
A-3. Development of endometrial hyperplasia in *Ezh2* cKO uteri. A–D: Hematoxylin and eosin staining of uteri from 8-month-old control (Ctrl; A) and *Ezh2* cKO (B–D) mice. B and C: Asterisks indicate cystic glands, whereas the dashed line shows an area with gland crowding, magnified in D. E and F: Vimentin staining in the uteri from control (E) and *Ezh2* cKO (F) mice at the age of 8 months. G and H: Ki-67 staining in some abnormal glandular structures in the uteri of *Ezh2* cKO mice at the age of 8 months. I–L: Ki-67 staining of control and *Ezh2* cKO uteri at the age of 5 months. $n = 3$ (E–H); $n = 2$ to 3 (I–L). Scale bars: 250 μm (A and B); 25 μm (C and D); 50 μm (E–H, J, and L); 100 μm (I and K). Original magnification: $\times 100$ (I and K); $\times 200$ (J and L). Myo, myometrium.



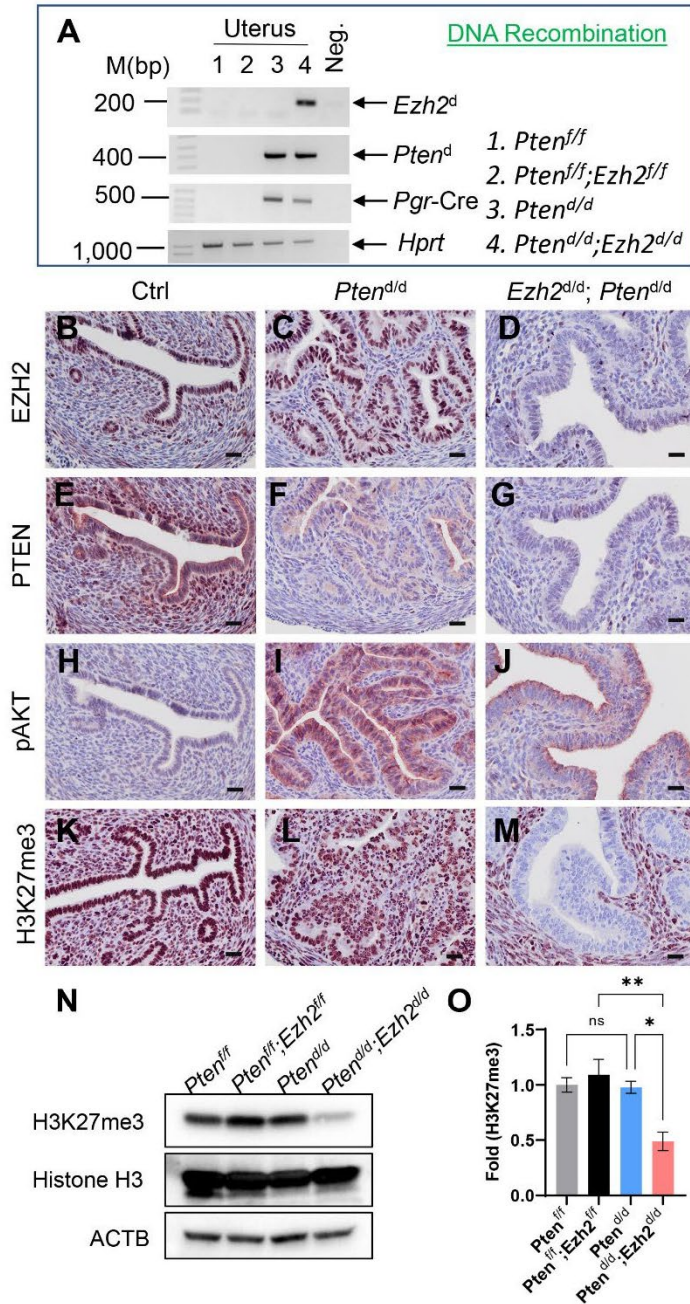
A-4. Expression of select genes associated with stratified uterine epithelia is not altered in *Ezh2* cKO mice at the age of 1 month. Real-time PCR analysis of *Fgfr2*, *Wnt4*, *Wnt7a*, and *Pten* mRNA expression in uterine tissues (A–D) and uterine epithelia (E–H) isolated from control (Ctrl) and *Ezh2* cKO mice. Data are expressed as means \pm SEM. $n = 4$ uterine tissues in Ctrl mice (A–D) and uterine epithelia in Ctrl and cKO mice (E–H); $n = 5$ uterine tissues in cKO mice (A–D).



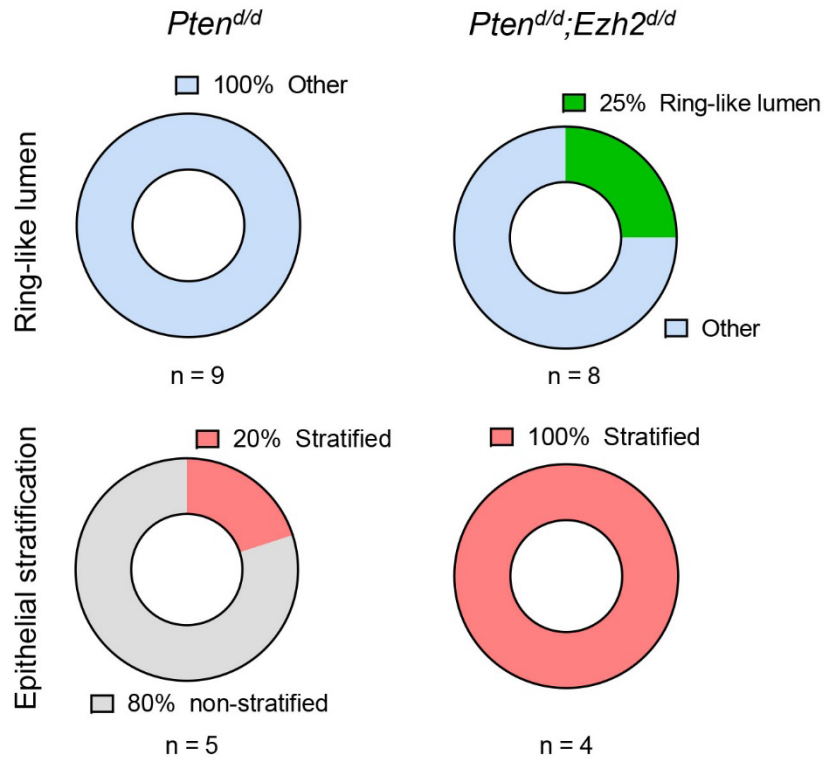
A-5. Elevated expression of basal cell markers in uterine epithelia isolated from *Ezh2* cKO mice. A–E: Real-time PCR analysis of expression of *TAp63*, $\Delta Np63$, *Krt5*, *Krt14*, and *Krt17* mRNA in uterine epithelia isolated from control (Ctrl) and *Ezh2* cKO mice at the age of 1 month. Data are expressed as means \pm SEM (A–E). $n = 4$ (A–E). * $P < 0.05$, ** $P < 0.01$.



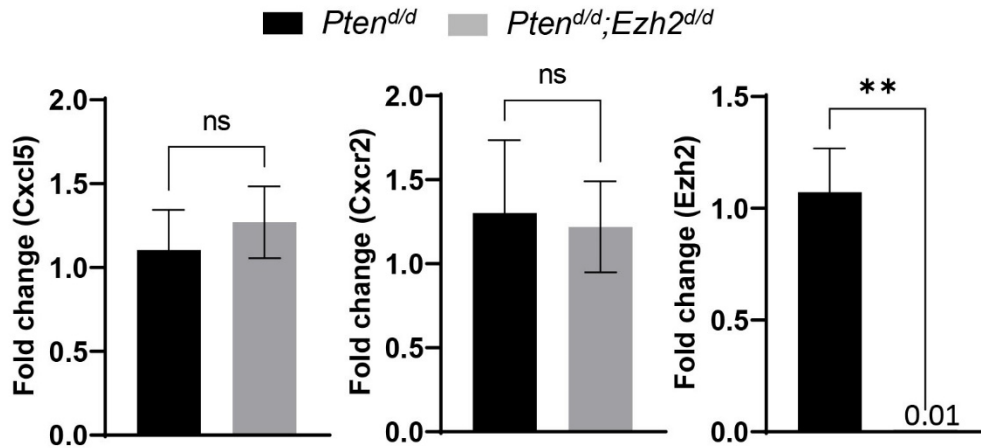
A-6. Expression analysis of genes associated with decidual differentiation and function in embryonic day 8.5 (E8.5) decidual tissues. (A) Gross images of uteri from control (Ctrl) and *Ezh2* cKO mice at E8.5. The arrow indicates a hemorrhagic site. (B) Real-time PCR analysis of genes involved in decidualization using E8.5 decidual tissues from control and *Ezh2* cKO mice. Data are expressed as means \pm SEM (B). $n = 3$ Ctrl mice (B); $n = 4$ cKO mice (B). ** $P < 0.01$.



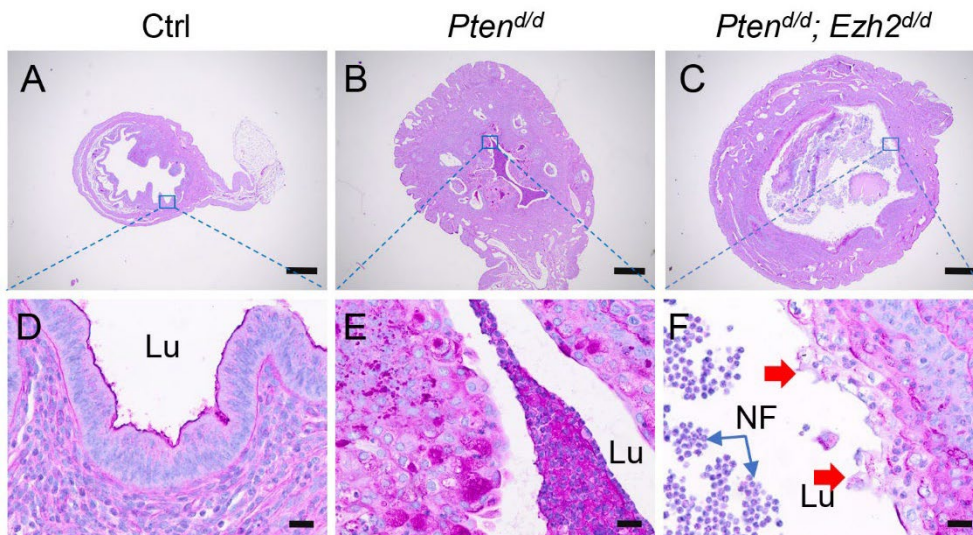
A-7. Generation and validation of mice with conditional deletion of *Ezh2* and *Pten*. **(A)** Analysis of DNA recombination of *Ezh2* and *Pten* alleles in the uteri of *Pten^{fl/fl}* (Ctrl), *Pten^{d/d}*, and *Pten^{d/d}; Ezh2^{d/d}* mice at 2 weeks of age. $n = 3$. **(B-M)** Immunostaining of EZH2 (B-D), PTEN (E-G), pAKT (H-J), and H3K27me3 (K-M) using uteri from 2-week-old *Pten^{fl/fl}* (Ctrl), *Pten^{d/d}*, and *Pten^{d/d}; Ezh2^{d/d}* mice. At least three independent samples were examined for each genotype. Scale bar = 20 μm (B-M). **(N)** Western blot analysis of H3K27me3 in the uteri from 2-week-old *Pten^{fl/fl}*, *Pten^{fl/fl}; Ezh2^{fl/fl}*, *Pten^{d/d}*, and *Pten^{d/d}; Ezh2^{d/d}* mice. Histone H3 was used as an internal control. **(O)** Quantification of western blot. Data were normalized to the control group (100%). $n = 4$. * $P < 0.05$ and ** $P < 0.01$. ns, not significant.



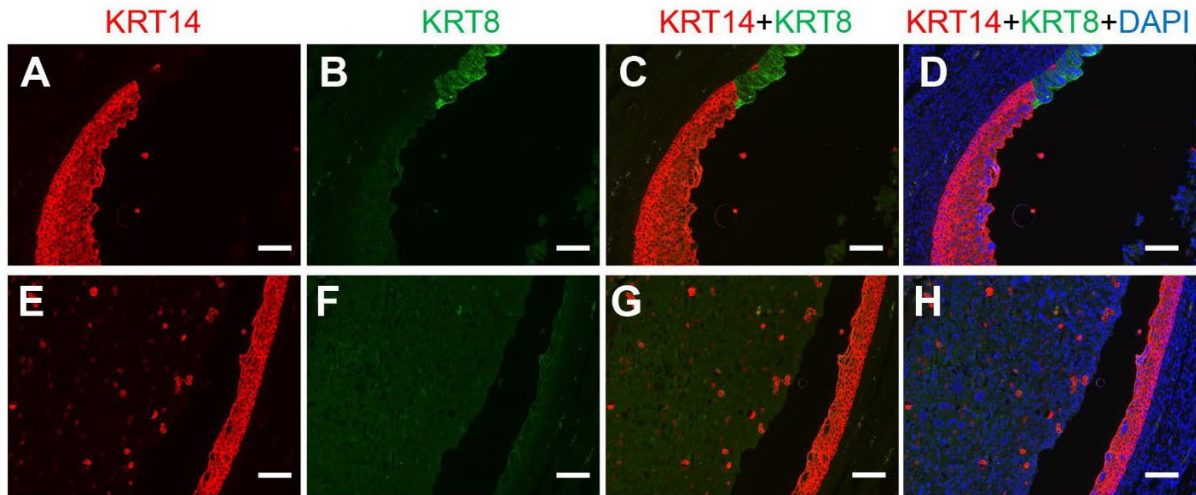
A-8. A summary of uterine histological features in *Pten*^{d/d} and *Pten*^{d/d};*Ezh2*^{d/d} mice at 1 month of age. The percentage of mice is used for the pie chart.



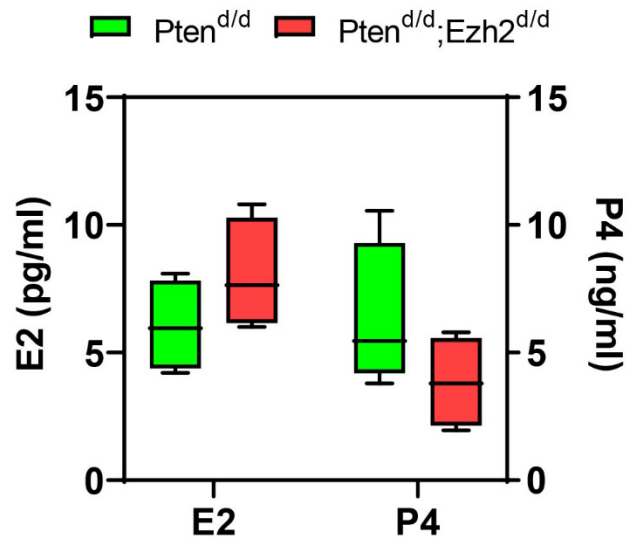
A-9. Levels of *Cxcl5*, *Cxcr2*, and *Ezh2* transcripts in uterine epithelial cells isolated from *Pten*^{d/d} and *Pten*^{d/d};*Ezh2*^{d/d} mice. Data are mean \pm s.e.m. $n = 4-5$. ** $P < 0.01$. ns, not significant.



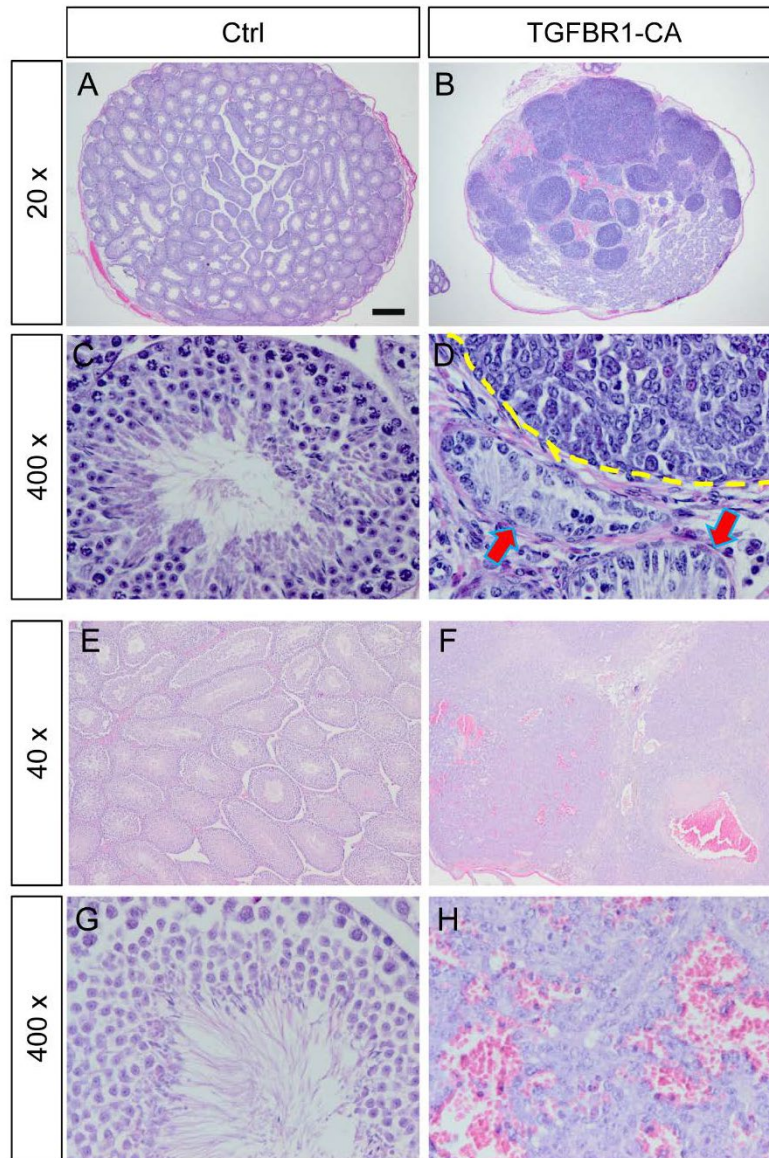
A-10. Intraluminal neutrophil infiltration in the uteri of *Pten*^{d/d} and *Pten*^{d/d};*Ezh2*^{d/d} mice. (A-F) PAS staining of uteri from 9-week-old Ctrl, *Pten*^{d/d}, and *Pten*^{d/d};*Ezh2*^{d/d} mice. Panels (D-F) are high power images of the boxed areas of panels (A-C), respectively. At least three independent samples were examined for each genotype. Red arrows indicate the sloughing epithelia. Lu, lumen. NF, neutrophils. Scale bar = 20 μ m (D-F) and 500 μ m (A-C).



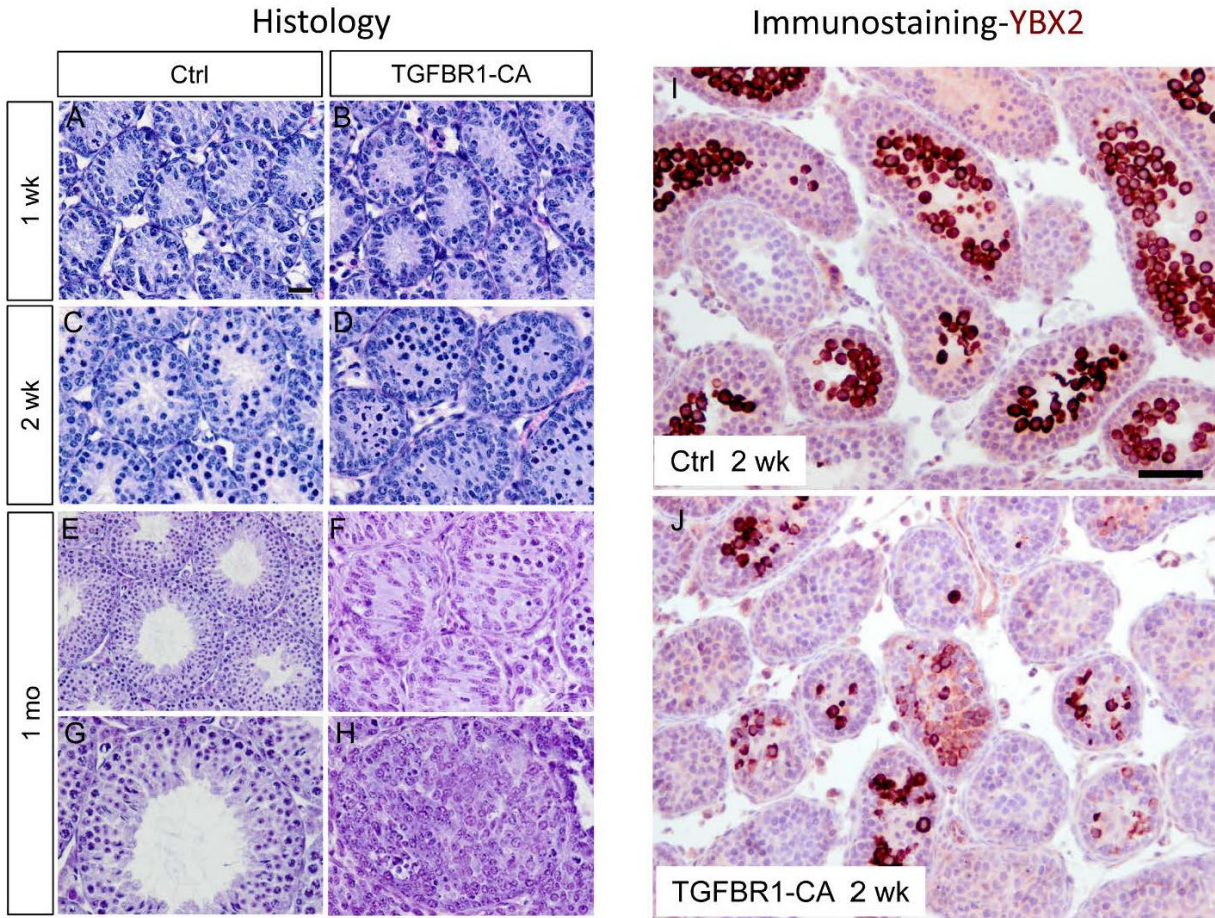
A-11. Immunofluorescence of KRT14 and KRT8 using uteri from 1-month-old *Pten*^{d/d}; *Ezh2*^{d/d} mice. DAPI was used to counterstain the nuclei. Scale bar = 100 μm.



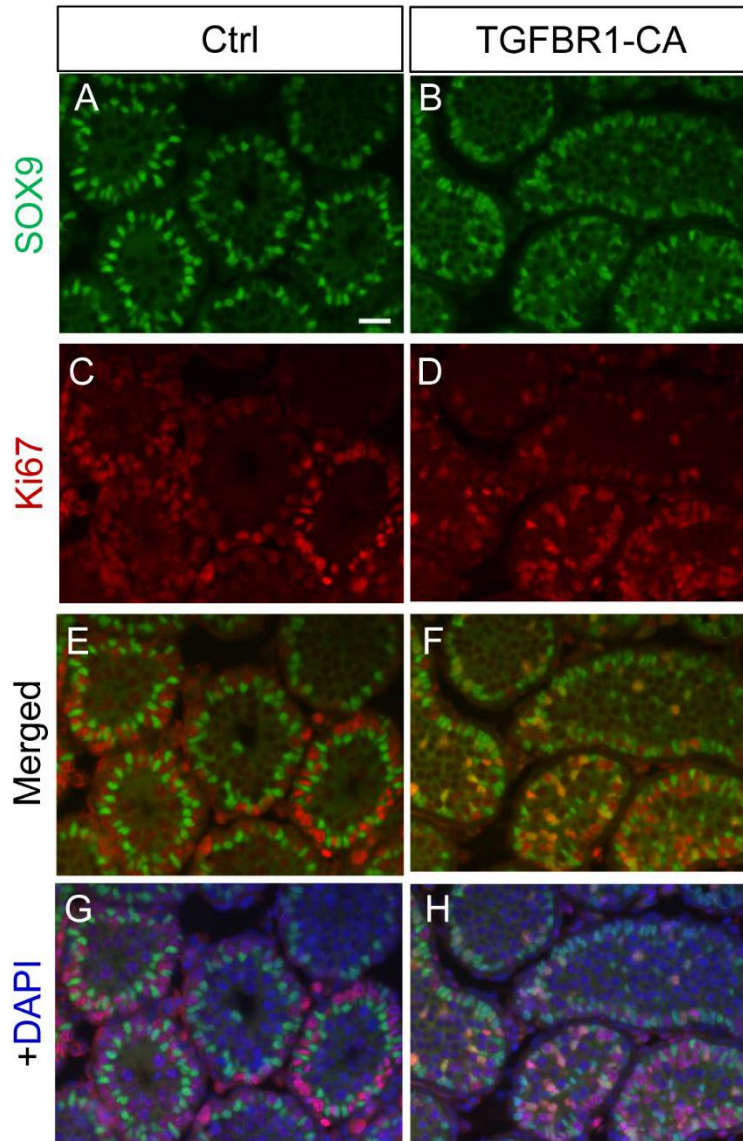
A-12. Serum estrogen and progesterone levels in *Pten*^{d/d} and *Pten*^{d/d}; *Ezh2*^{d/d} mice. Sera were collected from mice at the age of 9 weeks. *n* = 4.



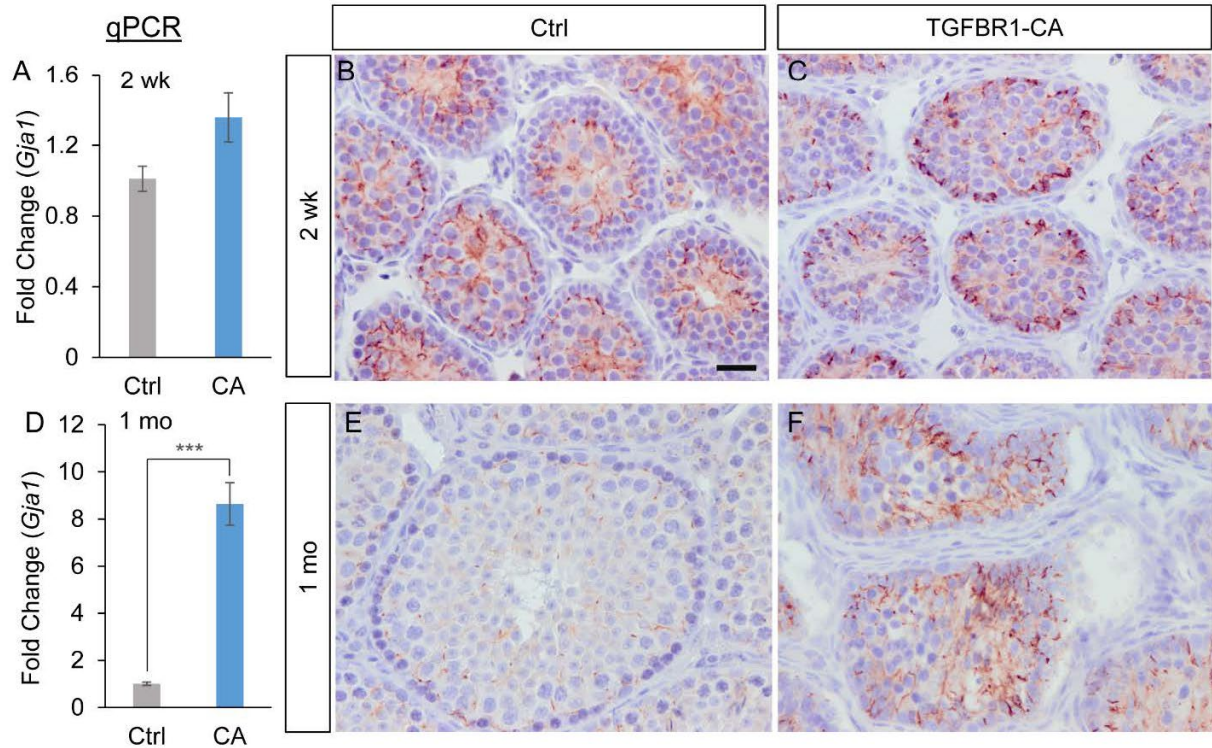
A-13. Histological analysis of testes from control and TGFBR1-CA^{Acrc} mice. (A-H) H & E staining of testes from normal control and TGFBR1-CA^{Acrc} mice at the age of 2 months (A-D) and 5-6 months (E-F). Note that the seminiferous tubules were displaced by circumscribed tumor nests in the testes of TGFBR1-CA^{Acrc} mice versus controls at 2 months of age (A-D). Panel (D) shows a tumor nodule (marked by dotted yellow line) and adjacent seminiferous tubules (arrows) near the edge of the testis that lack mature germ cells. At 5-6 months of age, tumors were more hemorrhagic (F and H). Control testes contained normal seminiferous tubule structures (E and G). Seven mice per group (5-6 months) were examined. Panels (C, D, G, and H) represent higher magnification images for the corresponding panels (A, B, E, and F). Scale bar is representatively shown in (A) and equals 20 μm (C, D, G, and H), 200 μm (E and F), and 400 μm (A and B).



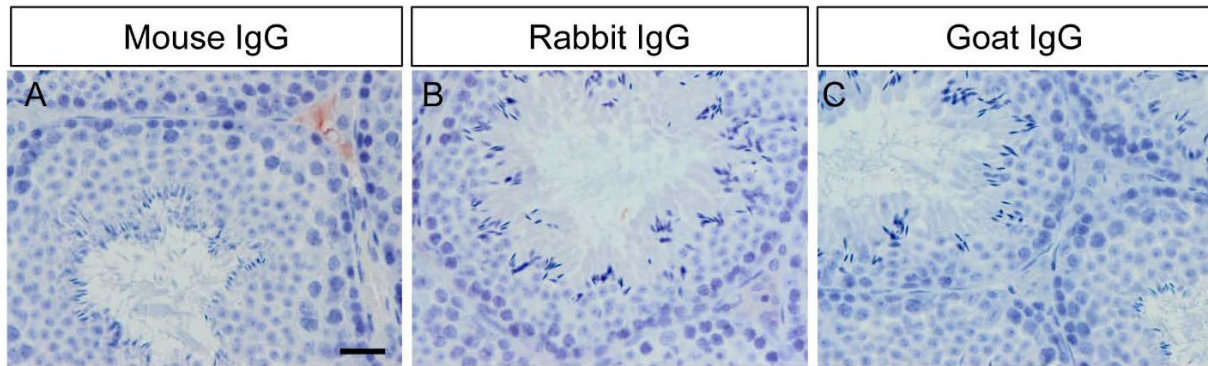
A-14. Histological analysis of testicular tumor formation in TGFBR1-CA^{Acre} mice during development. (A-H) H & E staining of testes from control and TGFBR1-CA^{Acre} mice at the age of 1 week, 2 weeks, and 1 month. Note the remarkable histological abnormalities of TGFBR1-CA^{Acre} testes (F and H) versus controls (E and G) at 1 month of age ($n = 4$). Dramatic structural alterations were not observed in TGFBR1-CA^{Acre} testes versus controls at the age of 1 week ($n = 2$) and 2 weeks ($n = 5$). Scale bar is representatively shown in (A) and equals 20 μm (A-D and F-H) and 40 μm (E). (I and J) Immunostaining of YBX2 in the testes of control and TGFBR1-CA^{Acre} mice at 2 weeks of age. Scale bar is representatively shown in (I) and equals 50 μm (I and J).



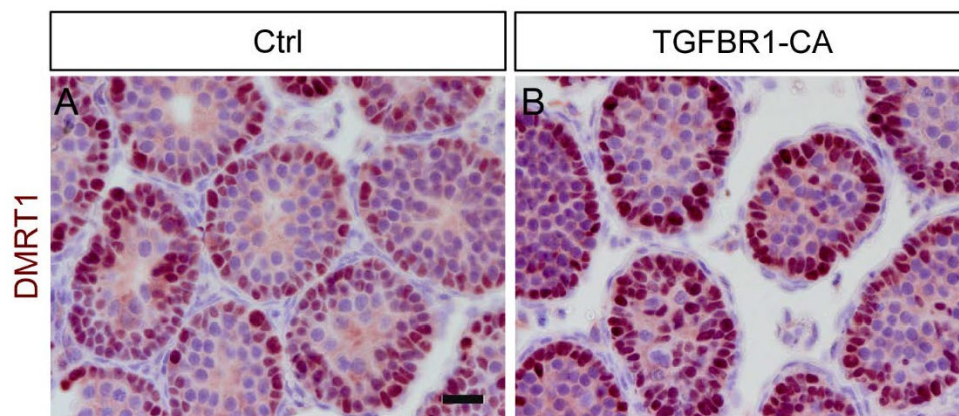
A-15. Immunofluorescence staining of SOX9 and and Ki67 using testes from control and TGFBR1-CA^{Acre} males at 2 weeks of age. Note the presence of double positive cells appearing in yellow/orange in TGFBR1-CA^{Acre} testes (F) but not controls (E). Scale bar is representatively shown in (A) and equals 20 μ m (A-F).



A-16. Expression and localization of GJA1 in the testes from control and TGFBFR1-CA^{Acre} males. (A-C) *Gjal* mRNA levels and protein localization in 2-week-old control and TGFBFR1-CA^{Acre} testes. (D-F) *Gjal* mRNA levels and protein localization in 1-month-old control and TGFBFR1-CA^{Acre} testes. Messenger RNA expression was analyzed using realtime-PCR (n = 5) and protein localization conducted using immunohistochemistry (n = 3). Data are presented as mean ± s.e.m. P < 0.001. Scale bar is representatively shown in (B) and equals 20 μm (B, C, E, and F).



A-17. Representative negative controls for immunostaining. (A-C) Isotype-matched IgG controls used for immunohistochemistry. Scale bar is representatively shown in (A) and equals 25 μm .



A-18. DMRT1 is expressed in control and TGFBR1-CA^{Acre} testes. (A and B) Immunostaining of DMRT1 in 2-week-old control and TGFBR1-CA^{Acre} testes. Sections were counterstained with hematoxylin. Three independent samples per group were used. Scale bar is representatively shown in (A) and equals 20 μm .